PURDUE UNIVERSITY

Purdue Research Foundation

Lafayette, Indiana

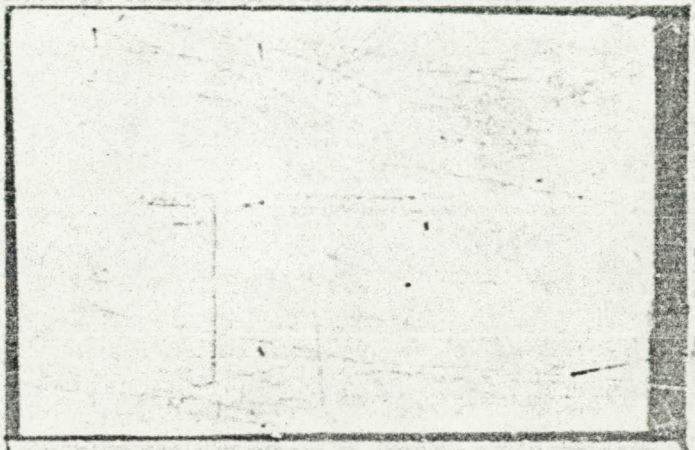

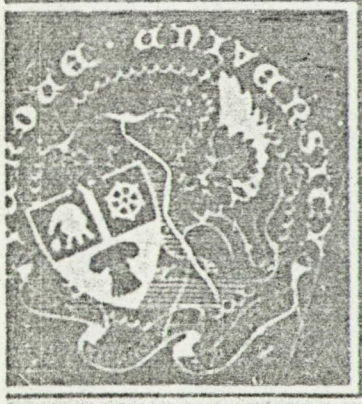

School of Mechanical Engineering

Heat Transfer Laboratory

33

THE STUDY AND CLASSIFICATION OF TWO AND MULTI-COMPONENT HIGH THERMAL CONDUCTANCE DEVICES

Interim Report

August 20, 1970

by

W. O. Barsch, E. R. F. Winter
R. J. Schoenhals, and R. Viskanta

THE STUDY AND CLASSIFICATION OF TWO AND MULTI-COMPONENT HIGH THERMAL CONDUCTANCE DEVICES

Interim Report

August 20, 1970

Submitted by

School of Mechanical Engineering
Purdue University
Lafayette, Indiana

Principal Investigators:

E.R.F. Winter, R.J. Schoenhals, and R. Viskanta

to

National Aeronautics and Space Administration
George C. Marshall Space Flight Center
Marshall Space Flight Center, Alabama 35812

Contracting Officer's Representative: B.G. McKinney

Contract Number: NAS 8-24015
Control Number: DCN 1-9-52-20010 (1F)

Authors: W. O. Barsch, R. J. Schoenhals, E.R.F. Winter, R. Viskanta

TABLE OF CONTENTS

LIST OF FIGURES

NOMENCLATURE

Basic Symbols

a	channel shape factor (eqn. 49)
A	dimensionless constant (eqn. 49)
A_a	area of artery (eqn. 104)
A_b	area of boiling heat transfer surface
A_L	area available for liquid flow
A_v	area available for vapor flow
A_w	area of wick normal to flow
b	dimensionless constant (eqn. 13), width of 2-D wick (Figure 51)
c	specific heat
d	screen mesh opening half width groove depth (Figure 52)
d_1	screen wire radius
D	diffusion coefficient
D_c	dimension parameter
D_ℓ	hydraulic diameter
g	gravitational acceleration
g_c	gravitational constant
G'	$Q/A_b \varepsilon h_{fg}$
h	elevation difference between evaporator and condenser (Figure 12)
	enthalpy
	convection heat transfer coefficient

h_f	film boiling coefficient
h_{fg}	latent heat of vaporization
h_{max}	maximum wicking height
H	net rate of heat addition per unit length
j	mass flux
K	permeability
	correction for channel shape (eqns. 48, 54)
	ratio of specific heats (eqn. 108)
k	thermal conductivity
l	length of heat pipe
ℓ'	characteristic dimension of wick surface
$\dot{m}$	mass flow rate
M	mach number
	molecular weight
n	number of channels
N	liquid transport factor
P	pressure
	power input to evaporator
P_{vap}	vapor pressure of liquid
ΔP_c	capillary pumping pressure
q	heat flux
q_r	radial heat flux
Q	heat transfer rate
r	radius
	meniscus radius
r_{min}	minimum effective radius

r_c	pore radius
r_{ch}	effective channel radius
r_b	radius of bubble nucleus
r_m	mean groove radius (eqn. 86)
r_1, r_2	meniscus radii of curvature in evaporator
R	channel half depth (eqn. 115)
	gas constant
S	constant (eqn. 16)
t	time
t_w	wick thickness
T	temperature
u	axial velocity component
V	velocity
v	cross-axial velocity component
w	groove width (eqn. 87)
w'	land width between grooves (eqn. 87)
x	wick length (Figure 10)
	coplanar heat pipe axial coordinate
y	coplanar heat pipe cross-axial coordinate
z	axial coordinate
α	wick inclination (Figure 10)
	aspect ratio of grooves (eqn. 89)
	accommodation coefficient
	thermal diffusion factor
β	inclination from vertical
	dimensionless pitch of grooves (eqn. 87)

δ	groove depth (eqn. 86)
	dimensionless constant (eqn. 51)
ϵ	wick porosity
θ	wetting angle
	inclination from horizontal
λ	second coefficient of viscosity
μ	viscosity, dynamic
ν	viscosity, kinematic
π	pressure tensor
ρ	density
σ	surface tension
τ	vapor blanket thickness (Figure 26)
Φ	viscous dissipation function
χ	mass fraction
ψ	depth ratio of grooves

Nondimensional Groups

Np	pressure number = $\rho_\ell \sigma g/P^2 g_c$
Pr	Prandtl number = $\mu c/K$
Re	Reynolds number = $r v/\nu$
Re_r	radial Reynolds number = $r_v V_r/\nu_v$
St	Stanton number = $h_f/C G'$

Subscripts

a	sonic
c	condenser
e	evaporator

eff	effective
f	effective flow
ℓ	liquid
m	mid-channel
o	condenser exterior
p	heat pipe container
s	liquid-vapor surface
sat	saturation
v	vapor
w	wick matrix, wall, or interface
x	axial direction
y	cross-axial direction
1,2	locations (Figure 10)
	components "1", "2"

ABSTRACT

A comprehensive literature review covering the period from 1964 through midyear 1970 on heat pipe technology is presented. A brief citation of early heat pipe work is followed by a presentation of heat pipe phenomenology in which the mechanism of operation, external boundary conditions, operational limits, the influence of noncondensable gases, and startup behavior, are discussed. Experimental investigations directed at determining the suitability of various substances for use as working fluids and wicks are described. In addition, numerous experimental studies dealing with operational characteristics of heat pipes are evaluated. Several possible areas of heat pipe application including heat transfer, temperature control, heat flux conversion and control of thermal conductance are examined. A discussion of basic heat pipe theory together with numerous modifications and simplifications concludes the review.

An experimental program is described which consisted of three phases. The first phase involved the design and construction of an apparatus for the measurement of wicking properties such as the maximum wicking height and the

transient velocity characteristics in a porous sample. The second phase of the experimental program involved the design, construction, and testing of a conventional cylindrical heat pipe. Wall temperatures were measured along the pipe as a function of both heat input and pipe orientation. It was found that the temperatures at the evaporator end were extremely sensitive to orientation.

The third and final phase of the investigation consisted of experimentation with a coplanar heat pipe. The objective of this part of the study was to determine to what degree the components in a two component heat pipe separate. Both single component and water-methanol mixtures were used for the working fluid. The temperature distribution was measured under the wicks and in the vapor space for various combinations of power input, orientation, and methanol mass fraction. It was found that stratification had an influence on the temperature field within the vapor. The temperature profiles measured with water-methanol mixtures exhibited a consistent trend when compared to the profiles obtained with pure water. The behavior of the profiles suggests that a partial separation of components occurred. The phenomenon of complete component separation was not observed.

CHAPTER I: INTRODUCTION

In recent years it has become increasingly important to develop methods for the efficient transport of thermal energy from one location to another. The advent of the space age has moreover stimulated research for heat transfer devices which are light weight and have relatively long life expectancies. Such a device, although not for space application, was first proposed by Gaugler [1] of the General Motors Corporation in 1944. Unfortunately for Gaugler, the thermal transport problems of that time could be solved using more conventional heat transfer methods and devices, thus effectively concealing the true potential of his invention for some 20 years. In 1962 Trefethen [2] submitted a report to the General Electric Company in which he suggested the possible use of a passive thermal device for spacecraft applications. This device was to consist of a hollow tube with a porous liner covering the inside surface. Energy would be transferred from one end to the other by means of a capillary induced, continuous mass cycling. No experimental verification of this concept was attempted, however, and the suggestion was quietly buried in company files.

In 1964 Grover, et al. [3] of the Los Alamos Scientific Laboratory independently rediscovered a device similar to

Gaugler and Trefethen's and coined the name "heat pipe" to describe it. Grover and his co-workers were working in the area of spacecraft power generation at the time but they immediately recognized the potential of the heat pipe in other areas. A heat pipe is defined as a closed structure containing some working fluid which transfers thermal energy from one part of the structure to another part by means of vaporization of a liquid, transport and condensation of the vapor, and the subsequent return of the condensate from the condenser by capillary action to the evaporator. Because energy is transferred by the flow of a pure saturated vapor, a heat pipe is usually very nearly isothermal. However, heat pipes often operate nonisothermally if the saturated vapor is "contaminated" with a second gas. The second gas may either be introduced into the pipe intentionally for the purpose of control, or may be accidentally admitted through leaks or improper filling procedures. If the second gas (vapor) participates in the evaporation processes, then the pipe is called a "two component" heat pipe. If the second gas is unable to liquify and participate in the heat transfer, it is usually referred to as a noncondensable gas. Many investigators have had experience with noncondensable gases in heat pipes (usually unintentionally) but little has been done to investigate the operation of two or multicomponent heat pipes. This lack of activity has provided the motivation for the present research program.

Problem Formulation

The first paper which mentioned two and multi-component heat pipes was published by Cotter in 1965 [1]. He performed an elementary one dimensional analysis and concluded that for a heat pipe operating at steady state, the various components would separate and form a series of segments each containing a pure component which would operate as an "independent" heat pipe within the multi-component heat pipe. The temperature of each segment would adjust itself so that the pressure within the vapor is nearly constant throughout the entire pipe, thus forming a series of temperature plateaus. The most volatile component, of course, would be located at the condenser end of the heat pipe. S. Katzoff [5] analyzed the wall temperature distribution for a copper heat pipe containing a mixture of ethanol and methanol. He assumed that the energy needed for the leg with the more volatile (methanol) component is transferred past the ethanol-methanol interface primarily by conduction along the wall and wick structure. If this heat flow is sufficient to maintain circulation in the methanol segment, then the situation described by Cotter would exist, i.e., the two legs would operate independently and the temperature distribution in the pipe would comprise two plateaus. In the transition region between the two legs the composition of both the liquid and vapor would vary continuously, but

at each location the relative compositions would have to be such that the liquid and vapor are in equilibrium. Katzoff speculated that if on the other hand the conduction past the interface is not enough to maintain the methanol leg, then it may be possible for an ethanol-methanol mixture to exist along the entire pipe in both the liquid and the vapor. This would be possible if the composition varied both radially and axially instead of just axially.

Tien [92] measured the axial temperature distribution along the outside of a water-ethanol heat pipe. He determined the pressure inside of the pipe and compared this with the pressure which had to prevail if pure ethanol occupied the condenser and pure water occupied the evaporator. He concluded that separation into pure components in a heat pipe is extremely difficult, if not impossible, to achieve. Instead he found that if the initial composition was rich in ethanol, the data attested to the existence of a water-ethanol mixture in the evaporator while nearly pure ethanol (i.e., the azeotropic mixture) occupied the condenser section. All of Tien's data, however, were obtained with the pipe operating vertically with the evaporator below the condenser. If the pipe contains excess liquid such an arrangement is usually referred to as a reflux condenser because gravity forces, instead of capillary forces, can always return the condensate to the evaporator. In such cases results would have to be viewed with some caution

because the wick structure may or may not significantly alter the liquid vapor equilibrium conditions.

It is clear that present knowledge about even the fundamentals of multi-component heat pipe operation is rather limited. It was the objective of this study to extend this knowledge for the case of two component heat pipes. The aims of the research reported in this study were:

1) to perform a survey and evaluation of the heat pipe literature
2) to experimentally study and describe the basic physical behavior of a two component heat pipe, and
3) to analytically predict the qualitative temperature and concentration profiles in the vapor core of a two component heat pipe.

Because an understanding of a single component heat pipe and some of the problems associated with it is a prerequisite for the investigation of a two component heat pipe, chapter II contains a discussion of the general phenomenology of heat pipes. In chapter III a review of all literature pertaining to heat pipes is presented. The articles to be discussed include those published up to approximately March 1970. In addition to these, about twelve articles to be presented at the 1970 ASME Space Technology and Heat Transfer Conference, Los Angeles, California, June 21-24 will be referenced in an appendix to

this study. Due to the large number of references cited, chapter III is somewhat lengthy. Readers primarily interested in the experimental investigation may find it expedient to proceed directly to chapter IV.* The analytical formulation for a two component heat pipe is discussed in chapter IV. In chapter V the various apparatus used during the course of the current research are described in detail. Experimental results are presented in chapter VI together with the predictions from chapter IV. A number of appendices in which supporting information is contained concludes the study.

* Chapters II and III together with a modified introductory chapter are being published as a monograph entitled, "The Heat Pipe," in volume seven (7) of the "Advances in Heat and Mass Transfer," New York, Academic Press, 1971.

CHAPTER II: HEAT PIPE PHENOMENOLOGY

Description and Types of Heat Pipes

As evident from the definition given in the introduction, all heat pipes have a number of common features. First, all heat pipes incorporate what is usually referred to as an evaporator. This is the part of the heat pipe through which thermal energy from some external source is introduced into its walls and from there subsequently transferred to the working fluid. Second, all heat pipes include a condenser section. The working fluid condenses here and ultimately transfers its heat of condensation to an external sink. Many heat pipes contain also an adiabatic section located between evaporator and condenser. The adiabatic section, besides providing a passage for the fluid, serves no functional purpose other than separating the heat source and heat sink to make the heat pipe compatible with any given external geometric requirement.

In addition to the longitudinal sections, i.e., evaporator, condenser, and adiabatic section, a heat pipe may also be subdivided for the purpose of discussion into three radial components. The outermost shell is usually referred to simply as the "container." The container's sole mechanical purpose is to enclose the functioning parts

of the heat pipe and to lend it structural rigidity. Since the internal pressure is often different from the environmental pressure, the container must be capable of withstanding pressure differences without bulging or bursting. This constraint, along with cost and manufacturing considerations has led to the wide use of cylindrical "pipes" as containing structures. In addition to fluid and "pressure" containment, the container also acts as an important part of the heat flow path from the source to the sink (see Figure 2.1). Hence the container walls should be thin to minimize their thermal resistance. This feature is in direct opposition to the thick wall requirement for pressure containment and hence an opportunity for an optimization presents itself. The next radial element is usually referred to as the wick. For ease of the present discussion, this may be regarded simply as a porous material filled with small random interconnected capillary channels. Various types of wicks and their properties are discussed in greater detail later in this study. The wick returns the liquid from the condenser to the evaporator utilizing the surface tension forces of the liquid. Although it is not a requirement, the wick is usually firmly attached to or pressed against the inside wall of the container. Since the wick is in general saturated with a low conductivity working fluid (except in the case of liquid metals) the wick-fluid matrix represents usually the major resistance along the heat flow path. It

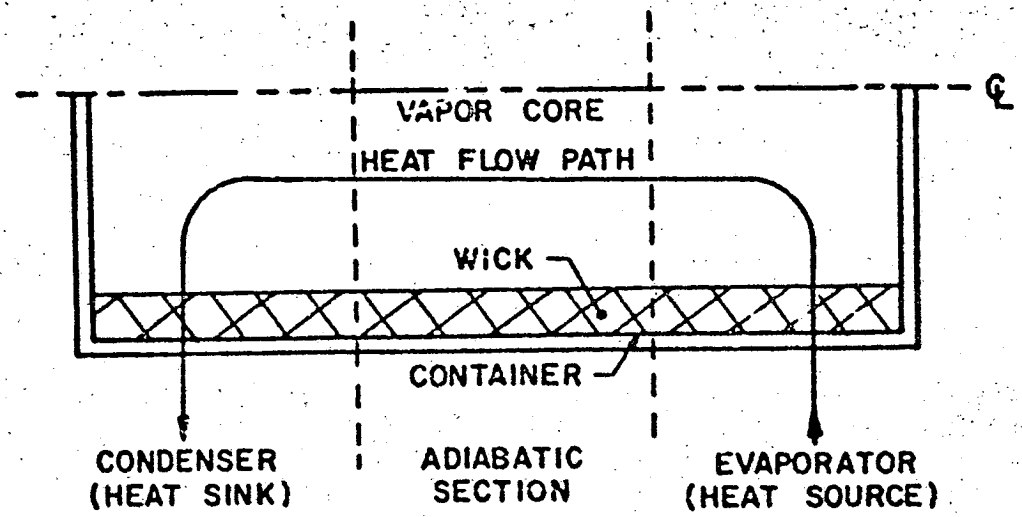

Figure 2.1 Heat Pipe Components

is therefore necessary to consider thermal properties as well as liquid transport properties when selecting a suitable wick. The interior space of the heat pipe is usually referred to as the vapor core which provides a passage for the vapor as it flows from the evaporator to the condenser.

It should now be evident that the heat pipe definition entails no geometric constraints in regard to its structure; and in fact a large number of heat pipes of many different shapes have been built and tested. Several conventional and unconventional heat pipes are depicted in Figures 2.2 through 2.4. A heat pipe, as originally conceived by Grover, et al. is illustrated in Figure 2.2-A [3]. This particular geometry exhibits two features which early investigators felt were important for efficient heat pipe

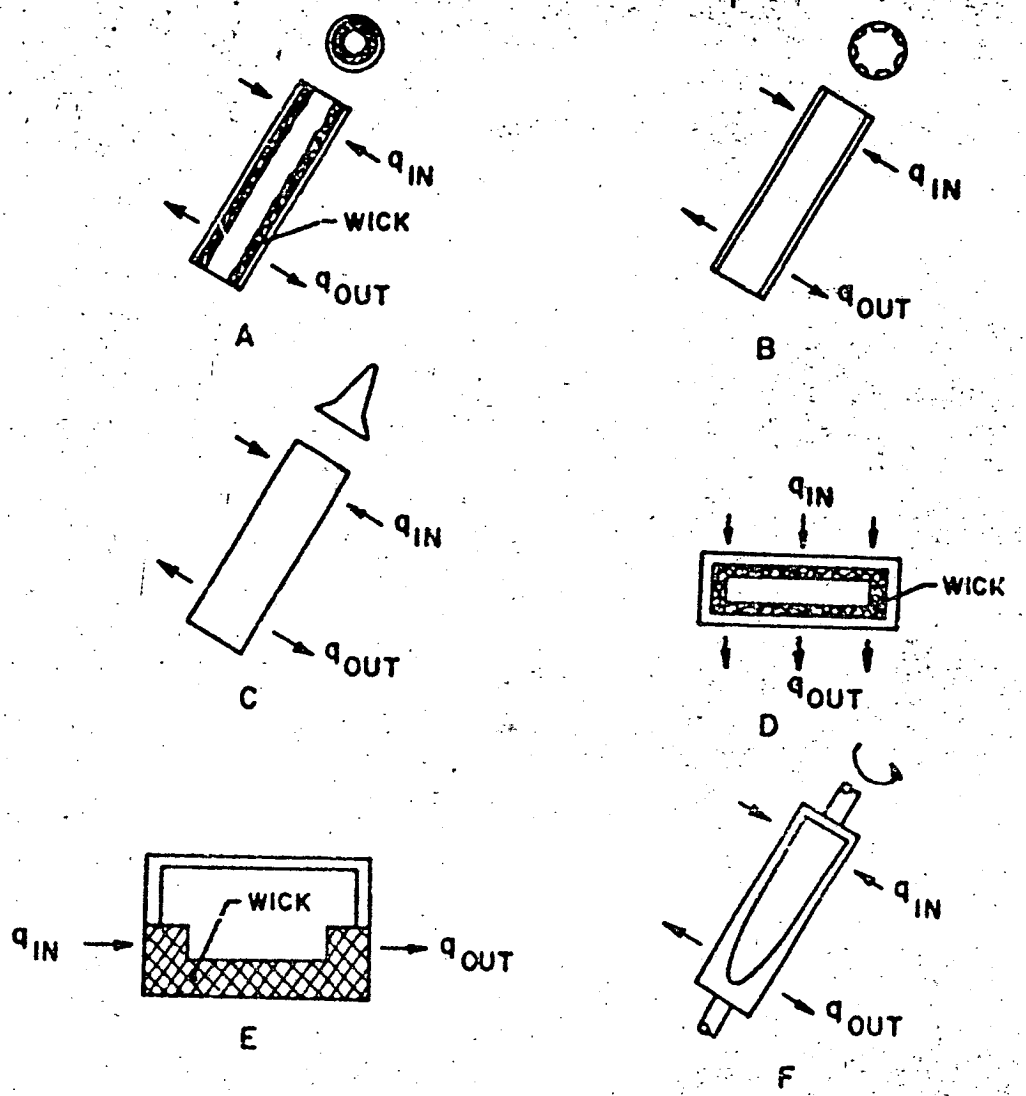

Figure 2.2 Typical Heat Pipe Geometries

operation, i.e., a relatively large length to diameter ratio, and a porous wick material which covers the inside surface of the structure. Figures 2.2-B and 2.2-C illustrate two typical heat pipe configurations which also have a large length to diameter ratio, but which provide for capillary transport of the liquid in grooves and crevices forming an integral part of the containing structure, contrary to the porous wicking material sketched in Figure 2.2-A, which is only held against the inside wall. The heat pipe shown ~~in~~ Figure 2.2-D has a very small length to diameter ratio. Heat pipes having such proportions are often called "vapor chambers" or "vapor chamber fins." The device shown ~~in~~ Figure 2.2-E also fits our definition of a heat pipe although the liquid and vapor flow paths are separated mechanically whereas in the more conventional heat pipe only the liquid-vapor interface separates the flow paths. Finally, the device depicted in Figure 2.2-F has recently been introduced [6] as a "rotating heat pipe." Here the liquid return is caused by centrifugal forces of the rotating contrivance. Although the rotating device appears promising for many thermal transport problems, it does not fit our definition of a heat pipe and hence will not be discussed in detail.

Evidently the variations in heat pipe shapes are unlimited; both Katzoff [5] and Conway and Kelley [7] have considered a doughnut shaped heat pipe. Several investigators [5, 8, 9] have proposed and designed flexible heat

pipes. RCA has built and operated heat pipes with a variety of geometries. Among these are the two illustrated in Figures 2.3-A and 2.3-B [10]. The configuration displayed in 2.3-A will effectively transport heat around a 90° bend. The five-pronged device in Figure 2.3-B allows the use of any combination of prongs as evaporators and of the remaining prongs as condensers. For ease of manufacturing, both types have cylindrical cross sections although this is not a requirement. In addition to the above geometries, several investigators [10, 11] have built and tested a so-called radial heat pipe. As illustrated in Figure 2.4, the radial heat pipe provides for thermal energy transport from a heat source to a concentric heat sink. The wick lining the inner walls of the annulus in this case is complimented by spokes consisting of additional wick materials. Here, as with most other heat pipe geometries, the relative positions of the condenser and evaporator may be interchanged in order to accommodate any particular thermal transport problem. The variety of geometries depicted above are by no means inclusive of all possible configurations and are presented only to illustrate the extreme versatility of the heat pipe for heat transfer problems.

Functioning of the Heat Pipe

At first glance, the operation of a heat pipe appears exceedingly simple. Thermal energy is transferred from the evaporator to the condenser by continuous mass cycling and

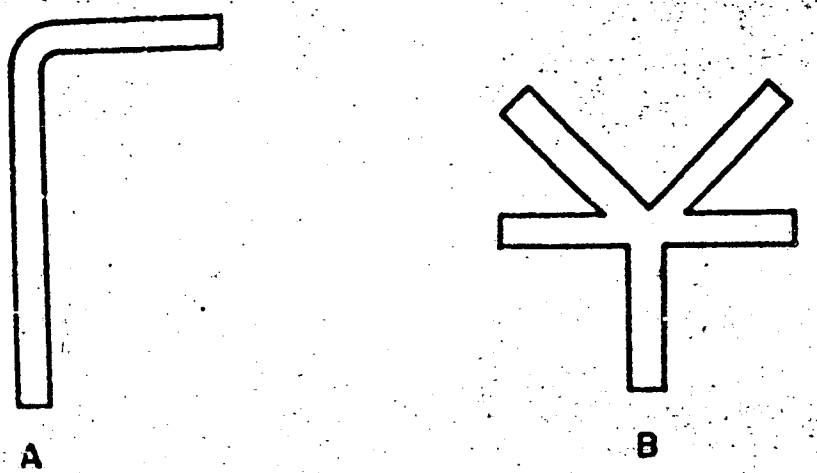

Figure 2.3 Various Heat Pipe Geometries [10]

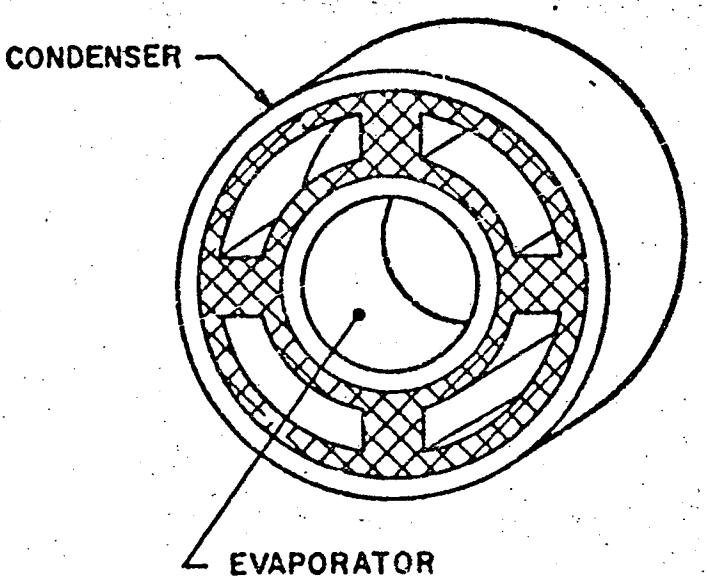

Figure 2.4 Radial Heat Pipe [11]

phase change of a suitable working fluid. The mechanism of phase change with the accompanying absorption or release of the latent heat of transformation has long been recognized as an efficient heat transfer process. Many gadgets, e.g., the coffee percolator and the reflux condenser, combine heat transfer by phase change with a gravity induced mass cycling. Boilers in many cases utilize a mechanical pump to continuously circulate and replenish the working fluid. In a heat pipe, however, the working fluid is continuously cycled by the surface tension forces of the fluid itself. It is this unique method of mass transfer which has both stimulated a growing interest in the heat pipe, and has also proved to be one of the major impediments for a successful heat pipe operation. To better understand the functioning and the limitations of heat pipes let us consider in more detail the physical effects occurring in a heat pipe.

The steady state operation of a heat pipe may be represented schematically as shown in Figure 2.5. The inside wall of the container is lined with a porous capillary structure which is saturated with some working fluid. A sufficient amount of fluid must be supplied in the container in order to fill (saturate) all the pores of the capillary structure. The penalty for having a slight excess of fluid is small compared to the possibility of heat pipe failure which might arise from a deficiency of fluid. The vapor in the core of the pipe is essentially at the saturation

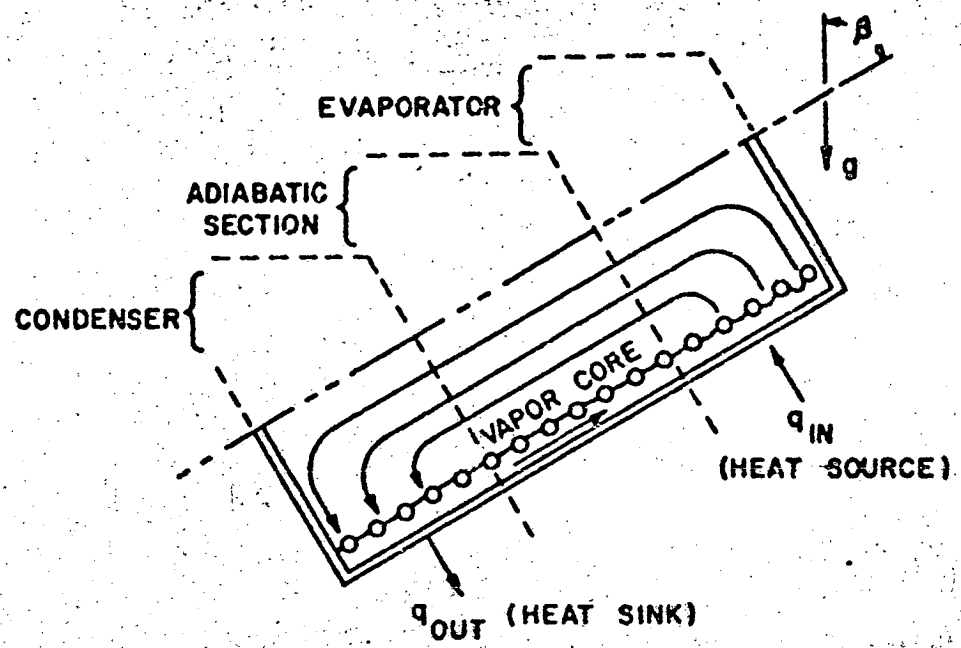

Figure 2.5 Heat Pipe Schematic

pressure corresponding to the liquid surface temperature. In actuality the saturation pressure of a vapor in equilibrium with a liquid surface depends also on the radius of curvature of the surface. The vapor pressure is greater than that acting on a plane surface if the liquid surface is convex, and less if the meniscus is concave. The effect is usually too small to warrant consideration and is not significant until the meniscus radius is of the order of one micron [12]. Since the typical capillary pores in most heat pipes are larger than one micron, no noticeable error is introduced by neglecting this effect.

The heat transfer from the source to the sink is affected mainly by six simultaneous and interdependent processes: 1) heat transfer from the source through the container wall and wick-liquid matrix to the liquid-vapor interface; 2) evaporation of the liquid at the liquid-vapor interface in the evaporator; 3) transport of the vapor in the core from the evaporator to the condenser; 4) condensation of the vapor on the liquid-vapor interface in the condenser; 5) heat transfer from the liquid-vapor interface through the wick-liquid matrix and container wall to the sink; and 6) return flow of the condensate from the condenser to the evaporator caused by capillary action in the wick. Let us now consider each of these processes separately and in more detail.

Heat transfer from the source to the liquid-vapor interface in the evaporator is essentially a conduction process. For low conductivity fluids, e.g., water or alcohols, the thermal energy is conducted through the wick-liquid matrix almost entirely by the porous wick material since the wick has a higher thermal conductivity than the fluid. For high conductivity liquid metals, however, the heat is conducted both through the wick structure and by the liquid in the pores. Heat transfer by convection is very small because the pores are too small for any significant convection currents to develop. The temperature drop associated with conduction across the wick-liquid matrix depends on the working

fluid, wick materials, wick thickness and the net radial heat flux. This temperature drop may range from a few tenths to several hundred degrees Fahrenheit and is one of the major temperature gradients along the heat path.

Once the thermal energy has been transferred to the vicinity of the liquid-vapor interface, evaporation of the liquid can take place. As the liquid evaporates, the net mass flow away from the surface causes the liquid-vapor interface to recede into the wicking structure. The resulting concave shape of the meniscus, shown in Figure 2.5, is responsible for the functioning of the heat pipe. A simple force balance on a single pore shows that for a spherical interface the pressure of the vapor exceeds the liquid pressure by an amount equal to twice the surface tension divided by the meniscus radius. This pressure difference is the basic driving force for both the liquid and vapor flows. It is opposed mainly by the gravitational and viscous forces acting on the liquid during circulation. The assumed form of the liquid-vapor interface sketched in Figure 2.5 is probably quite realistic for relatively low heat fluxes. As the heat flux increases, however, the meniscus recedes even further into the wick and assumes a more complex shape [13] which may eventually interfere with the liquid flow in the capillaries. Once the liquid has absorbed the latent heat of vaporization and is evaporated, the vapor begins to move through the core of the pipe towards the condenser. The

flow is caused by a small pressure difference prevailing in the vapor core. This pressure difference is caused by the slightly higher temperature (saturation pressure) in the evaporator as compared to the temperature (and hence lower saturation pressure) in the condenser. This temperature drop is often used as a criterion for successful heat pipe operation, and if the difference is less than 1 or 2°F, the heat pipe is often said to be operating in the "heat pipe regime" i.e., isothermally [3, 14, 15]. As the vapor flows toward the condenser, additional mass is added from the downstream portions of the evaporator and consequently the mass flow rate and velocity in the axial direction continue to increase throughout the evaporator. Inverse conditions prevail in the condenser section of the heat pipe.

The vapor flow in the evaporator and condenser of a heat pipe is dynamically identical to pipe flow with injection or suction respectively through a porous wall. The flow may be either laminar or turbulent depending on the operating conditions of the heat pipe. As the vapor flows through the evaporator (and the adiabatic section) the pressure continues to decrease due to both viscous and acceleration effects. Once the condenser section is reached and the vapor begins to condense on the liquid-wick surface, a partial dynamic recovery in the decelerating flow tends to increase the pressure in the direction of fluid motion. It should be mentioned that the driving pressure in the vapor

core is somewhat smaller than the vapor pressure difference of the fluid in the evaporator and condenser. This is so, because the vapor pressure of the liquid in the evaporator must exceed the pressure in the adjacent vapor in order to maintain a continued evaporation process. Likewise, the pressure of the condensing vapor must exceed the vapor pressure of the adjacent liquid in order to maintain continued condensation.

As the vapor condenses the liquid saturates the pores in the condenser. The meniscus has a very large radius of curvature, and in fact it may be considered essentially infinite. Any excess working fluid in the pipe collects on the condenser surface thus virtually insuring a plane interface. The heat of condensation is conducted through the wick-liquid matrix and container wall to the heat sink. If excess liquid is present, the temperature drop from the interface to the outside of the container will be larger than the corresponding temperature drop in the evaporator. In fact, some investigators [14, 16] feel that the thermal resistance in the condenser is one of the major parameters to be considered in heat pipe design.

Finally, the condensate is "pumped" through the wick to the evaporator by capillary action. The liquid flow is generally regarded to be laminar and assumed to be dominated by viscous forces. The pressure along the liquid flow path decreases due to both the viscous losses and the increase in

elevation if the heat pipe is operated in a gravity field. Operation of the heat pipe in presence of gravity with the condenser above the evaporator actually defeats the purpose of the wick since gravity can be used to return the condensate along the inside of the container wall with less viscous loss than liquid flow in the wick would cause. In this mode of operation the heat pipe is said to have degenerated into a reflux condenser or thermosyphon. Therefore, in this monograph, the pressure loss due to gravity will always be considered greater than zero (evaporator above condenser) or equal to zero (horizontal orientation of heat pipe simulating a gravity free environment).

Because the vapor temperature, or operating temperature as it is sometimes called, of the heat pipe is essentially determined by the coupling of the heat pipe to the heat source and the heat sink, a brief discussion of possible source-sink combinations and their effect on the heat pipe operation is warranted. The vapor temperature adjusts itself in such a way that the temperature drop across the wick-liquid matrix and the container wall in evaporator and condenser is adequate to transfer the given heat flow from heat source to heat sink. In other words, the absolute vapor temperature is established in response to the temperatures imposed on both the evaporator and condenser by the source and sink. The temperatures at the outside wall of the heat pipe may be either "fixed" or "floating" depending

on the type of constraints imposed by source or sink. At the evaporator, a "floating" temperature is usually the result of forcing some sort of heat flux boundary condition upon the heat source. This is easily accomplished by employing resistance heaters, induction coils, RF coils or radiative heating for the heat source. At the condenser, a "floating" temperature is commonly effected by radiative cooling. A fixed temperature can be maintained at either end of the heat pipe with constant temperature baths or by utilizing the heat of evaporation or condensation of a secondary working fluid for heat addition or removal respectively, at constant temperatures.

Let us now consider possible qualitative temperature profiles along the heat flow path (see Figure 2.1) for several source-sink combinations. Figure 2.6-A depicts the temperature profile which would be obtained if both the source and the sink were of the constant "fixed" temperature type. For such a situation, only one axial heat flow rate is possible. The vapor temperature in the heat pipe is quite close to the average of the source and sink temperatures and probably tends to be somewhat closer to the source temperature since the thermal resistance in the liquid-wick matrix is larger in the condenser than in the evaporator. Figure 2.6-B illustrates the temperature profile which results if the sink temperature is fixed and the source temperature is allowed to float. This particular combination

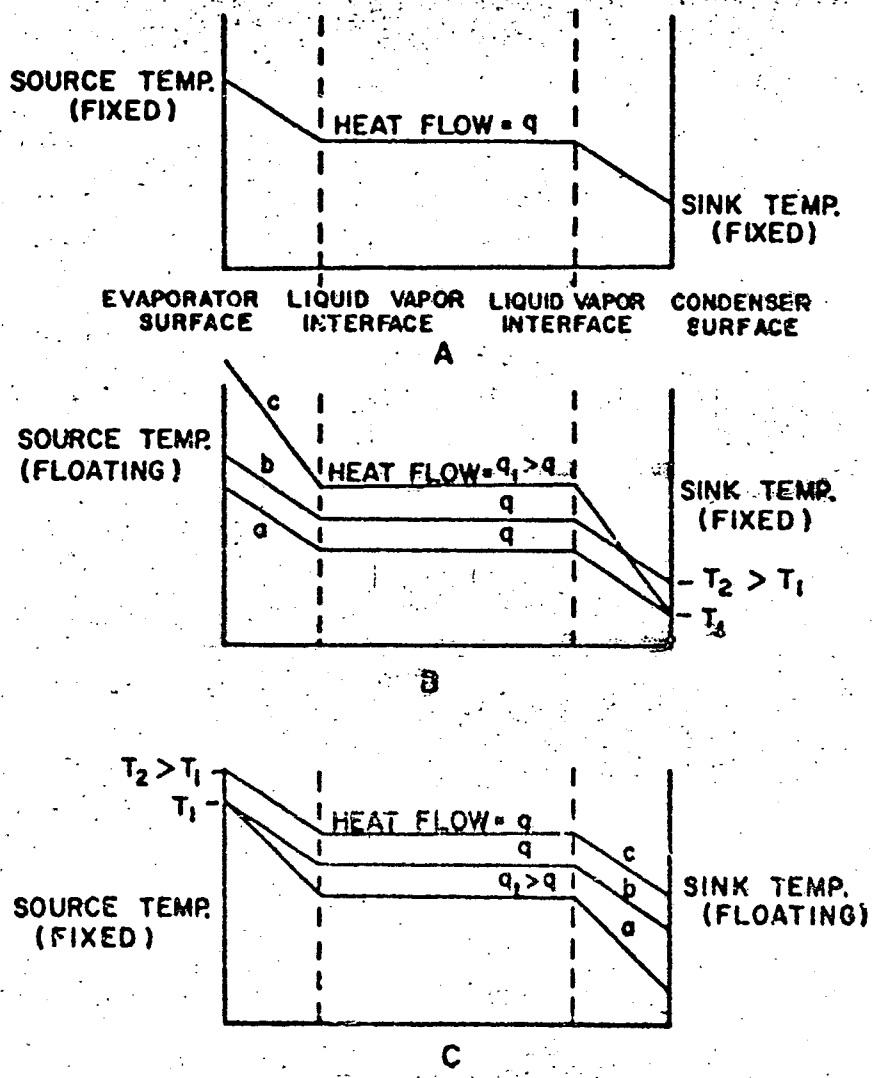

Figure 2.6 Qualitative Temperature Profiles Along Heat Flow Path

of source and sink is commonly found in laboratory testing of low temperature heat pipes (resistance heating and water jacket cooling). As shown by profiles a and c, the source temperature and the vapor temperature increase with increasing heat flux. Conversely, if the heat flux is maintained constant and the sink temperature is increased as in profiles a and b, the vapor temperature and the source temperature again increase, but now the temperature gradients in the evaporator and condenser remain the same. Figure 2.6-C describes the profiles which are obtained if the source temperature is fixed and the sink temperature is allowed to float. Here we see from profiles a and b that the vapor temperature must drop in order to accommodate a larger heat flux for a fixed source temperature and conversely it must rise for a given heat flux if the source temperature is increased. A significant omission from Figure 2.6 is the case where both the source and the sink temperature are allowed to float, a situation often encountered during the laboratory testing of high temperature liquid metal heat pipes (induction or RF coil heating and radiative cooling). For this case the operating temperature of the heat pipe adjusts itself to a value at which the total heat input equals the total heat rejection. Since this self-adjustment depends on the exact type of source and sink used, and possibly on certain properties of the container wall itself, e.g., electrical resistivity or emissivity, an exact

statement about the operating temperature cannot be made. In general, increased heat fluxes cause an increase in the operating temperature of the heat pipe.

The proper functioning of heat pipes depends also upon a continuous circulation of the working fluid; consequently, it is not surprising that virtually all of the limitations (limits) for successful heat pipe operation are associated in one way or another with the interruption of this mass circulation. The limit discussed and analyzed most often in the literature is the so-called "wicking limit." This condition is reached when a given heat flux causes the liquid in the liquid-wick matrix to evaporate faster than it can be supplied by capillary pumping in the wick (wicking action). Once this condition occurs, the liquid-vapor meniscus continues to recede into the wick until all of the liquid has been depleted. The wick in the evaporator becomes dry and the container temperature increases without bound until a "burnout" condition is reached which usually results in destruction of the pipe. Of course, the burnout condition can only be reached if the source is of the floating temperature type. For a fixed temperature source, the heat pipe would simply cease functioning once the capillary limit is achieved, and no mechanical damage would occur.

Two additional limits of heat pipe operation are commonly associated with heat pipe "startup" and low operating temperature conditions. One of these is called "sonic limit",

a condition found in heat pipes in which the source temperature is kept constant while the sink temperature is lowered. The vapor density decreases and the vapor velocity increases correspondingly until the velocity becomes sonic. The vapor flow "chokes" at the evaporator exit, just as it does when the sonic condition is reached at the throat of a convergent nozzle [17]. Once choking occurs, a further decrease of the sink temperature, in analogy to a reduction of the exit pressure in a nozzle, does not result any longer in an increase of the total heat flow.

A so-called "entrainment limit" is reached when the vapor velocity is high enough and the vapor stream shears off droplets from the liquid interface entraining and carrying them to the condenser. Quite frequently the droplets can be heard as they impinge upon the end cap of the heat pipe [18]. The premature depletion of the working fluid from the wick means that less liquid can reach the evaporator where it is needed for successful heat pipe operation. The entrainment limit depends to a large extent on the surface pore size of the wick material and also on the surface tension of the working fluid. The use of small pore sizes and fluids having large surface tensions is perhaps the most effective way of avoiding liquid entrainment.

The relative position of the operating limits in a heat flow Q, versus temperature T plot, is illustrated in Figure 2.7. Here Q represents the total axial heat transfer rate

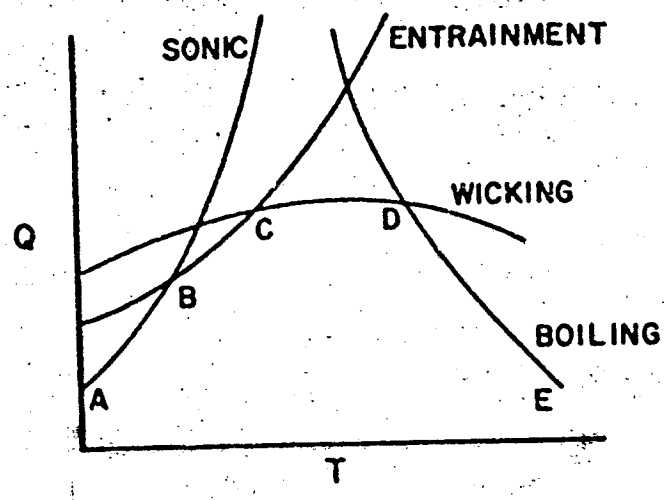

Figure 2.7 Limits to Heat Pipe Operation [18]

and T is the average vapor temperature in the heat pipe. Successful heat pipe operation is possible only under conditions existing below the curve ABCDE. The shape of the area under the curve may vary drastically depending on the wick material and working fluid used; however, the basic shape of each limit curve should remain as shown. Numerical examples for these various limits will be presented later in the text of this thesis.

The presence of a noncondensable gas in a heat pipe may have a detrimental effect on heat pipe performance. The noncondensable gas can be added intentionally for the purpose of control, or it can be the result of improper filling procedures, container leaks, or chemical reactions between the working fluid and the container or wick material. Neglecting the control aspect for the present, the most common

noncondensables are air (from leaks) and hydrogen (from chemical reactions). During heat pipe operation the noncondensable gas is swept to the condenser and forms a stagnant gas layer. The temperature in this zone adjusts itself in such a way that the total pressure in the vapor core remains approximately constant throughout. Heat is transferred through this zone to the liquid-wick surface primarily by conduction. Because this mode of heat transfer is extremely slow compared to that taking place in a normal condensation process, the zone containing the stagnant gas is effectively eliminated as a functioning part of the heat pipe. The result is an effective shortening of the pipe, thus reducing its total axial heat transfer capability. The length of the noncondensable gas zone depends on the operating temperature and pressure in the system. For increased axial heat fluxes and the corresponding increased pressures, the zone will contract and allow more of the condenser to become operative again. Conversely, for decreased operating pressures, the gas zone expands and reduces the area available for condensation. If the quantity of noncondensable gas or the operating pressures are such that the entire condenser section comes to lie within the stagnant gas zone, heat pipe operation ceases. The possibility of using a noncondensable gas for the variation of the effective condenser area as a control technique will be expanded upon later.

The preceding discussion has dealt exclusively with steady state heat pipe behavior. Of equal importance for the practical use of these devices is an understanding of the transient operating conditions through which a heat pipe passes during startup. Cotter [19] conceived three basic modes of startup which may be recognized by the shape of the developing temperature profiles. The three modes are experienced when the evaporator is heated uniformly over its entire length at constant heat flux which may, however, be varied with time. The condenser is cooled uniformly either by radiation or heat conduction to a sink kept at uniform temperature. The various modes of startup are illustrated in Figure 2.8, the abscissa of which represents the distance along the heat pipe axis and the ordinate the vapor temperature. The uniform startup in Figure 2.8-A takes place when the vapor density is high at the ambient temperature so that the working fluid begins to reflux throughout the pipe immediately in response to an increase in the heat flux. This type of startup procedure may be accomplished very rapidly without detrimental effects to the pipe. The frontal startup in Figure 2.8-B is encountered when the vapor density is very low at ambient temperature, a case often observed when starting liquid metal heat pipes from room temperature. In this case the vapor density is so low that the molecule mean free path exceeds the vapor core diameter. As the heat flux is increased, the vapor density in the evaporator section rises

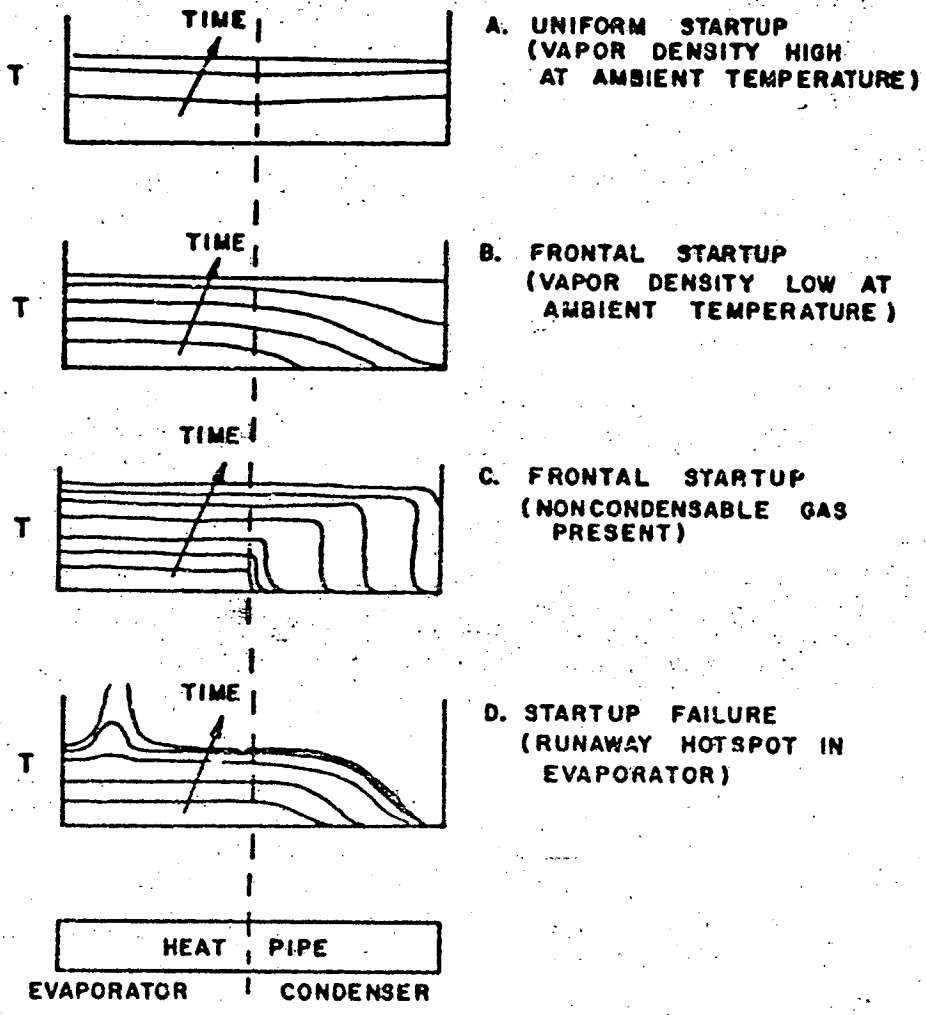

Figure 2.8 Transient Temperature Profiles of Heat Pipes During Various Startup Modes [19]

and the molecule mean free path becomes small compared to the vapor core diameter. The vapor in the evaporator section enters the continuum flow regime while the vapor in the condenser remains in the free molecule flow regime with, of course, a transition region located in between. This mode of startup is further complicated by compressible flow effects since transonic vapor velocities are achieved. Finally, the vapor may condense into liquid droplets in the vapor core since the vapor is nearly saturated in the evaporator but subcooled in its expanding flow toward the condenser. The frontal startup in Figure 2.8-C illustrates a situation which can be expected if a significant amount of noncondensable gas is present, a case in which the evaporator heats up relatively uniformly. As the vapor temperature and hence pressure increase the noncondensable gas is moved toward the condenser where it collects in a fairly well defined zone. The temperature in this zone adjusts itself so that the total pressure in the vapor core is approximately constant. As the heat flux is increased and the vapor pressure and temperature increase, the noncondensable zone is further compressed thus causing the temperature profiles displayed in Figure 2.8-C. This mode of startup may also be accomplished very rapidly. The startup modes described above are somewhat idealized and various intermediate modes may be observed depending on the vapor density at initial temperature and the amount of noncondensable gas present.

Figure 2.8-D illustrates a common failure encountered during startup. A hot spot is formed in the evaporator and the temperature increases without bound until failure results. The failure is usually a consequence of either the attainment of the wicking or boiling limit during the startup sequence of heat pipes having a floating temperature source.

CHAPTER III: LITERATURE SURVEY

General Literature

A very extensive research effort has been devoted to heat pipes since 1964 when Grover and his co-workers [3] at the Los Alamos Scientific Laboratory, Los Alamos, New Mexico, first reported the successful operation of a heat pipe. A 347 stainless steel container lined with five layers of 100-mesh 304 stainless steel screen saturated with 40 gm of sodium became the prototype of all subsequent heat pipes. Five chromel-alumel thermocouples were welded along the 9-cm-long pipe. The temperature distribution was measured for various input power levels ranging from 50 to 600 watts. Of particular interest among the experimental results reproduced in Figure 3.1 are the constant temperature plateaus extending from the heated end of the pipe revealing the zones which were refluxing. The temperature drops occurring at the unheated end were attributed to stagnant hydrogen gas formed by the impure sodium at elevated temperatures. The measured temperature gradient in the refluxing region amounted to less than .05°K/cm. If the heat pipe were considered a solid rod, it would have an effective thermal conductivity in excess of 24,000 Btu/hr ft°F. It is not surprising that a device capable of such

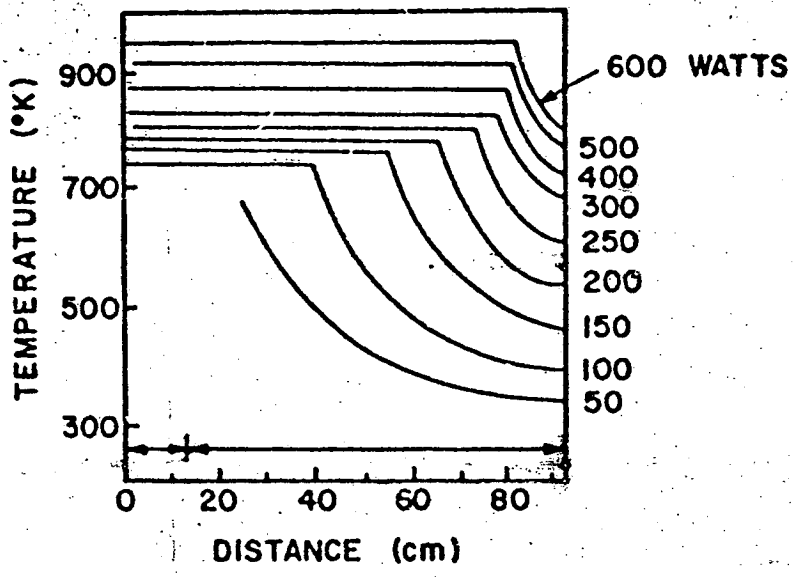

Figure 3.1 Temperature Profile Along Heat Pipe, Grover et al. [3]

performance stimulated considerable interest among large numbers of researchers. Subsequently, research and development programs were initiated simultaneously in many university and industrial laboratories leading to considerable duplication of the research efforts. Much of this effort was focussed on the determination of basic material properties, especially wicking properties. Because of the large number of papers published in a relatively short period of time, it is very difficult to present a chronological discussion of the references. Instead, the literature will be dealt with by subject in the following order: material properties, operating characteristics of heat pipes, heat pipe applications, heat pipe control and heat pipe theory. It should not be overlooked that several very useful review

articles [20, 21, 22] have appeared in the literature, and while they did not add new experimental or theoretical information, they probably encouraged further research and hence contributed to the growing field of heat pipe technology.

Material Tests

Working Fluids

The choice of a working fluid for a heat pipe application is dictated to a large degree by several physical properties of the fluid and by the chemical compatibility of the fluid with the container and the wick. Deverall and Kemme [23] were the first investigators to formulate the requirements for suitable heat pipe fluids: 1) high latent heat of vaporization, 2) high thermal conductivity, 3) low viscosity, 4) high surface tension, 5) high wetting ability, and 6) suitable boiling point. Parker and Hanson [24] have pointed out that the vapor pressure curve dictates the temperature range of applicability for a given fluid. In general, a fluid should be used in a steeply sloped region of its vapor pressure-temperature curve so that the temperature change associated with the given pressure drop is minimized. In addition, the vapor pressure should be reasonably high, since a low vapor pressure would result in low vapor densities and high pressure drops in the vapor flow.

as a function of temperature [8, 26, 27, 28, 29,30]. In addition, Frank et al. [30] have published extensive property group plots for water, sodium, and cesium while references [31, 32] yield values of liquid metals for possible heat pipe application. Langston and Kunz [13] have presented a table comparing the value of N for several low temperature fluids including the freons, alcohols, and glycols. Basiulis and Dixon [33] have assembled some property data on potential w rking fluids which are electrically insulating.

The choice of a particular fluid, of course, depends on the specific application; however, a few general conclusions can be drawn. For high temperature, high heat flux heat pipes, the liquid metals are definitely superior to non-metallic liquids due to their vapor pressure characteristics, high surface tension, and high latent heat. The outstanding fluid for low temperature work appears to be water due to primarily its high surface tension and latent heat. No valid statements can be made at this time regarding the suitability of cryogenic fluids for low temperature heat pipe applications.

Wicks

Prior to the recent interest in heat pipes, the majority of work on flow through porous materials came from such diversified fields as soil mechanics, petroleum engineering, water purification and ceramic engineering. The particular type of flow in porous bodies under study was usually either

a gravity induced flow or a forced or pressurized flow. Many publications in these fields as well as the fundamental theories on flow through porous media are presented and discussed in a book by Scheidegger [34]. Instead of gravity or mechanical work, the heat pipe on the other hand, utilizes capillary induced fluid flow for its operation. This particular feature, along with several other prerequisites to be discussed subsequently, has led to considerable research efforts aimed at developing or finding existing wick materials suitable for employment in heat pipes.

As mentioned earlier, the primary requisite for a heat pipe wick is that it acts as an effective capillary pump. That is, the surface tension forces developed between the fluid and the wick structure must be sufficient to overcome all viscous and other pressure drops in the pipe and still maintain the required fluid circulation. Because the heat pipe may often be required to operate in a gravity field with the evaporator located above the condenser, the wick should be capable of lifting the working fluid to heights equal to or greater than the maximum difference in elevation between the evaporator and condenser. The requirements are of opposing nature since on one hand large pore sizes are called for to minimize the viscous loss in the wick and on the other hand small pore sizes are needed to provide for sufficient capillary pumping and maximum lift height. As a result, some sort of pore size optimization procedure

appears warranted and in fact numerous authors have addressed themselves to this problem and their work will be treated later.

The property data on potential wicking materials, which have been accumulated to date, originate primarily from wicking height measurements and the measurement of the permeability, which is defined as a proportionality constant between the flow rate and the pressure drop in a porous body. The techniques used and the values obtained for these properties will be discussed later. In addition to the operating characteristics, several mechanical features must be considered when examining potential heat pipe wicks. Of special importance is the reproducibility of a wick structure so that future heat pipe investigators may rely on data generated during earlier investigations. The wick should be mechanically stable and should be rigid enough so that its flow properties do not change in response to wick sagging or stretching. The ease of wick fabrication and the cost are also important and it is conceivable that these considerations could someday be the major criteria for wick selection, if heat pipes are ever mass-produced.

A wide variety of wicks have been successfully employed in heat pipes. As mentioned earlier, the first wick, and also probably the most widely used to date, consists of several layers of fine mesh screen. Various methods have been used to guarantee mechanical contact between the screen

and the container. Neal [28] rolled the screen on a mandril and upon insertion into the pipe removed the mandril. The screen was held against the heat pipe wall by its own resilience, but Neal found that the resilience varied from screen to screen and hence the performance of the pipe was not reproducible. Deverall and Kemme [23] forced a steel ball through a heat pipe, after the screen layers had been inserted, and apparently achieved good contact between the wick and the wall. However, no attempt was made to check the reproducibility of the wick structures. Kemme [17] has constructed rigid screen wicks using the following procedure. Several layers of stainless steel screen were wrapped around a copper tube. The structure was placed into another copper tube and drawn through a die to compress the screen layers; the copper was removed chemically. The screen tube was then heated to 1000°C in a vacuum oven to bond the structure. Finally the baked, rigid screen tube was inserted into a heat pipe where the screen and the crescent annulus between screen and wall formed an effective wick structure with reproducible qualities. Numerous other techniques for screen wick preparation have either been used or suggested. McKinney [35] has employed a coiled spring to hold a screen wick firmly against the heat pipe wall. Katzoff [5] constructed wicks in which a single layer of screen is metallically bonded to the wall. One construction technique consisted of electroplating a thin coating of indium or tin

onto both the screen and the wall, pressing the two firmly together and baking them in an oven (200°C for indium and 275°C for tin). Excellent results were also obtained by diffusion bonding stainless steel screens to stainless steel plates. The bonding was effected by pressing the screen against the plate with a pressure of 15 psi while baking them at 1100°C for 2 hours in a vacuum oven.

In addition to using screens as wicks, several investigators have employed screens only as a retaining structure. Heat pipes constructed at North Carolina State University [36, 37, 38, 39, 40, 41] have utilized wicks consisting of various types of beads packed in an annulus between a retaining screen and the heat pipe wall. Wicks of this type have been successfully constructed using beads of monel, glass, and stainless steel of various diameters.

Several different textile fabrics have also been employed as wicks. Haskin [25] used a rayon cloth as wick for a nitrogen heat pipe. The cloth was held firmly against the heat pipe wall by sliding together two halves of a slotted, diagonally cut retaining tube. Shlosinger [42, 43] and Shlosinger, et al. [44] selected a quartz fiber cloth as a wick for their experiments with flexible heat pipes, in which the cloth was pressed against the wall with springs. Attempts to bond the cloth to the heat pipe wall met only with limited success. It was found that ordinary rubber cement produced acceptable bonds for operating

temperatures up to 50°C if the rubber was allowed to cure and become "tacky" before the wick was pressed against the wall. Experiments with higher temperature silicon rubber failed because low molecular weight silicon compounds were released in the curing process and effectively waterproofed the wick. Good bonding was achieved by applying heat sealable film materials, such as thermosetting and thermoplastic sheets of the polyester resin and polyethylene-type.

Other investigators experimented with commercially available porous metals as potential heat pipe wicks. Neal [28] constructed a heat pipe using a sintered copper fiber wick. Unfortunately the wick was not bonded to the heat pipe wall and poor results were obtained. Porous metal wicks are extremely difficult to machine and normal cutting techniques such as band-sawing, shearing and grinding tend to close the surface pores along the cut. The use of a filler material which could be removed after cutting is not generally recommended, since it is difficult to completely remove the filler, which changes the wetting characteristics of the porous material. Langston and Kunz [13] have microscopically examined porous metals, which were cut by electrodischarge machining (EDM) and electrochemical (ECM) machining techniques. They found that EDM tended to erode the surface whereas ECM cut the porous material very cleanly with a minimum of pore distruction. A technique to avoid the machining of porous metals completely was recently

developed [45]. The technique entails the application of a mixture of particular matter, binder, and solvent to a surface. As the solvent evaporates the surface tension of the fluid draws the particles together, compacting them, yet leaving open pores. Of special significance is the fact that with this technique wicking structures can be applied to geometrically complex surfaces. Wick structures have been successfully fabricated from powders of Al_2O_3, SiC, aluminum, copper and nickel.

With the exception of screen wicks, the wicking structures which have received the most attention are the so-called low resistance and composite wicks. Bohdansky et al. [46] first suggested the possibility of using channels, cut into the interior surface, running axially the length of the tube. Busse and his co-workers [47] constructed several heat pipes employing such an integrated type of wick and found that the structure was very stable and the pore size was easily controlled. Kemme [17] has advocated the use of "composite" wicks with a fine pore size at the liquid-vapor interface to provide good capillary pumping and a larger pore size underneath for the return flow of the liquid. He fabricated such a composite wick from several layers of screen of different mesh sizes with the finer screens installed on the inside to provide capillary pumping forces and the coarse screen located in the annulus between the fine screen and the wall to serve as flow passage. Another

type of composite wicks made of axially cut grooves or channels covered with a fine mesh screen has been successfully tested by Kemme [17] and Hampel and Koopman [32] . Katzoff [5] constructed a low resistance wick by forming a single cylindrical passage or artery out of the same sheet of screen material which covered the interior of the pipe. A variety of other schemes have been devised for the construction of low resistance wicks. Ranken and Kemme [48] have employed a slotted corrugated stainless steel sheet which was formed into a cylinder and inserted into a heat pipe. The triangular passages formed between successive corrugations served as low resistance fluid return paths. Calimbas and Hulett [49] modified the basic screen wick by placing nickel ribbon spacers between the layers of screen to create a series of concentric annuli. McSweeney [50] made a wick by using a series of 1/16" diameter rods wrapped with 10 mil wire to space them apart. The rods were held against the pipe wall by a coarse screen. Turner and Harbaugh [51] and Turner [52] attempted to construct a noncircular heat pipe such that the corners of the tube would supply the capillary pumping force. His "configuration pumped heat pipes" were not very successul due to structural deficiencies causing the pipes to bulge and distort under even minor pressure differences between the interior and the surroundings.

A wick property of major importance is the maximum height to which a wick lifts a given working fluid. Two

reasons must be cited to underline its importance for heat pipe operation. First, the maximum lift height places a constraint on the dimensions of a heat pipe if it is to be operated in a gravity field with the evaporator located above the condenser. Second, the measurement of the maximum lift height represents an efficient method for the evaluation of the capillary pumping capability of a potential wick. The capillary pumping pressure must be greater than the sum of all viscous pressure losses and gravity losses if the pipe is to function at all. Once the maximum lift height has been determined, the minimum effective radius of the capillary structure can be calculated with equation (3-2)

$$h_{max} = \frac{2\sigma \cos\theta}{\rho_\ell \, g \, r_{min}} \qquad (3\text{-}2)$$

Equation (3-2) is obtained from a simple static force balance performed on a meniscus located a distance, h, above a free surface in a cylindrical tube. After r_{min} has been determined, the capillary pumping pressure is obtained from equation (3-3)

$$\Delta P_c = 2\sigma / r_{min} \qquad (3\text{-}3)$$

which is derived from a simple force balance. The idea of designating a pore radius or diameter is of course an idealized approach because in general capillary pores consist of irregular non-circular channels. This irregularity in channel size has prompted investigators at North Carolina

State University [36, 37, 38, 39, 40, 41] to define both a "rising" and a "falling" capillary equilibrium height. In general the height to which a liquid will rise in a wick (rising height) is less than the height to which the liquid will fall in the same wick after it has first been completely soaked (falling height). Katzoff [5] has indicated that the difference between the two levels is typically of the order of 25 per cent and attributes this to wetting difficulties associated with the rising fluid.

Several investigators have experimentally measured capillary equilibrium levels in various wicks. Ferrell and his co-workers [40] measured the falling equilibrium height of water in packed beds consisting of stainless steel particles (40 to 100 mesh) and glass beads (80 to 100 mesh). Further work [41] indicated that the equilibrium height as a function of particle diameter could be closely predicted by assuming that the beads were arranged in a cubic array. Phillips and Hinderman [53] measured the maximum capillary pressure for a 200 mesh screen of stainless steel, bronze and nickel using water, methanol and benzene respectively. In addition, several metal "foams" and "felts" were tested with these fluids. (The porosities of the samples ranged from 89% to 96%.) Capillary pressures were determined by the standard technique of measuring the equilibrium height and the pressure necessary to force an air bubble through a saturated wick. Both methods gave comparable results and

the latter approach proved to be easier and less time consuming. For the screens, capillary pressures ranged from .12 psi to .36 psi and for the porous metals from .02 psi to .13 psi. Katzoff [5] measured the lift capability of six screens and found the values of the minimum effective meniscus radius ranging between .75 and .90 times the spacing of the wires in the screen. Ernst [54] studied Katzoff's data and concluded that the effective meniscus radius can be expressed by $(d + d_1)$, where d is the mesh opening half width and d_1 is the radius of the wire in the mesh. Langston and Kunz [13, 55] measured the equilibrium height of water and Freon 113 in 23 wick samples. The samples consisted of three classes of porous materials: sintered metal screens, sintered metal powders, and sintered metal fibers (the porosity of the samples varied from 47.7% to 91.8%). Equilibrium heights greater than 16" were found for several of the sintered nickel fiber samples with water as test fluid. In a study not directly concerned with heat pipes Ginwala et al. [56] examined 178 potential wicking materials which included cellular types, textile and synthetic fibers, filter papers, inorganic fibers, porous ceramic and refractory products, porous and fibrous metals, etc. Equilibrium heights were measured for the fifteen most promising materials. Maximum rise heights were obtained with the Silica Vitreous fibers and filter papers while acceptable heights were observed in Viscous Rayon.

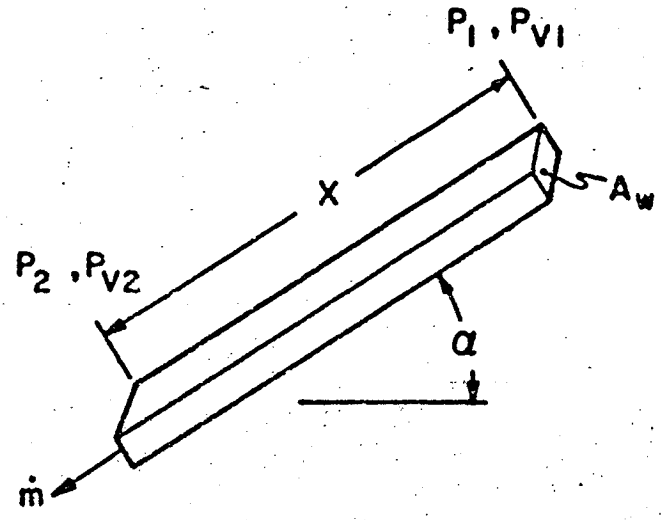

Figure 3.2 Measurement of Permeability

A property of great importance when selecting a wick is its permeability. Permeability (K) has the dimensions of length squared and is defined by Darcy's law given by the following relationship:

$$\dot{m}_\ell = \frac{KA_w\rho_\ell}{\mu_\ell x}\left[(P_1-P_2) - \rho_\ell g \; x \; \sin\alpha\right] \qquad (3\text{-}4)$$

The permeability is dependent upon the dimensions and the geometry of the passages in the wicking material and can be determined experimentally by passing a liquid through a wicking material and measuring the pressure drop in the direction of the flow (see Figure 3.2). The pressure drop and the measured liquid mass flow rate along with the area normal to the flow and the fluid properties are then used in equation (3-4) to evaluate the permeability. The flow through the porous body may be either forced or gravity

induced since static pressure variations due to gravity are accounted for in the second term in brackets. Unfortunately, no correlations between permeability and more easily measured wick properties have been found which apply to general wick configurations. Attempts to correlate permeability with porosity have been unsuccessful [34] since porosity in no way accounts for the coupling of one pore to another. For wick materials whose geometry is easily identified, as for example spheres in a cubic array, correlations can readily be found as shown by Carnesale, et al. [36] and Ferrell and Alleavitch [41] who measured the permeability of several beds of packed spheres of different diameter. For comparable packing the porosity of all beds was 40% and a correlation between permeability and particle diameter was obtained.

Numerous investigators have measured the permeability of more complex wicks for which no correlations exist. Ginwala, et al. [56] measured the flow rate of distilled water flowing through various types of felts, fibrous materials, and cellular materials for three different pressure heads. Their experiments indicated that the flow rate under constant pressure head decreased with increasing time for all wicking materials. This behavior was thought to be caused by an accumulation of gases and microscopic particles in the wick initially dissolved and suspended in the liquid. Langston and Kunz [13, 55] experimentally determined the permeabilities for a number of sintered metallic materials

fabricated from felted fibers, powders, and screens. Special care was taken to degas the fluids before their use. The permeability was found to be independent of the nature of the fluid, time, flow rate and fluid temperature. A special test in which water was intentionally aerated before being passed through the sample was performed to evaluate the effect of dissolved gases in the fluid. The results showed that, with a high degree of air saturation, the permeability of the wicks decreased by about 18% in about 50 hours of operation. Using both equilibrium height and permeability data, values for a capillary pumping parameter defined as the product of maximum lift height and permeability were then evaluated for all samples. The magnitude of this pumping parameter is a direct measure of the efficiency with which a material might function as a pipe wick. The data attested that sintered metallic fibers as a group make the best heat pipe wicks while sintered powders were the next best and screens were the worst. Phillips [29] and Phillips, et al. [53] measured the permeability of sintered metal screens, fibers, and foams using forced flow, gravity flow, and condenser flow in an operating heat pipe. For the force flow test the permeability was found to decrease for increasing flow rates. This is contrary to Langston and Kunz's results which demonstrate that permeability is independent of the fluid flow rate. The disparity may perhaps be explained by the fact that for comparable

samples Phillips et al. used a much wider range of flow rates than Langston and Kunz did (by a factor of almost four). Their data showed for a 96% porosity nickel foam wick a variation in permeability of approximately 23% over the entire range of flow rates. Gravity induced flows were used to measure the permeability of very thin wicks (such as one or two layers of screen or sintered metal samples less than .050 inches thick) as a function of meniscus radius and flow rate. The meniscus radius was maintained constant along a sample by adjusting the flow rate or angle of inclination in such a way that the viscous pressure drop was exactly countered by the increase in static head. This procedure assured pressure constancy throughout the liquid. The meniscus radius was varied by changing the gas pressure on the vapor side of the vapor-liquid interface. For thin wicks the data revealed the permeability as a strong function of meniscus radius and for some samples (especially single layers of screen) also as a strong function of the liquid flow rate. Permeability values measured by forced and gravity induced flow techniques were in general not in agreement. The gravity induced flow technique yielded permeability values up to 2 1/2 times those measured by the forced flow method. The disagreement was attributed to the manner in which the samples were mounted. For the forced flow tests, the wicks were completely enclosed and the measured permeability was based

on flow solely in the porous structure. In case of the gravity flow tests a fluid fillet formed along the edge of the wick which allowed some of the liquid to bypass the wick, leading to an erroneous and high value for the permeability. Several attempts were also made to measure permeability of a wick in an operating heat pipe. The pressure distribution in the wick was measured at five locations in the condenser and the fluid flow rate was determined from the product of the measured heat transfer rate and the known latent heat of vaporization of the liquid. Unfortunately the results were erratic and consequently their reproducibility for identical experiments was very poor.

Farran and Starner [57] measured the capillary pressure and the permeability of a compressible wick of braided SiO_2 fibers. They noticed that the capillary pressure (referring to Figure 3.2) is defined as,

$$\Delta P_c = P_{v_1} - P_1 \qquad (3\text{-}5)$$

could be evaluated from (P_1-P_2) if the lower end of the wick was submerged and the meniscus had an infinite radius of curvature thus equalizing the pressure in both phases, $P_2 = P_{v_2}$ (it is assumed that $P_{v_1} = P_{v_2}$). Equation (3-4) transforms to

$$\dot{m} = \frac{\Delta P_c \rho_\ell A_w K}{\mu_\ell}\left[\frac{1}{x}\right] - \frac{\rho_\ell^2 g A_w K \sin\alpha}{\mu_\ell} \qquad (3\text{-}6)$$

or inserting the relation for the mass flow rate in terms of the fluid velocity leads to

$$\frac{dx}{dt} = \frac{K\Delta P_c}{\mu_\ell} \cdot \frac{1}{x} - \frac{\rho_\ell g K \sin\alpha}{\mu_\ell} \qquad (3\text{-}7)$$

Two techniques were selected to evaluate the pressure difference, ΔP_c, and the permeability. The first technique (displayed schematically in Figure 3.3-A) consisted of the measurement of the steady state mass flow in the wick. The fluid was removed from the top of the wick by evaporation. The second technique involved the measurement of the transient rise of a liquid in a previously unsaturated wick (displayed schematically in Figure 3.3-B). Inspection of equations (3-6) and (3-7) then reveals that if $\dot{m}$ (or dx/dt) were plotted as a function of 1/x, the resulting plot (Figure 3.3-C) should be a straight line and the permeability and the capillary pressure could be found from the intercept and the slope, respectively. Data obtained by both methods failed to yield the expected linear relationship. For near horizontal wicks ($\sin\alpha \approx 0$) the capillary pumping pressure and the permeability turned out to be constant and the two methods yielded values which differed by about 10%. For $\sin\alpha \neq 0$ both methods indicated that ΔP_c was proportional to $(x \sin\alpha)$ and the reciprocal of the permeability was approximately proportional to $(x \sin\alpha)^2$. This behavior is perhaps best explained in terms of the existence of an optimum capillary radius corresponding to an optimum capillary flow area through which a maximum mass flow rate is

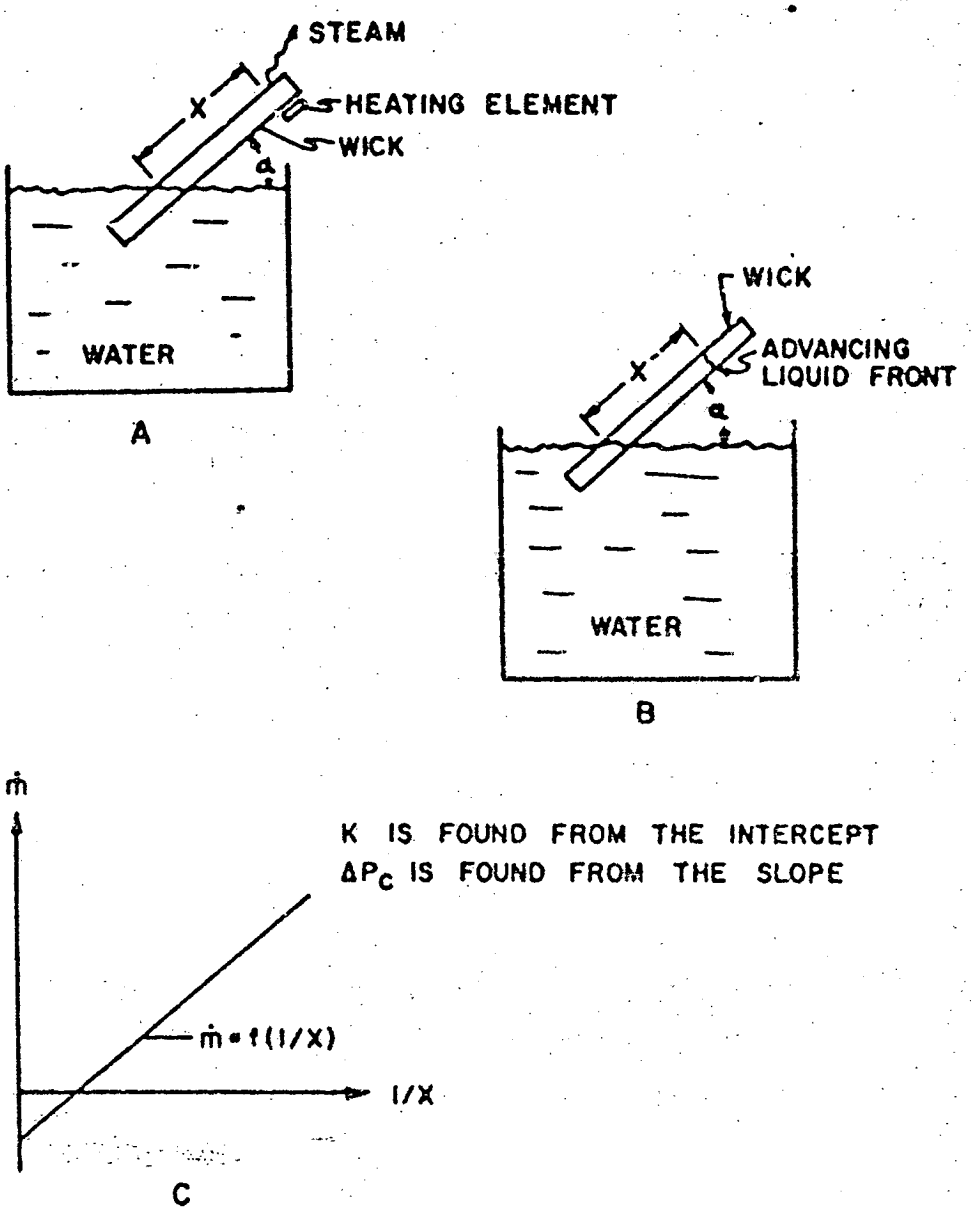

Figure 3.3 Determination of the Capillary Pumping Pressure and Permeability, Farran and Starner [57]

pumped by capillary action. Farran and Starner showed an inverse variation of this radius with x sinα; and furthermore, they observed that if the optimum radius exists along the entire wick, ΔP_c should be proportional to (x sinα) and 1/K to $(x \sin\alpha)^2$. They hypothesized that if the pore size distribution is large enough at any particular position, x, enough optimum sized pores would be available to dominate the flow. However, a determination of the pore size distribution was not made for the test samples thus leaving the hypothesis unchecked. Finally it is quite noteworthy that Feldman [8] has collected and presented a table summarizing permeability values for a variety of wicks including the sintered metals and some compressible materials.

Compatibility of Components and Life Tests

The choice of suitable materials for heat pipe construction is dictated by a compatability criterion of the different materials. Many of the problems associated with long term heat pipe operation are a direct consequence of material incompatibility which usually manifests itself in chemical reactions. In general, improper selection of components results in a gradual appearance of noncondensable gases. For high temperature liquid metal heat pipes, improper material selection furthermore accelerates corrosion and dissolution of the wick structure. Grover and his associates [3] were the first to encounter and describe the generation of noncondensable gases. In their experiment, which is described

earlier, the temperature profile along the heat pipe dropped suddenly at the condenser (see Figure 3.1). This was attributed to a pocket of hydrogen gas produced from impure sodium in the reaction, $NaH \rightarrow Na + \frac{1}{2}H_2$. Andeen, et al. [16] tested a water-brass heat pipe and experienced severe problems with noncondensable gas. No attempt however, was made to determine the source of the gas. Schwartz [58] noticed the occurrence of a noncondensable gas in several water-stainless heat pipes. Samples of the gas were withdrawn from one of the pipes and their composition analyzed with a mass spectrometer. The results of the chemical analysis indicated that the noncondensable gas was composed of over 97% hydrogen. Schwartz hypothesized that the hydrogen was formed as a result of a chemical reaction between the iron in the stainless steel and water. He suggested that the problem of noncondensable gas generation could be avoided, either by choosing a heat pipe whose metal components range below hydrogen in the electromotive series or if the metals have an electrochemical potential above hydrogen, by using a nonreacting working fluid other than water. To test this concept, an ammonia-stainless steel heat pipe was built and operated continuously for 3 months with no measurable sign of noncondensable gas formation. Conway and Kelley [7] were also troubled by noncondensable gases in a water-stainless steel heat pipe. Although no tests were made to determine the origin of the gas, it was certainly most likely

that hydrogen was produced in the same chemical reaction which plagued Schwartz. Grover [59] has suggested a possible solution to the problems caused by hydrogen formation in low and moderate temperature heat pipes. He recommended to fabricate the condenser end cap out of palladium allowing hydrogen to diffuse to the outside while retaining the working fluids. The prohibitive cost of palladium, however, limits its use to only the most amply funded experimental programs and as yet, the concept has not been tested. Deverall and Kemme [60] have reported the successful operation of a water-stainless steel heat pipe for over 3000 hours without accumulation of noncondensable gas. The stainless steel tube and screen were first degreased in acetone and then bright-dipped to guarantee clean surfaces which were subsequently degassed at 6000°C in a high vacuum oven. Since the other investigators who encountered hydrogen formation in water-stainless steel heat pipes reported no extensive cleaning procedures, it may be speculated that for the particular case of water-stainless steel, hydrogen formation is more a function of the techniques used in processing the materials than of the materials themselves. Jeffries and Zerkle [27] have commented on work done by Lyons who tested several fluids in capsules of aluminum alloy 6061 at temperatures from 155°F to 322°F for durations in excess of 500 hours. Strong evidence of corrosion was found with methanol and ethanol; n-Butane (155°F) and

Monsanto Cp-34 (321°F) showed moderate corrosion; whereas no corrosion was evident with n-Pentane (310°F), Benzene (310°F), Heptane (320°F), Toluene (322°F), Ammonia (159°F), Freon-11 (156°F), and Freon-113 (155°F). In addition, a capsule of 321 stainless steel was tested with water at 320°F. Definite signs of gas evolution were evident during the test, which proved in a qualitative mass spectrometric analysis to be hydrogen.

The most severe compatibility problems are encountered when heat pipes are operated at elevated temperatures. A considerable effort was expended by workers at Los Alamos [15, 23, 48, 59, 61] to study this problem. A heat pipe was constructed selecting tantalum as container and wick material, and silver as the working fluid. The pipe was operated at 1900°C for 100 hours. Examination of the sectioned pipe revealed that the wick in the condenser had almost disappeared while the wick in the evaporator was clogged with tantalum. This behavior was attributed to the dissolution of the wick in the working fluid. In this case, small amounts of structural material were dissolved by the working fluid in the condenser section, transported to the evaporator section and deposited there as the working fluid evaporated. The amount of tantalum deposited indicated a solubility of tantalum in silver of approximately 10 ppm. Dissolution and transport of the wick material also occurred in an indium-tungsten heat pipe which was operated at 1900°C

for 75 hours. Recent tests have attested to the potential of a silver-tungsten heat pipe for high temperature operation. Such a pipe has been operated for 1000 hours with no noticeable deterioration in performance. Burse and his co-workers [47, 62, 63] have conducted an extensive experimental program to determine material compatibility at the temperatures employed in thermionic converters, i.e., 1000°C for the collector and 1600°C - 1800°C for the emitter. Special care was taken to select materials for which no known intermetallic compounds exist. For many material combinations, they found that the dissolution of the container or wick led to eventual heat pipe failure due to clogging of the wick in the evaporator. Other material combinations produced ultimate heat pipe failure due to a weakening of the wall caused by intergranular corrosion and wall penetration. It was also noticed for a particular thermionic converter-heat pipe system that the lithium working fluid diffused through the wall at rates sufficient to significantly lower the power output of the converter. Three systems, however, proved to be promising for operations longer than 1000 hours at 1600°C: W/Li, W/Pb, and SGS-Ta/Tl. In the 1000°C temperature range, Na and Cs have operated for 1000 hours in a Nb-1Zr container with no significant corrosion. Workers at RCA [10, 64, 65, 66, 67, 68] have also investigated material compatibility at thermionic temperatures. Examination of a lithium - TZM alloy heat pipe

employing a molybdenum wire wick revealed about 10 ppm of the alloy in the lithium working fluid after 600 hours of continuous undegraded operation. Another Li-TZM heat pipe has been operated successfully for 1,400 hours while a K-Ni heat pipe has supposedly been working continuously for 26,000 hours. At lower temperatures, a water-copper heat pipe has accumulated 8500 hours of operating time with no degradation in performance. Ernst et al. [69, 70, 71] have reported the successful operation of a Li-TZM heat pipe for up to 5000 hours. Some deposits were noted in the evaporator and it was speculated that it was probably titanium oxide; however, no attempt was made to determine the composition of the substance. Johnson [72] investigated the compatibility at thermionic temperatures of the working fluids Ag, Ba, Ca, In, Li, Pb, and Tl with containers made of Cb-1Zr, Ta-10W, and TZM. The fluids (metals) were placed into reflux capsules which were heated for times up to 1000 hours. The capsules were then sectioned and examined by x-ray diffraction analysis. Results indicated that indium is not suitable for long term heat pipe operation. Only minor intergranular attack was observed when calcium was used as working fluid, while other material combinations showed varying degrees of attack and corrosion.

In summary, for low temperature heat pipes, care must be taken when selecting components to avoid any combination for which a possible chemical reaction exists which could

lead to the formation of noncondensable gases. Cleanliness and material treatment techniques also seem to govern to a large extent the ultimate compatibility of heat pipe materials. For high temperature heat pipes, due consideration must be given to the formation of possible intermetallic compounds, solubility of one metal in another, and diffusion effects. Obviously a great deal of systematic research is called for in high temperature applications since very little is known about the crucial properties of metals at these temperatures.

Operating Characteristics of Heat Pipes

General

In addition to the experiments concerned with basic investigations of potential heat pipe materials, many investigators performed experiments to determine the operating characteristics of heat pipes. In early investigations often little more than the successful operation of a heat pipe was reported. Shortly after the work performed at Los Alamos had been published, Bainton [73] reported the successful operation of two sodium-stainless steel heat pipes. Temperature uniformity over most of the length of the pipe was verified by infra-red photography. Workers at RCA [66] related the successful operation of a lithium heat pipe for over 9000 hours claiming that, as a thermal energy transfer device, this heat pipe operated 1000 to 10,000 times more

efficiently than the thermal conduction process in an equivalent rod of metals such as copper or silver. Hall [74] tested a lithium-TZM heat pipe and verified that fluxes sufficient in magnitude to operate a thermionic converter could be obtained. Fluxes on the order of 40 watts per square centimeter were achieved for both a lithium and a sodium heat pipe. Bowman and Crain [75] operated a water-copper heat pipe at near ambient temperatures. The temperature profile along the axis of the pipe was measured to confirm heat pipe operation. An electrically insulating fluid was employed by Basiulis and Dixon [11] in a radial heat pipe which could successfully dissipate 900 watts regardless of its orientation with respect to gravity. Although no mention was made concerning the uniformity of the flux across the condenser surface (see Figure 2.4), it is most probable that the flux around the circumference of the condenser was a function of its orientation in regard to gravity.

Investigations of Heat Transfer Limits

Several investigators have experimentally determined the wicking limit of heat pipes as a function of vapor temperature and/or geometric parameters. Bohdansky et al. [76] measured the maximum possible heat flow in a sodium-niobium heat pipe in the temperature interval from 500°C to 800°C. The pipe was 50 cm long and had a 2 cm inner diameter. The capillary system consisted of 85 grooves of rectangular cross section with a width of .4 mm and a depth

of .46 mm. The pipe was heated with an RF coil and cooled through a variable resistance helium thermal bridge with cooling water on the other end. In subsequent experiments the inclination of the pipe was varied in order to change the lift height, h, between evaporator and condenser. Upon each variation in orientation the power input was increased until a hot spot appeared at the far end of the evaporator indicating that the wick was no longer capable of supplying sufficient fluid to this part of the evaporator. The temperature variation was measured with thermocouples which were mounted at the outside wall of the pipe. Bohdansky et al. [76] plotted the heat flow rate versus operating temperature shown in Figure 3.4, where the detrimental effect of lift height on the maximum heat transfer can be recognized. Occurrence of maximum heat flows for each experiment performed at a constant lift height is attributed by Bohdansky et al. to the decrease of the surface tension with increasing temperature. They even further illustrated the effect caused by elevation (lift) by replotting the maximum heat transfer values as a function of height as shown in Figure 3.5. Neal [28] in a qualitatively similar representation for a water-stainless steel heat pipe fitted with four layers of 105 mesh screen as a wick structure confirmed the results of Bohdansky et al. It should be noticed that the shape of the curves in Figure 3.4 corresponds to the form of the qualitative wicking limit curve

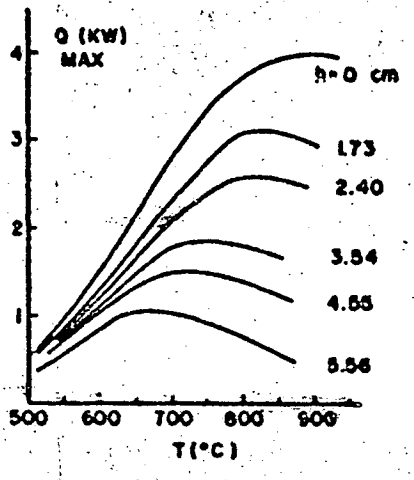

Figure 3.4 Heat Flow in a Na-Nb Heat Pipe as a Function of Temperature and Elevation, Bohdansky et al. [76]

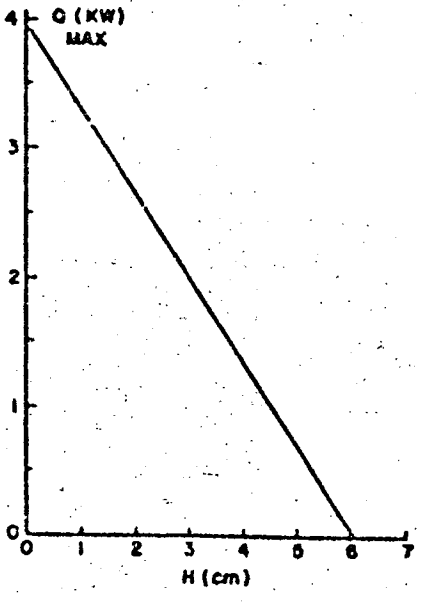

Figure 3.5 Maximum Heat Flow at 850°C as a Function of Elevation, Bohdansky et al. [76]

displayed in Figure 2.7. The curves can be compared qualitatively because the wall temperature and vapor temperature are closely related for heat pipes operating under steady state conditions.

Cosgrove et al. [37] investigated two water-brass heat pipes in which the wick structures consisted of packed monel beads which were held in an annulus between a retaining screen and the wall. For a particular wick structure and pipe orientation, the maximum heat transfer was considered reached when a hot spot began to form in the evaporator which was concurrently detected with thermocouples installed in the packed beads. The vapor temperature remained relatively constant in all experiments in which the primary variables were the pipe orientation and the diameter of the monel beads. Figure 3.6 illustrates the effect of particle diameter, and consequently pore size, on the maximum heat transfer as a function of inclination. For a given particle diameter, the maximum heat transfer decreases with increasing elevation once more reaffirming the results of Bohdansky and co-workers depicted in Figure 3.5. Notice, that for a selected pipe inclination the maximum heat transfer increases with decreasing particle diameter. This effect is caused by the increased capillary pressure resulting from the smaller pore sizes. Cosgrove could not explain why the curve with the smallest particle diameter intersected with the other curves. If the pore sizes were decreased indefinitely

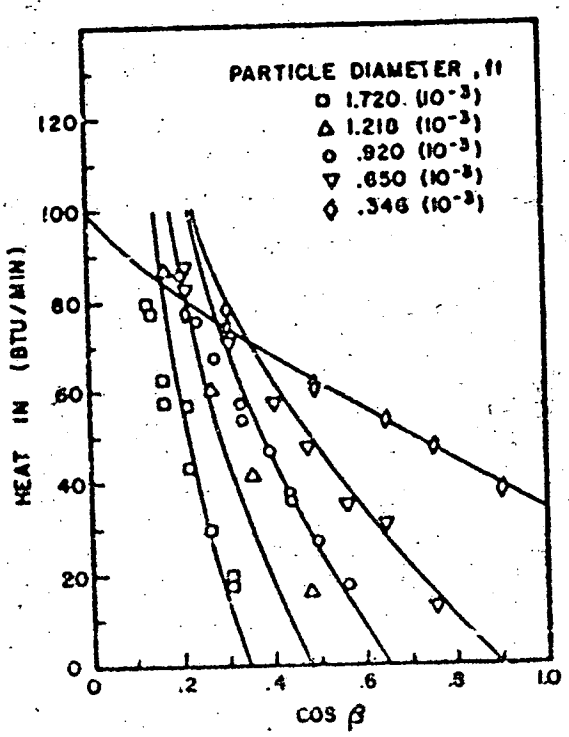

Figure 3.6 Maximum Heat Flow as a Function of Inclination and Particle Diameter, Cosgrove, et al. [37]

however, eventually an optimum pore size would be obtained at which the viscous drag in the capillaries would become dominant and the maximum heat flow should decrease again.

The results obtained by Bohdansky and Cosgrove and their co-workers suggest that the capillary limiting curve depicted in Figure 2.7 is in reality a family of curves, each depending on the pipe orientation in the gravitational field. Moreover, the entire family of curves depends on the geometry of the heat pipe, and in particular on the characteristics of the wick structure.

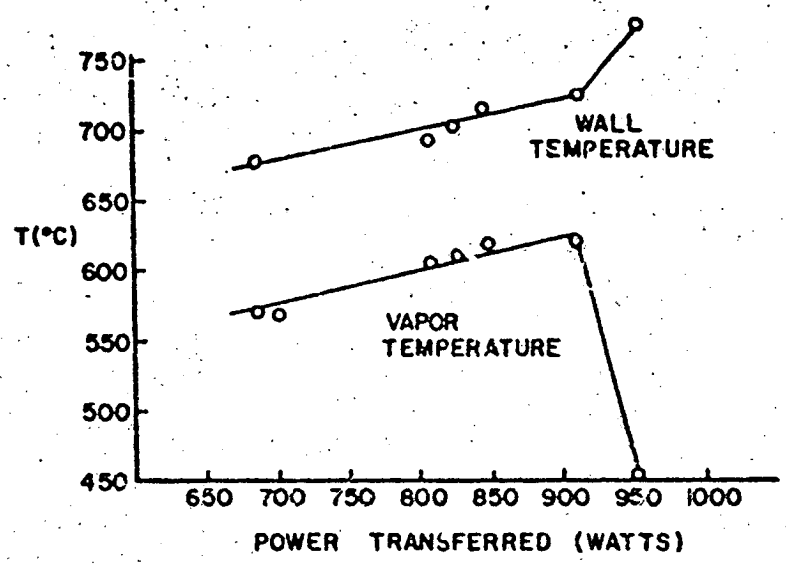

Figure 3.7 Heat Pipe Dryout, McSweeney [50]

While Bohdansky et al. and Cosgrove et al. installed thermocouples in the wall and wick to signal the formation of a hot spot, McSweeney [50] has found that the vapor temperature is a much more sensitive indicator of wick dryout. He experimented with a Na-Stainless Steel heat pipe and monitored both the vapor and the wall temperature as a function of increased power input. From his data shown in Figure 3.7 it is evident that the vapor temperature at dryout changes more rapidly in response to power increase than the wall temperature. The vapor temperature decrease under dryout condition is somewhat puzzling to say the least. Unfortunately the location of the thermocouple probe in the vapor space was not mentioned. However, it appears most probable that the probe was located in the proximity of the condenser. Possibly the termination of the heat flow

caused by the dryout of the wick resulted in considerable temperature variations within the now stagnant vapor core with rising temperatures in the evaporator and decreasing temperatures in the condenser which was still cooled. It is entirely possible that this type of behavior occurs only in heat pipes with a fixed temperature boundary condition imposed on the condenser. If a floating temperature sink were employed the entire vapor temperature would most likely increase once the dryout condition is reached.

In related studies, Shlosinger [43] found that for compressible wicks specifically, the manner in which the wick is retained against the heat pipe wall may significantly affect its wicking characteristics. For instance, if a helical spring is used to retain the wick, the fluid may have to travel by capillary action over a much longer spiral path from the condenser to the evaporator than otherwise would be necessary with a different type of retaining structure. This effect, of course, would not be present for more rigid wicking materials or for the commonly used axial slots. For instance, Busse et al. [63] found that heat pipes with axial grooves serving as a wick often formed a hot spot on the top side of the evaporator when the pipe was operated in the horizontal position. They attributed this behavior to the missing interconnections between the parallel grooves, thus preventing any cross flow between grooves in the evaporator. In the condenser, however, the excess liquid

tended to reside at the lower side of the pipe thus making the lower grooves the preferred paths for liquid transport. Their explanation was verified experimentally by shielding the lower side of the condenser of a W/Pb heat pipe. The shield forced the vapor to condense on the upper side of the pipe and subsequently no hot spot was formed. In a heat pipe in which the grooves are interconnected by circumferential grooves for instance, local overheating should not occur in the horizontal mode of operation. A few investigators have studied the problem of heat transfer and boiling in wicks. In a research project not directly related to heat pipes, Allingham and McEntire [77] measured boiling film heat transfer coefficients on a horizontal copper tube which was surrounded by a ceramic wick and immersed in a pool of water. For lower heat fluxes they measured values for the boiling film heat transfer coefficient in excess of those established under similar conditions in conventional pool boiling. The higher values were attributed to an increase in effective heat transfer surface area and also to an increase in active nucleation sites.

At higher heat fluxes, however, the trend reversed itself and the values of boiling film heat transfer coefficients decreased for wick boiling below the corresponding values of normal pool boiling. The reason for the decrease appears to be two-fold. First the very presence of the wick prevents agitation of the liquid otherwise so common

in pool boiling. Second the vapor escaping through the pores impedes the liquid counterflow directed towards the heating surface. The data were reduced and an implicit function of the boiling heat transfer coefficient as a function of the radial Reynolds number, based on four times the hydraulic radius of the capillary pores is plotted in Figure 3.8.

Likewise, Anand [78] and Anand et al. [79] tested a water-stainless steel heat pipe which had a 100-mesh stainless steel screen wick. The wall and vapor temperatures were recorded for different axial heat flows and the wick boiling heat transfer coefficient, h_f, was calculated. Anand claims that the data can be correlated by

$$St = .0051\ Pr^{-.6}\ Np^{-.2}\ Re^{-1.43} \qquad (3\text{-}8)$$

However, the data were plotted using

$$St = .00051\ Pr^{-.6}\ Np^{-.2}\ Re^{-1.43} \qquad (3\text{-}9)$$

Moreover, the ordinate on their graph was in error by a factor of ten. Allingham and McEntire corrected Anand's graph and presented it in Figure 3.9 along with their own correlation. Both correlations show the same trend and are in relatively good agreement considering that one represents wick boiling on the outside of a tube, and the other one wick boiling in the interior of a heat pipe. The validity of Anand's results, however, may be somewhat questionable in view of the mistake made in their graphical presentation.

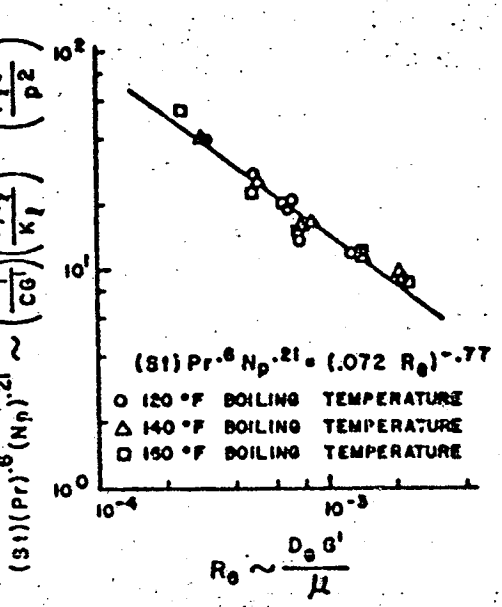

Figure 3.8 Wick Boiling Heat Transfer Correlation, Allingham and McEntire [77]

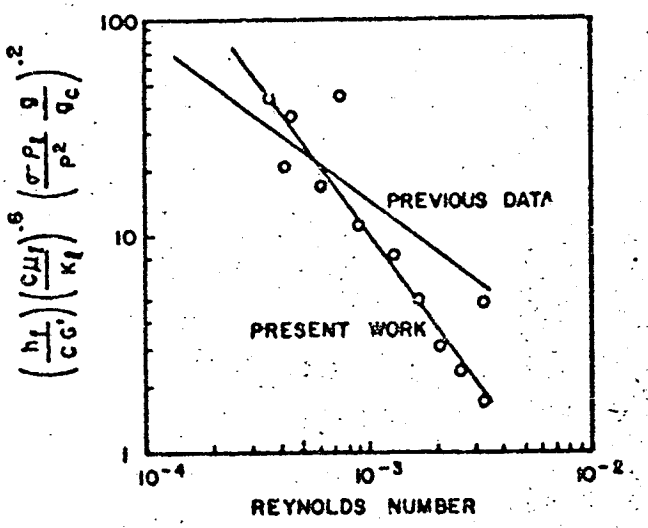

Figure 3.9 Wick Boiling Heat Transfer Correlation, Anand [78] and Anand, et al. [79]

Marto and Hosteller [80] studied the problem of wick boiling using a so-called everted heat pipe. A sectional view of their heat pipe is given in Figure 3.10. The unique feature of this pipe is a vapor space enclosed in an annulus between an interior tube and a confining envelope. The wick consisted of four layers of 100 mesh stainless steel screen attached to the outside of the inner pipe. Heat addition and removal were accomplished using a resistance heater and a tap water cooling system both installed within the inner tube. The outer envelope was made of glass to facilitate visual observation of wick boiling. The results obtained with water as working fluid are demonstrated in Figure 3.11, from which it becomes apparent that lower superheats were required under boiling conditions in a wick than in conventional pool boiling. As the radial heat flux was increased, dryout of the wick occurred at the same flux value whether or not boiling was observed. The authors concluded that wick boiling could exist in a heat pipe with no detrimental effect on its operation. The system pressure was also varied for both water and ethyl alcohol and it was found that for a given heat flux, the superheat decreased as the absolute pressure increased. In addition, for a given superheat the heat flux in the case of water was almost one order of magnitude larger than that obtained with ethyl alcohol. This disparity in heat fluxes is expected in view of the higher surface tension and latent heat of water

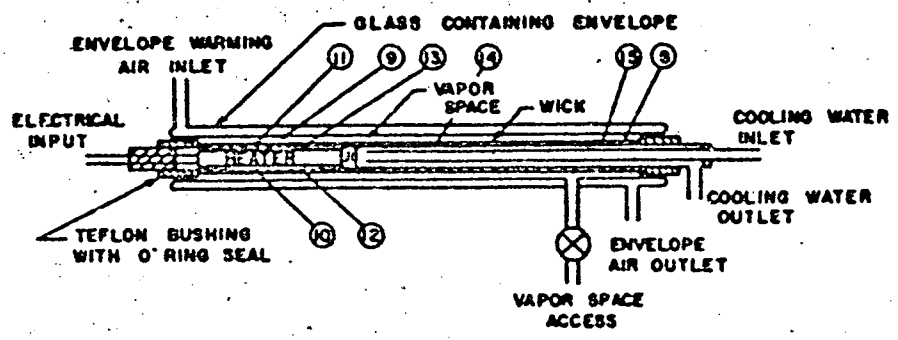

Figure 3.10 Sectional View of Everted Heat Pipe, Marto and Mosteller [80]

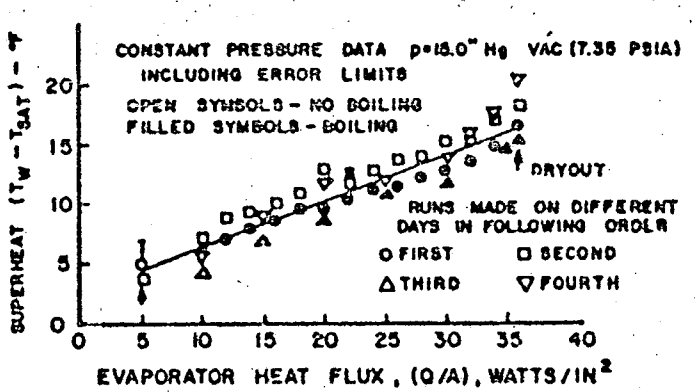

Figure 3.11 Observed Superheat vs. Radial Heat Flux, Marto and Mosteller [80]

compared to the same properties of the alcohols. In a study involving much larger superheats, Langston and Kunz [13] measured the heat flux through several wick samples as a function of the superheat. They found that for superheats of the order of 15°F and larger the flux through the sample wicks became much smaller than for boiling on a flat plate, thus confirming the results reported by Allingham and McEntire. The samples used by Langston and Kunz included sintered nickel powders and sintered nickel screens.

In another series of experiments on boiling in heat pipes, Moss and Kelley[51] employed a neutron radiographic technique to measure the liquid content (i.e., liquid thickness) in the wick of the evaporator in a co-planar heat pipe. The wick was made of sintered stainless steel screen (1/4" thick) and the working fluid was water. Measurements proved that only under conditions of zero heat transfer did the wick in the evaporator remain completely saturated. As soon as heat was supplied to the evaporator the liquid interface receded into the wick reducing the extent of saturation in the wick. In addition, the data demonstrated that under normal operating conditions the degree of saturation of the wick in the evaporator was inversely proportional to the heat flux. The authors concluded that a vapor blanket formed at the base of the wick and that the existence of this blanket manifested itself in the reduced saturation of the wick. Two analytical models were formulated in an

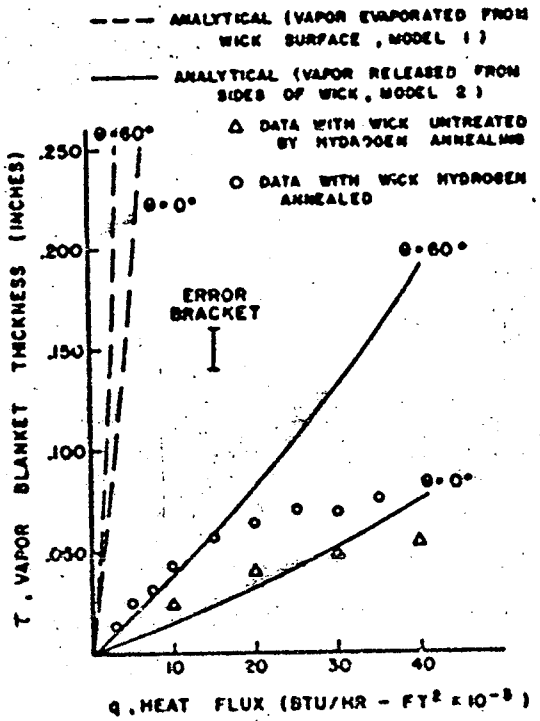

Figure 3.12 Vapor Blanket Thickness vs. Heat Transfer Rate, Moss and Kelley [81]

attempt to describe the heat transfer characteristics of the partially saturated wick. In a conventional model it was assumed that vaporization takes place at the liquid vapor interface. In the other model, however, the formation of a vapor blanket thickness as a function of the heat transfer rate and contact angle is shown in Figure 3.12. For heat fluxes smaller than 15,000 Btu/hr ft^2 the second model more closely predicts the measured values than the more conventional first model. The results led to some allegations that the study did not pertain to heat pipe operation since

it is generally believed that vaporization should take place at the liquid vapor interface during successful heat pipe operation. The authors countered these allegations by insisting that their measurements indicated beyond any doubt that the previously accepted idea of heat transfer through wicks is in error. At the present time, however, there are more data available supporting the model of conduction through the wick, with vaporization taking place at the liquid vapor interface, than results sustaining the observations made by Moss and Kelly. For example, Ferrell and Alleavitch [41] measured the heat flux through packed beads saturated with water. Their data for 30-40 mesh monel beads are displayed in Figure 3.13. It is seen that the data fall very close to the line predicted by assuming pure conduction through the saturated bed. The curve obtained from the conduction model was calculated under the assumption that heat flows by conduction through a thin liquid-bead layer in contact with the heating surface. The thickness of the liquid layer was determined by the location of the minimum pore diameter in the bead configuration. It is somewhat surprising that such good agreement was found between their theory and experiments since in the experiments the bed of beads was completely flooded to a level well above the upper surface of the bed; hence, no such thin liquid-bead layer existed in actuality. Recent work by the same authors has included heat transfer measurements in a similar apparatus, except

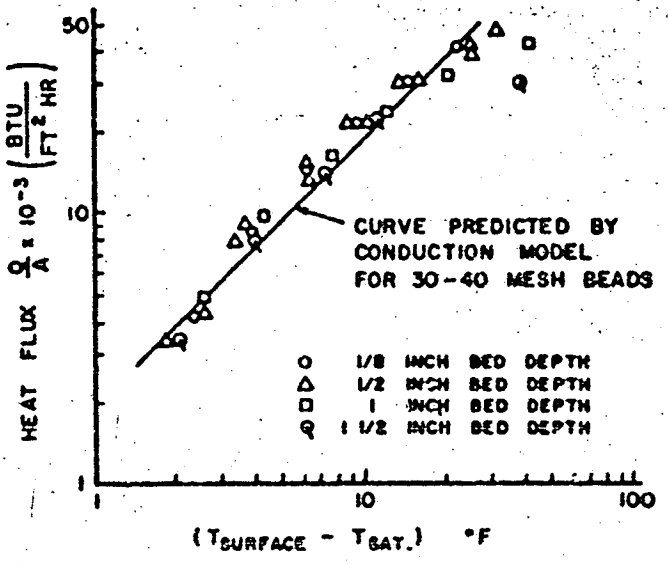

Figure 3.13 Experimental Results for Surface Covered with 30-40 Mesh Monel Beads, Ferrell and Alleavitch [41]

that now the bed was not flooded and the liquid was drawn to the evaporator section by capillary action identical in manner to an operating heat pipe. The more recent data showed excellent agreement with the conduction mechanism discussed above.

Similarly, Phillips [29] and Phillips and Hindermann [53] measured the heat flux through a composite wick of nickel foam and stainless steel screen using water as a working fluid. The fluid was supplied through an artery and moved by capillary forces. A typical sample of their data is illustrated in Figure 3.14. It is again obvious that conduction was the mode of heat transfer for low values of ΔT. The wick exhibited a hysteresis effect after

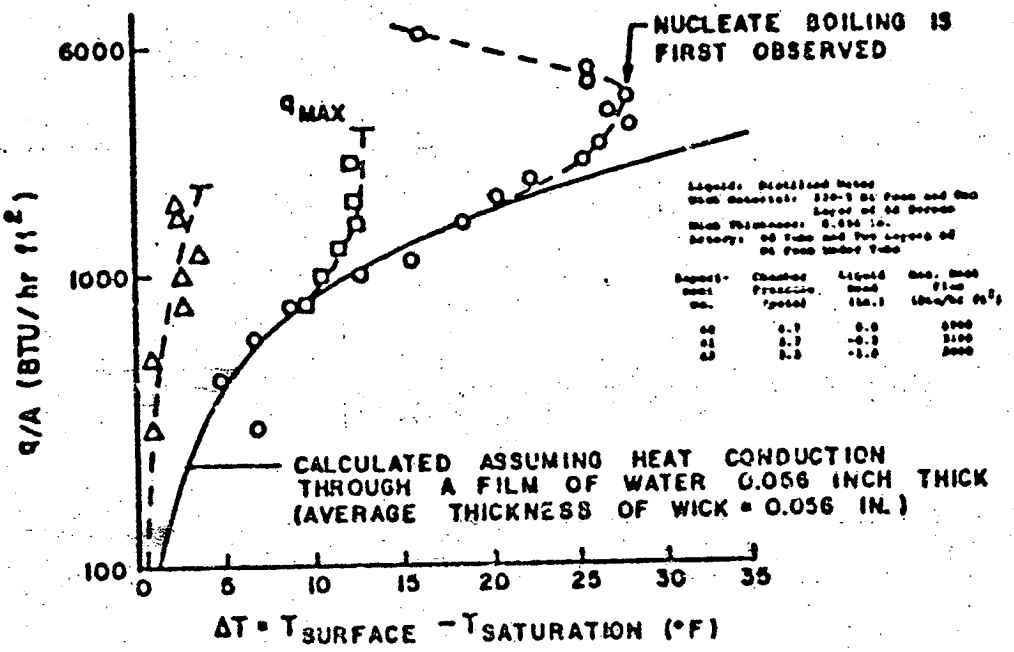

Figure 3.14 Experimental Results for Distilled Water and Nickel Foam, Phillips [29] and Phillips and Hindermann [53]

nucleate boiling was first observed. In addition, the maximum heat flux decreased with decreasing chamber pressure. The reduction was attributed to the significantly increased size of the vapor bubbles formed during nucleate boiling at decreased pressure; hence causing a premature burnout due to vapor blockage in the wick. The blockage occurred because the vapor was forced to vent through the top of the wick by purposely sealing its sides. The same effect was observed in experiments performed by Costello and Redeker [52]. They concluded that proper venting of the vapor was necessary if the full capabilities of the capillary supply

system were to be utilized. It is interesting to note that at the present time, no consideration is given to proper vapor venting of the wick in heat pipe design.

In addition to the capillary and boiling limits which restrict the heat transfer capability of all heat pipes, those transporting heat of the order of kilowatts instead of watts, are often limited by the sonic and/or entrainment limits. These limits are often encountered during startup procedures from near ambient conditions where the initial vapor pressure is very low and the resulting velocities in the vapor core are consequently very high. Kemme [17] investigated the sonic limit using several different liquid metals as working fluids. The heat pipes were heated by an induction coil and cooled through a gas gap with a water calorimeter. The use of different mixtures of argon and helium in the gap allowed heat pipe temperature variations at a constant heat input, or heat input variations at a constant heat pipe temperature. Figure 3.15 illustrates data obtained during the startup of a sodium heat pipe. The dashed line indicates the sonic limiting curve based on the vapor temperature existing in the evaporator exit. The heat flow was increased in discrete steps and the pipe was allowed to reach steady state before the heat flow and wall temperature measurements were made. The evaporator exit temperature followed the sonic curve until it reached 560°C. For temperatures lower than 560°C, the flow in the condenser section

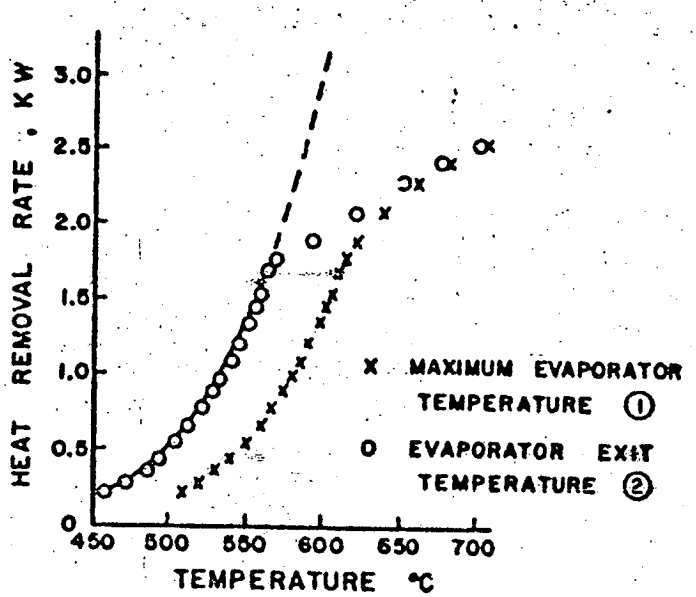

Figure 3.15 Startup Behavior for Sodium Heat Pipe, Kemme [17]

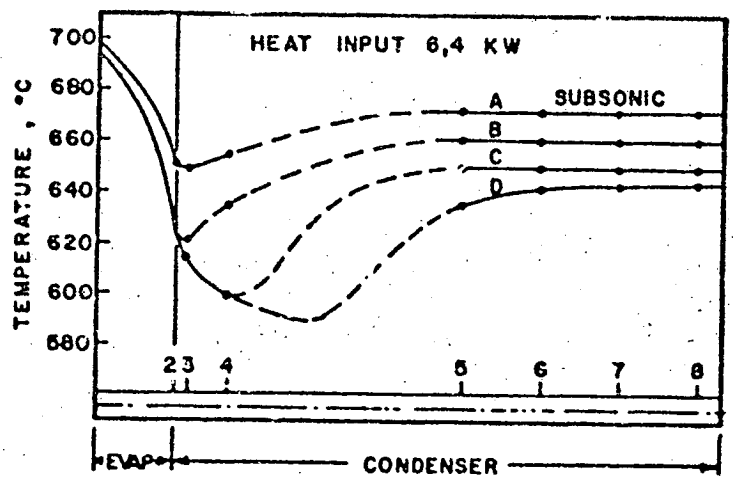

Figure 3.16 Transonic Conditions in Sodium Heat Pipe, Kemme [17]

consisted of continuum flow at the entrance and free molecule flow at the far end of the condenser. Hence, only that part of the condenser in which continuum flow existed contributed significantly to the heat removal from the pipe. As the heat flux increased, eventually the entire condenser region was in the continuum flow regime and once this occurred, the heat removal area of the system remained fixed, so that a further increase in heat input now resulted in a larger temperature rise at the evaporator exit than was previously possible. The subsequent vapor density increase allowed the velocity at the evaporator exit to become subsonic. Further experiments indicated the occurrence of supersonic velocities at the condenser entrance. Figure 3.16 shows results obtained from steady state measurements at a constant heat input of 6.5 kw. The condenser temperature was adjusted by varying the concentration of the gas mixture confined in the gap described earlier. Curve A describes a condition in which the vapor velocity remained subsonic throughout the heat pipe. As the pressure in the condenser was decreased, the velocity became sonic at the evaporator exit (curve B). The existence of subsonic flow between curves A and B is evidenced by the changes in the condenser temperature and pressure which were transmitted to the evaporator where corresponding changes occurred. When the pressure in the condenser was further decreased, as shown by curves C and D, the evaporator pressure conditions

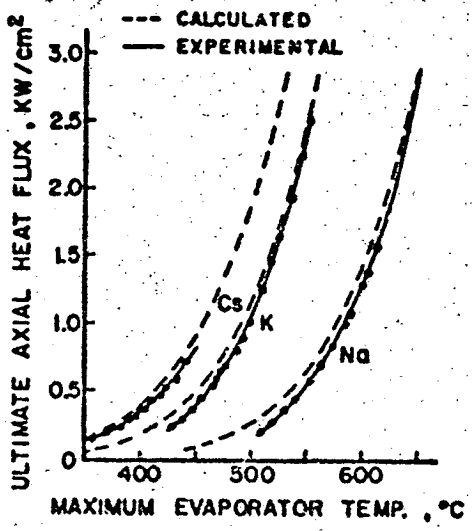

Figure 3.17 Comparison of Sonic Limits in Sodium, Potassium and Cesium Heat Pipes, Kemme [17]

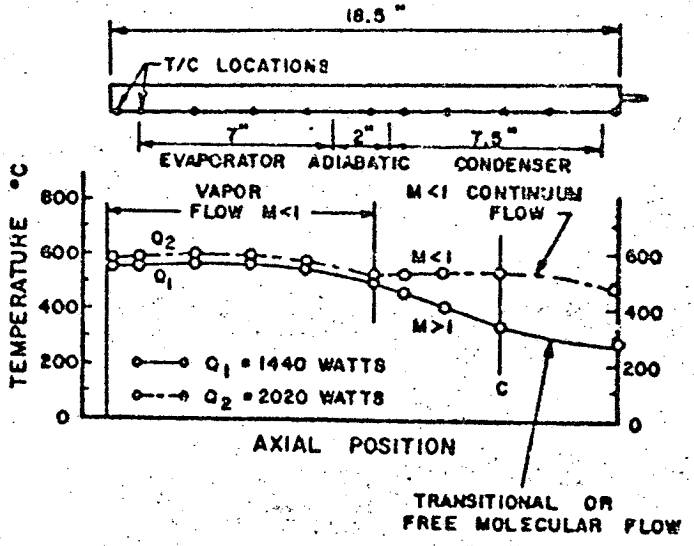

Figure 3.18 Axial Temperature Profiles for Sodium Heat Pipe, Dzakowic, et al. [83]

remained constant. The vapor velocity did not decrease immediately upon entering the condenser but continued to expand and became finally supersonic followed by a more abrupt pressure recovery than was evidenced for subsonic flow. Figure 3.17 demonstrates the effect of different fluids on the sonic limit. Good agreement between experimental results and theoretical predictions was achieved. The sonic limiting curve (see Figure 2.7) is highly dependent on the working fluid and is also dependent on the pressure and temperature at which the heat pipe is operating.

In a similar study, Dzakowic, et al. [83] confirmed the results obtained by Kemme. A sodium-stainless steel heat pipe with five layers of 60 mesh screen serving as wick was employed to study the vapor velocity limit in heat pipe operation. Figure 3.18 is a plot of the axial temperature profiles obtained for two different heat inputs. It is interesting to see that with increasing heat flow the transition from supersonic to subsonic flow at the condenser entrance took place at nearly the same heat flow rate and temperature as measured by Kemme (see Figure 3.15). This emphasizes again the dependency of the sonic limit on the selection of the working fluid and operating conditions of the pipe and deemphasizes its dependence on a particular pipe geometry. Various startup tests were also conducted. The data are presented in Figure 3.19 along with the calculated capillary (or ΔP) and sonic limits. Note the data of

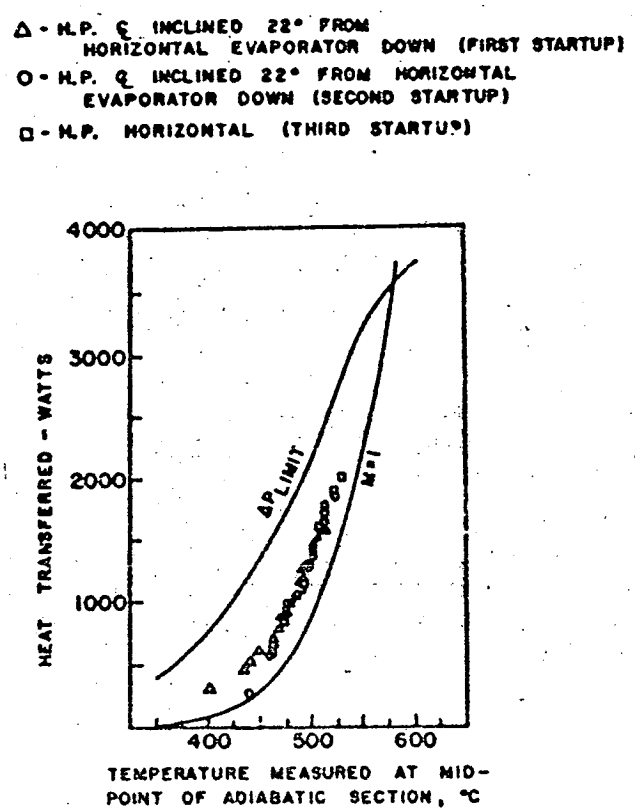

Figure 3.19 Heat Transfer Rate vs. Temperature at the Adiabatic Section, Dzakowic, et al. [83]

Dzakowic, et al. fall to the left of the sonic limit curve while Kemme's data (Figure 3.17) fall consistently to the right of the curve. An explanation for this discrepancy may be derived from the fact that Kemme plotted his data as a function of the maximum evaporator temperature, while Dzakowic et al. used the temperature measured at the mid-point of the adiabatic section. It appears that perhaps the use of the evaporator exit temperature would move both sets of data closer to the predicted curve. Dzakowic et al.

attributed their observed temperature discrepancy to possible supersaturation of the vapor and to a lesser degree, to the uncertainty in values of sonic velocity and specific heat of the vapor.

The sonic limit is not the only factor which contributes to startup problems of heat pipes. Obviously the starting technique is also of major importance. Busse, et al. [47] found it impossible to start a magnesium heat pipe unless the entire pipe was first preheated. Ernst, et al. [69] experienced that the method of orienting the heat pipe during startup had a significant affect on its final operating condition. Figure 3.20 depicts the evaporator temperature drop as a function of difference in elevation between the evaporator and the condenser. For height differences of less than 4.4 inches, no effect depending on pipe orientation was evident. Once the pumping limit was reached, however, the temperature drop was greatly influenced by the method used to attain the elevation difference. The upper curve represents the situation where the pipe was first placed into the desired position and subsequently heated, while the lower curve represents the case where the pipe was first heated horizontally and then subjected to the desired orientation. No satisfactory explanation was given for the difference in heat pipe behavior. McSweeney [50] measured the temperature in the vapor space of a sodium heat pipe which during the startup transient period unexpectedly

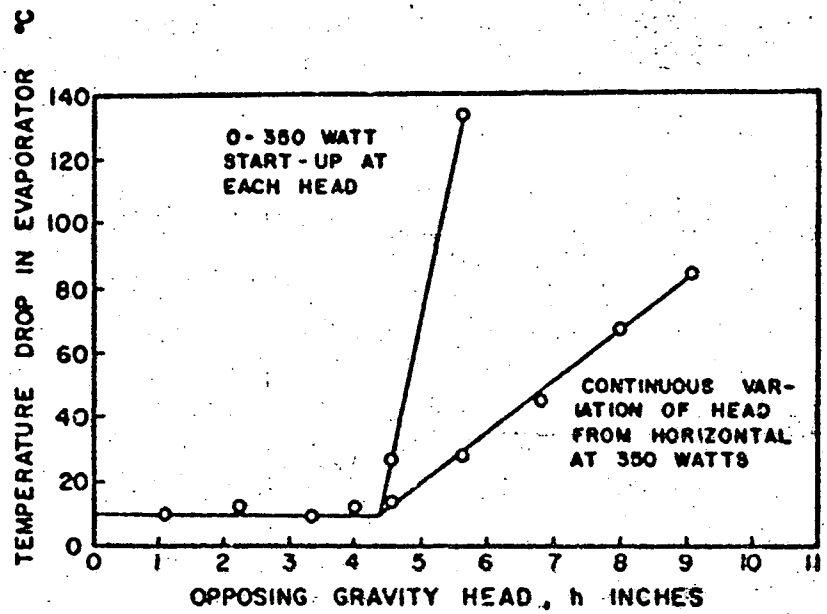

Figure 3.20 Temperature Drop in Evaporator vs. Opposing Gravity Head for 580°C Sodium Heat Pipe Operating at 350 watts, Ernst, et al. [69]

oscillated with an amplitude of nearly 50°C and a period of approximately 10 seconds. Oscillations were also observed for steady state operation of the pipe when the heat removal was highly concentrated by localized calorimeter cooling. As long as cooling was effected by free convection and radiation, no such oscillations were observed and the vapor temperature remained nearly uniform throughout the vapor space. The oscillatory behavior was attributed to either non-linear wick characteristics or the presence of non-condensable gases.

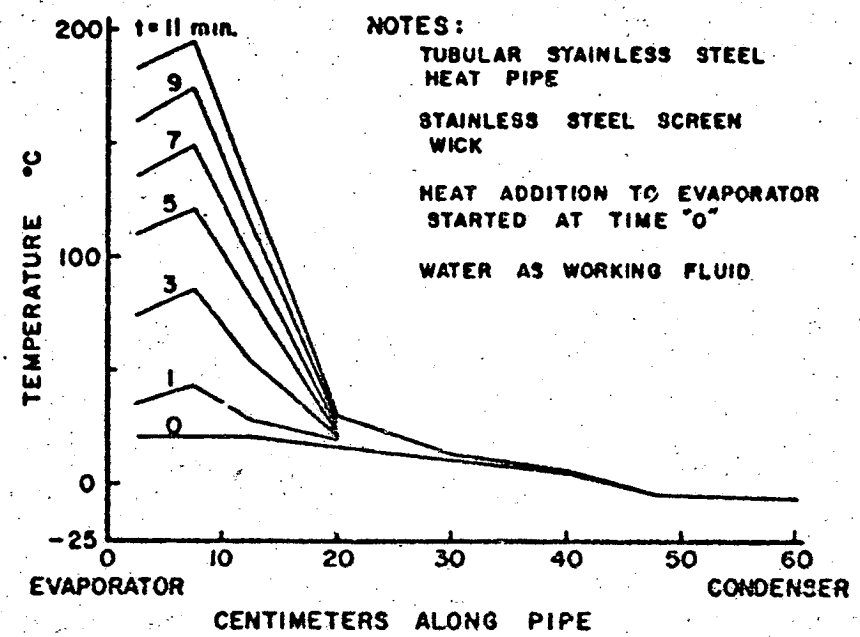

Figure 3.21 Transient Temperature Profile Along Partially Frozen Heat Pipe, Shlosinger [43]

Neal [28] and Shlosinger [43] studied the startup behavior of low temperature heat pipes with the working fluid initially frozen. The transient temperature profile along a water heat pipe in response to 50 watts of heat input is illustrated in Figure 3.21. Even such a moderate heat input of only 50 watts caused wick dryout and subsequent overheating in the evaporator section before the entire pipe thawed out and could begin to operate in its normal mode. With a heat input of 15 watts, however, the pipe thawed without wick dryout and normal operation began after approximately one hour. In an attempt to shorten the transient period, an auxiliary heat pipe which employed a

working fluid with a lower melting point was bonded to the primary heat pipe. The use of the auxiliary pipe greatly enhanced the thawing of the primary heat pipe without local overheating and the transient period of time was reduced by a factor one half. Initially the pipe was frozen only in the condenser section and liquid was present in the rest of the pipe. Deverall et al. [84] investigated the startup behavior of a water heat pipe which was initially frozen over its entire length. Ten watts of power were supplied and the transient temperature profile, shown in Figure 3.22, was measured. From the shape of the developing temperature profiles, Deverall deduced the following sequence of events: First heat was transferred in association with vapor flow along the full length of the pipe. The vapor was formed by sublimation in the evaporator. Since the wick was still frozen no liquid returned to the evaporator to replace the sublimated fluid. The lack of return fluid resulted in a rapid rise in evaporator temperature until it (see stations 1, 2, and 3) rose above the melting point. Water was then wicked into the heater area, and the temperature rise was temporarily arrested. Since most of the fluid was still frozen, not enough liquid was supplied to the heater. Dry-out occurred and the temperature of the evaporator increased rapidly to above 100°C. When the entire working fluid was finally melted, sufficient liquid was wicked into the

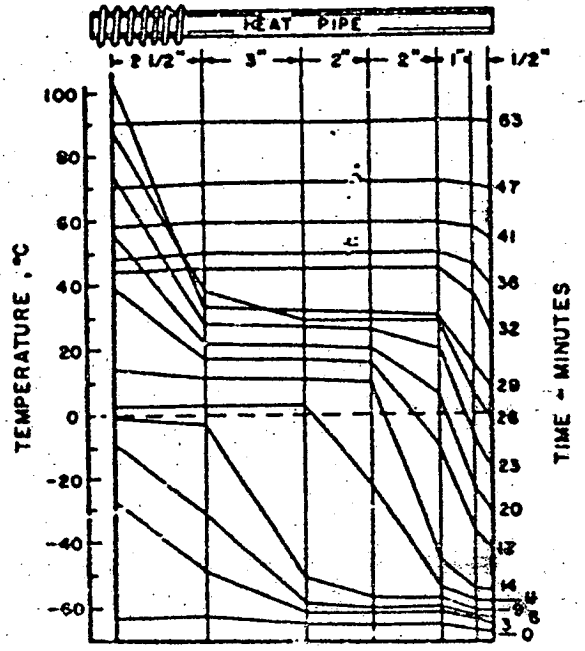

Figure 3.22 Transient Temperature Profile Along Completely Frozen Heat Pipe, Deverall, et al. [84]

evaporator and the temperature fell suddenly to 44°C. Normal operation began and the pipe became isothermal.

Startup data were also obtained for a (nonfrozen) water heat pipe placed in earth orbit. Telemetry data indicated a frontal startup of the type illustrated earlier in Figure 2.8-B. The startup procedure and steady state operation of the heat pipe in orbit were similar to those experienced in laboratory tests.

Phenomena associated with the startup behavior of high performance heat pipes have been studied by Kemme [85, 86]. He found that it was virtually impossible to start several

sodium heat pipes with wicks consisting of axial channels (grooves) running the length of the pipe. The difficulty was attributed to the attainment of the entrainment limit. As mentioned earlier, this limit is reached when a high velocity vapor stream shears liquid out of the wick and impedes a continuous supply of fluid to the evaporator. The entrainment limit is dependent primarily on the characteristics of the wick surface. Figure 3.23 shows test data obtained for three wick surface configurations. The maximum heat transfer was significantly improved by covering the channels with a layer of screens. The experimental curve labeled 4 is a good example of the entrainment limit and its shape confirms the curve initially depicted in Figure 2.7. In another experiment, the effect of "screen fit" was studied and is shown in Figure 3.24. The mechanical fit of the screen was very important in establishing the heat transfer limit of the heat pipe. The higher limit with the loose fitting screen was probably caused by the extra fluid paths available in the annulus between the screen and the outer wall. The curve calculated for the contacting screen in Figure 3.24 was based on the capillary limit and not the entrainment limit. The capillary and entrainment limits are both dependent on the wick structure and it is impossible to theoretically or experimentally change one without also altering the other. This dependency associated with the fact that the entrainment limit is generally attained only

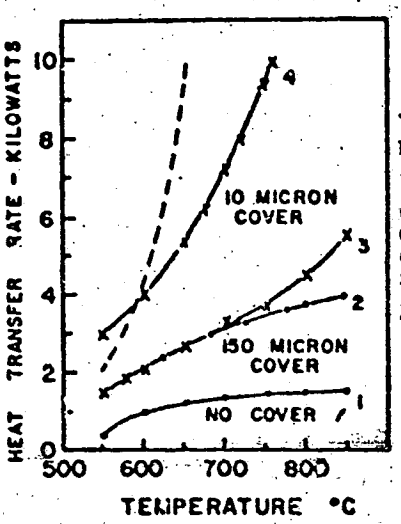

Heat Pipe Structure	Test Number 1	2	3	4
Material	Ni	Ni	S.S.	S.S.
System Length, cm	30	30	85	85
Evaporator Length, cm	8	8	8	8
Condenser Length, cm	22	22	77	77
Channel Width, mm	0.16	0.16	0.75	0.75
Channel Depth, mm	0.40	0.40	0.75	0.75
Screen Pore Size,	-	150	150	10
Screen Wire Diam,	-	115	115	46
Tube o.d., cm	1.82	1.82	1.82	1.79
Vapor Flow Area, cm^2 (cross section)	1.70	1.58	1.48	1.46

Figure 3.23 Heat Transfer Limit vs. Temperature for Different Wick Surface Configurations, Kemme [85, 86]

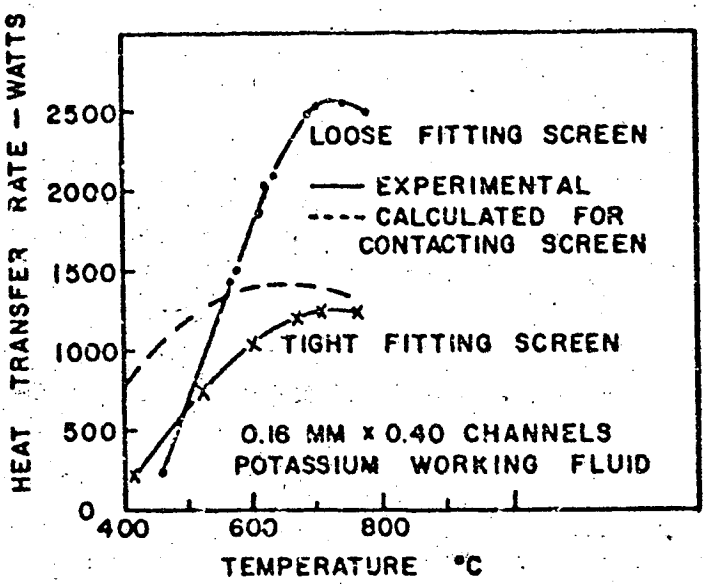

Figure 3.24 The Effect of Screen Fit on Axial Heat Flow in a Sodium Heat Pipe with Channels, Kemme [85, 86]

in a relatively narrow temperature range (between B and C in Figure 2.7) has somewhat curtailed the investigation of this particular limit of heat transfer in heat pipes.

Basic Studies

The investigations discussed in the preceding section have dealt primarily with the limits to heat pipe operation and startup characteristics. A number of additional studies have yielded information contributing to the rapidly growing heat pipe technology. Deverall, et al. [60, 84, 87, 88] operated a water-stainless steel heat pipe in an earth orbit and its performance was monitored by telemetry at several tracking stations during fourteen revolutions. Results indicated that there was no degradation of the heat pipe performance in a zero gravity field. In further tests [26, 89] a similar heat pipe was subjected to various sinusoidal and random vibrations to determine the influence of a vibratory environment on heat pipe performance. The experiments proved that vibration was not detrimental to heat pipe operation. On the contrary, vibration enhanced the wetting of the wick, forcing liquid into all parts of the wick structure, and thus actually improved heat pipe performance. Calimbas and Hulett [49] confirmed these results in a series of vibrational tests performed with a water-stainless steel heat pipe.

Haskin [25] measured the total radial temperature drop in the evaporator and condenser in a low temperature nitrogen

heat pipe. He found that for low heat loads (less than 36 watts) the temperature drop in the condenser was larger than in the evaporator. The difference was assumed to be caused by the extra liquid which accumulated in the condenser during operation. For larger heat loads, the temperature gradient in the evaporator became greater. This was attributed to partial drying of the wick and to the formation of a superheated vapor film on the inner metal tube surface. Similar measurements were made by Schwartz [58] with a water-stainless steel heat pipe. For the same range of heat loads, but much higher temperatures obtained with different fluids he found that the temperature drop across the wall and wick in the evaporator was consistently higher than in the condenser. Hence, a higher condenser temperature drop is not the rule, but instead, the relation between condenser and evaporator temperature drops is dependent on the given geometry and the nature of working fluids.

In yet another study, Ranken and Kemme [48] measured the temperature variation along the length of a lithium heat pipe operating at about 850°C as shown in Figure 3.25. The measured points have been fitted with a smooth curve which was corrected for the temperature drops arising from radial heat flows. Vapor pressure values associated with measured temperatures and with the temperature minimum are also displayed in Figure 3.25. The temperature reaches a minimum between the evaporator and condenser. In addition a pressure

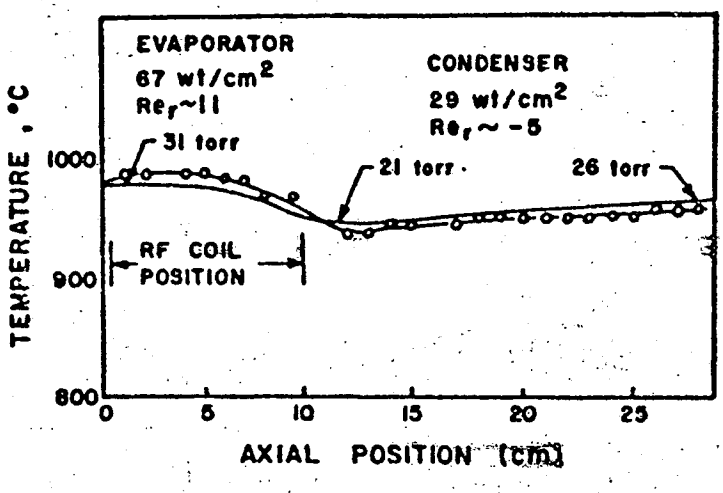

Figure 3.25 Experimental Observation of Pressure Recovery in Lithium Heat Pipe, Ranken and Kemme [48]

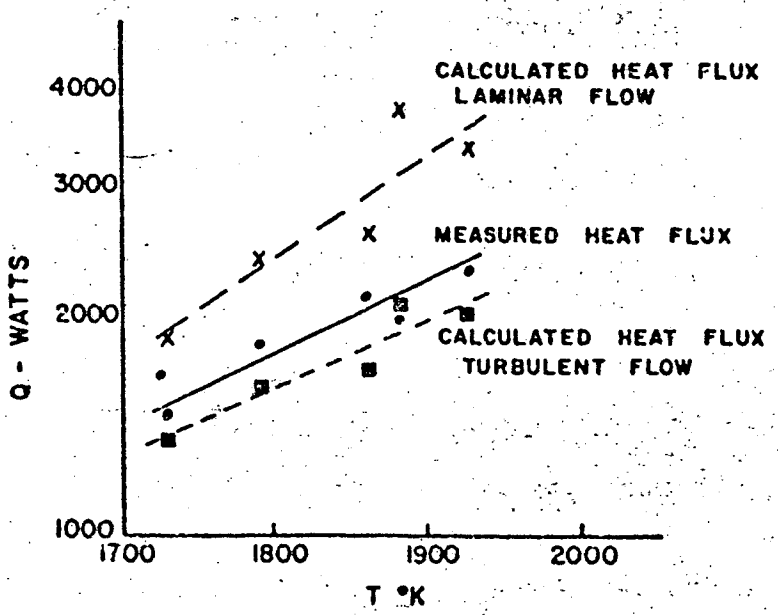

Figure 3.26 Results of Bohdansky Heat Transfer Determinations Compared to Theoretical, Ranken and Kemme [48]

recovery of .5 has occurred which compares favorably with theoretical predictions to be discussed in a later section. Ranken and Kemme compared data, obtained by Cohdansky and Schins [90] using a lead-tantalum heat pipe, with predicted values for both laminar and turbulent flow, Figure 3.26. Blasius' turbulent flow equation gave considerably better results than the laminar flow equation, which was expected, because the axial flow Reynolds' numbers were well over 1000 for this experiment. McKinney [35, 91] conducted extensive tests on a series of water heat pipes in a moderate temperature range (temperatures up to 400°F). Among other conclusions, which have already been amply discussed, he found that the magnitude of the radial Reynolds number had little or no effect on heat pipe operation.

Tien [92] measured the axial temperature distribution along the outside of a water-ethanol heat pipe. He determined the pressure inside of the pipe and compared this with the pressure which had to prevail if pure ethanol occupied the condenser and pure water occupied the evaporator. He concluded that separation into pure components in a heat pipe is extremely difficult, if not impossible, to achieve. Instead he found that if the initial composition was rich in ethanol, the data attested to the existence of a water-ethanol mixture in the evaporator while nearly pure ethanol (i.e., the azeotropic mixture) occupied the condenser section. All of Tien's data, however, were obtained with the

pipe operating vertically with the evaporator below the condenser. If the pipe contains excess liquid such an arrangement is usually referred to as a reflux condenser because gravity forces, instead of capillary forces, can always return the condensate to the evaporator. In such cases results would have to be viewed with some caution because the wick structure may or may not significantly alter the liquid vapor equilibrium conditions.

Heat Pipe Applications

Theoretically the heat pipe may be applied to almost a limitless number of thermal transport problems, which in general, can be subdivided into four broad topical categories [8, 9, 10, 20] depending on the particular feature of a heat pipe which is to be exploited. These areas of possible application are: 1) Temperature Flattening, 2) Source-Sink Separation, 3) Heat Flux Transformation, and 4) Constant Flux Production.

The temperature equalizing feature of the heat pipe has prompted numerous suggestions and actual uses for the maintenance of a desired constant temperature environment. Much of the emphasis has been, and is still, focused on the problems of thermal control of spacecraft. It is well known that large temperature variations may occur on the surface of a spacecraft resulting from nonuniform heating of the craft. These temperature variations can cause a host of problems including undesirable thermal stresses. Katzoff [5] together

with several other investigators [7, 93, 94, 95] recommended the use of long heat pipes, wrapped around the circumference of a spacecraft, to accomplish the necessary equalization of the temperature distribution. Naturally the evaporator sections of the circular pipes would have to face the sun while the radiation cooled condensers have to remain in the shadow of the craft. According to Katzoff such an arrangement of heat pipes would reduce the temperature variations around a spacecraft with a circumference of ten meters from 275°K to 44°K. Anand et al. [96, 97] reported the successful employment of two Freon-11 heat pipes which reduced the temperature differences between transponders located in different parts of a Geos II spacecraft. Deverall utilized the isothermal walls of a heat pipe to measure the total hemispherical emissivity of variously prepared surfaces [23, 98]. Several heat pipe containers were plated or sprayed with different materials, and the resulting emissivities were determined over a wide range of temperature with an estimated accuracy of ±2%. Schretzmann [99] employed an isothermal surface of a heat pipe as a metal source in a study of the effect of electromagnetic fields on the evaporation of metals. Bohdansky and Schins [100] used a heat pipe for the determination of pressure-temperature relations of metal vapors at high temperatures and pressures. Feldman and Whiting [9] have suggested the construction of an isothermal flat plate for the installation of electronic components. They conceived a sandwich type plate, the interior filled with

many interconnecting honeycombed heat pipes, which would rapidly distribute any localized heat flow and maintain the plate at a uniform temperature.

Another use of the heat pipe would allow separation of the heat source from the heat sink. Again, possible spacecraft applications of heat pipes have received considerable attention since the heat source, for instance electronic components, is often located in the interior of the craft and the waste heat must often be transferred over some distance for ultimate rejection to outer space. Moreover, any sizeable temperature drop between the source and the radiator may induce a significant weight penalty because a larger radiator area will be required at lower temperatures to dissipate the same amount of energy. Since the heat pipe is both light weight and nearly isothermal it appears to provide ideal solutions to many thermal dissipation problems encountered in spacecraft. Many investigators [46, 101, 13, 102, 103, 104, 61] have considered its application to such energy dissipation systems and have cited numerous advantages including greater heat transfer per unit weight, and some degree of meteor protection when used in parallel arrangement. Werner and Carlson [104] have reported that heat pipes can operate sixty times more effectively as radiators than solid rods based on heat transfer rates per unit weight. Deverall and Kemme[23] support this claim by reporting that a silver heat pipe is 520 times more effective than an equivalent

solid tantalum rod. A team of investigators of RCA [20, 51] has designed, constructed and successfully tested a space radiator composed of one hundred individual heat pipes. The system which weighs less than twelve pounds is capable of rejecting 50,000 watts of thermal energy at a temperature of 1420°F. McKinney [35] recommended the installation of cryogenic heat pipes around cryogenic storage tanks. If the heat pipes contained a working fluid having a lower boiling point than the stored fluid it should be feasible to transfer the heat, leaked from the immediate surroundings into the storage vessel, to a remote sink for dissipation. Researchers at Los Alamos Scientific Laboratory explored a unique scheme in which the construction of a heat pipe plasma oven was proposed. The disposal of waste heat given up by electronic components at remote locations has already been mentioned several times [11, 49].

Another feature of the heat pipe, which has generated much enthusiasm, is its ability for thermal flux transformation. Heat addition to and heat removal from a heat pipe are feasible across heat flow areas of different size. This potential for heat flux transformation has stimulated thermionic specialists to consider the conversion of low heat fluxes generated by radioactive isotopes, for instance, into a sufficiently high heat flux which is required for the operation of a thermionic converter. Leefer [64] achieved a flux transformation with a flux concentration ratio of

approximately ten to one equivalent to an output flux density of 250 watts/cm^2 which is more than adequate to meet the requirements of a thermionic converter. Other investigators also reported measured flux conversions of a ratio of ten to one [107] and even twelve to one [74, 68]. A number of papers have appeared in the literature [23, 64, 65, 67, 71, 108 to 117] extolling the virtues of heat pipes when used in conjunction with thermionic converters. Numerous heat pipe-thermionic converter assemblies have been built and tested. The results have generated much optimism and it is believed that the heat pipe applied to thermionic converters will reach technical maturity in the near future.

Heat pipes may also be used to "flatten" flux variations supplied by an unsteady heat source. Researchers at RCA [107] have developed a "classified" radioisotope powered heat pipe which supposedly maintains a constant thermal output flux independent of variations in thermal input flux for at least three half lives. A qualified thermodynamicist might want to study these more exotic schemes in view of their compatibility with the requirements of the Second Law of Thermodynamics.

Two particular potential heat pipe applications have been proposed by investigators at the Lawrence Radiation Laboratory. Hampel and Koopman [32] suggested the utilization of the heat pipe concept for the control of small, fast-spectrum, high temperature reactors. Their scheme is based on the

capability of the heat pipe to respond to a sudden increase in heat flux with an increase in evaporation rate. If the evaporator ends of a sufficient number of heat pipes, filled with special working fluids having a negative void coefficient, were installed in the reactor core, an increase in core heat flux would result in a decrease of the total mass contained in the core (evaporators). Such a hypothetical mass transfer device may eventually be used to provide some sort of reactor safety control. Werner [118] proposed to employ lithium heat pipes as tritium producers in the blanket structure of a reactor. The scheme calls for the transport of the tritium within the heat pipe to an accessible processing point outside of the blanket where it could be removed by diffusion or equivalent means and then be used to replenish the tritium consumed in the core.

Heat Pipe Control

Inasmuch as the heat pipe transfers energy between two points utilizing a continuous mass circulation, it is apparent that some degree of heat pipe control may be exerted by controlling the mass flow. Katzoff [5] suggested several concepts to accomplish thermal control with the heat pipe serving as a variable thermal conductor. One technique involves the intentional introduction of a noncondensable gas into the vapor space. As discussed earlier, the gas tends to collect in the condenser where it forms a relatively stagnant gas zone which effectively eliminates any working

fluid condensation. The length of the gas zone, of course, depends on the working pressure in the pipe; the zone length decreasing with increasing pressures. The gas layer can be exploited in several ways. For example, suppose it is desired to always furnish solar energy to an instrument inside of a spacecraft regardless of the craft's orientation with respect to the sun. The task could be accomplished by mounting the instrument in the center section of a heat pipe containing some noncondensable gas. If the amount of gas was such that it filled slightly less than half of the pipe, then the instrument would always receive energy from the sun. The end of the heat pipe on the shaded side of the spacecraft should remain inoperative due to the blocking effect of inert gas and thus minimizing heat losses. The opposite problem could be solved by using a partially dry heat pipe. Now the dry part of the heat pipe, and hence the inoperative part, could always face the sun, and the instrument which might generate heat could reject this heat by radiation from the shaded side of the spacecraft to outer space. Besides Katzoff, Wyatt [119] and Anand et al. [79] have suggested the use of thermostatically controlled valves and/or bellows to supply or withdraw the noncondensable gas. Such an arrangement would allow the effective condenser area to be varied independently of the operating pressure prevailing in the pipe. Katzoff has also recommended a control technique which involves the interruption of the liquid flow

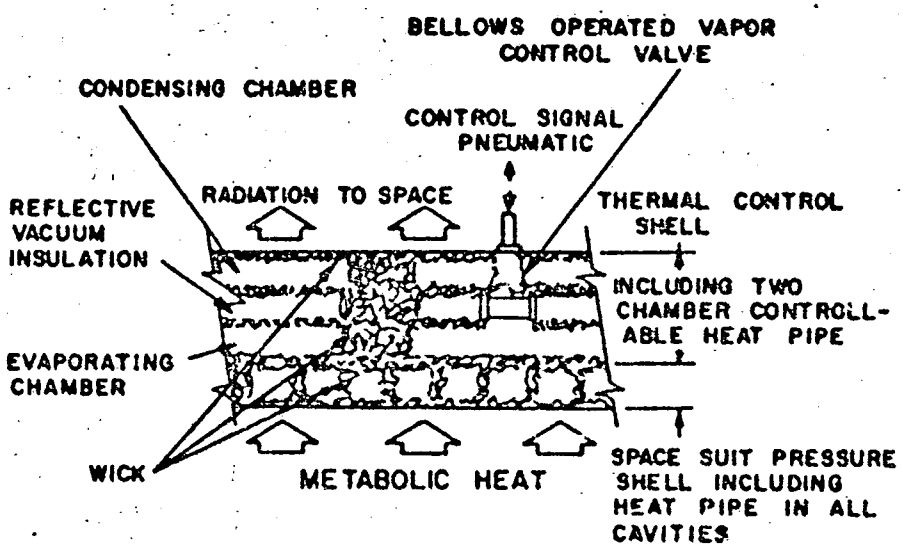

Figure 3.27 Schematic Cross Section of Variable Conductance Space Suit Shell, Shlosinger [42, 43, 44]

in the wick. This control technique would be practical only in wicking structures in which the bulk of the flow takes place in an artery. A thermostatically controlled valve could be used to impede, or stop the flow in the artery, in response to the control requirements. Anand et al. [79] and Shlosinger et al. [44] have also considered a similar arrangement for the control of the vapor flow. Shlosinger [42,43] used this concept into the design of a variable conductance space suit. His design is illustrated in Figure 3.27. The design concept provides for both insulation when the valve is closed and for heat rejection when the valve is open during periods of high metabolic heat generation of the space suit wearer. Experimental results

were interpreted to consider such a technique as feasible, but calling for much more research. Anand et al.[79] recommended a control technique involving the use of two fluids whose pressure-temperature curve intersect at the desired operating temperature. In anticipation of the difficulty of finding such fluids, this method of control has received only minor attention. Workers at Honeywell [27] have studied the concept of bellow controlled feeder wicks which are either in contact with the heated surface thus providing a path for the condensate return, or the contact is interrupted, thus preventing fluid return and hereby shutting off the heat pipe action. Heat pipes acting as "thermal switches" were built primarily in an effort to develop variable conductance walls. Conductivity ratios of 150 have been reported depending on the position of the feeder wick.

Obviously a great many possibilities for heat pipe control exist; however, most of these concepts remain still in the dreaming stage, and few controllable heat pipes have actually been built to date. Much more research will have to be devoted to this particular area of heat pipe application so that eventually some thermal problems can be solved with controllable heat pipes.

Heat Pipe Theory

The heat pipe theory developed up to date is due, in large part, to a stimulus provided in a theoretical study performed by Cotter [4]. He formulated the governing

equations describing the processes taking place in the heat pipe and also developed a model to predict the capillary limit of heat pipe operation. His results have been used by other investigators who have often simplified or modified his equations to suit their particular assumptions and/or geometries. Because this has been done so extensively, Cotter's analysis will be presented in necessary detail. The description of the analysis will be followed by a number of modified theories and by several other analytical approaches, all of which are concerned with the capillary limit. Derivations for the predictions of the other limits of heat pipe operation are given subsequently and finally several analyses which deal with specific problems conclude the analysis section.

Cotter studied a heat pipe as shown in Figure 3.28. The capillary structure is assumed to have a pore radius, r_c, and to be completely saturated with a working fluid. The radius of curvature of the meniscus surface is thought to be dependent on the distance, z, and the pressure difference across a surface as a function of position is given by

$$P_v(z) - P_\ell(z) = 2\sigma/r(z) = 2\sigma\cos\theta/r_c \qquad (3\text{-}10)$$

where r(z) is the local meniscus radius of curvature. In equation (3-10), of course, it is assumed that the meniscus is represented by one radius of curvature only. If, in fact, a complex meniscus shape were formed, the term

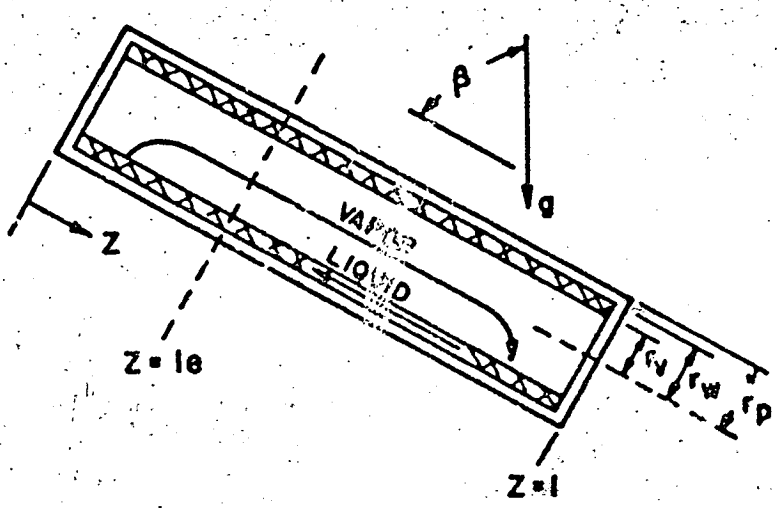

Figure 3.28 Cylindrical Heat Pipe Structure, Cotter [4]

$(2/r(z))$ in equation (3-10) should be replaced by $\left(\frac{1}{r_1} + \frac{1}{r_2}\right)$ where r_1 and r_2 are the two radii of curvature necessary to describe a three dimensional surface. If a heat pipe is to be operated in a gravity field, then the maximum length, z_{max}, of the pipe is restricted by the lifting ability of the combined wick and liquid system. The maximum length is given by the well known relation

$$z_{max} \cos\beta = \frac{2\sigma\cos\theta}{\rho_\ell g\, r_c} \qquad (3\text{-}11)$$

Cotter next considered the steady state operation of a heat pipe and applied the conservation of mass principle to arrive at the relation

$$\dot{m}_v(z) + \dot{m}_\ell(z) = 0 \qquad (3\text{-}12)$$

where the two mass flow rates are both positive in the plus z-direction.

The pressure gradient in the liquid was determined from the Navier Stokes equation for steady, incompressible, constant viscosity flow. By neglecting the inertial term and by modifying the viscous term with a dimensionless constant to account for different wicks, the pressure gradient in the z direction was found to be

$$\frac{dP_\ell}{dz} = \rho_\ell g \cos\beta - \frac{b\mu_\ell \dot{m}_\ell(z)}{\pi\left(r_w^2 - r_v^2\right)\rho_\ell \varepsilon r_c^2} \qquad (3\text{-}13)$$

where the dimensionless constant, b, is defined as $\varepsilon r_c^2/K$ and has a value of approximately 8 for non-connected parallel cylindrical pores, and 10-20 for more realistic capillary structures with tortuous and interconnected pores. The radial pressure gradient has been assumed negligible as will be the case for long thin pipes; that is, for those pipes for which $r_v l \gg r_w^2$.

The pressure gradient in the vapor was found by employing the results of Yuan and Finkelstein [120] and Knight and McInteer [121]. These authors assumed incompressible laminar flow and uniform injection or suction at the vapor space boundary. The applicability of these results is based on the value of the radial Reynolds number, Re_r, which is defined by

$$Re_r = -\frac{\rho_v r_v v_r}{\mu_v} = \frac{1}{2\pi\mu_v}\frac{d\dot{m}_v}{dz} \qquad (3\text{-}14)$$

It is positive for evaporation and negative for condensation. For $|Re_r| \ll 1$, the vapor flow is dominated by viscous forces

and the velocity profile approximates the usual parabolic shape for Poiseuille flow. For this case the vapor pressure gradient is given by

$$\frac{dP_v}{dz} = -\frac{8\,\mu_v\,\dot{m}_v}{\pi\rho_v\,r_v^4}\left(1 + \frac{3}{4}\,Re_r - \frac{11}{27}\,Re_r^2 + \cdots\right) \qquad (3\text{-}15)$$

For $|Re_r| \gg 1$, however, the flow is qualitatively different in evaporator and condenser. For high evaporation rates, the velocity profile is not parabolic but is proportional to $\cos\frac{\pi}{2}\left(\frac{r}{r_v}\right)^2$, which was verified experimentally by Wageman and Guevara [121], and the pressure decreases in the direction of flow. For high condensation rates, on the other hand, the velocity profile is nearly constant across the vapor space with the transition to zero velocity occurring in a thin layer near the wall, and the pressure increases in the direction of motion due to a partial dynamic recovery in the decelerating flow. For $|Re_r| \to \infty$, the pressure gradient is found to be

$$\frac{dP_v}{dz} = \frac{-S\,\dot{m}_v}{4\rho_v\,r_v^4}\,\frac{d\dot{m}_v}{dz} \qquad (3\text{-}16)$$

where $S = 1$ for evaporation and $S = 4/\pi^2$ for condensation. Furthermore, Cotter hypothesized that for some situations where the $Re_r = 0$ and the average vapor velocity is high, as might exist in heat pipes with a long adiabatic section, fully developed turbulent flow may occur. For such a case, Cotter recommended using

$$\frac{dP_v}{dz} = - \frac{.0655\ \mu_v^2\ Re^{7/4}}{\rho_v\ r_v^3} \qquad (3\text{-}17)$$

in lieu of equation (3-15).

The relation between vapor and liquid pressures and the mass flow rates is next given by a formula supplied by the kinetic theory.

$$\frac{d\dot{m}_\ell}{dz} = - \frac{d\dot{m}_v}{dz} = \frac{\alpha r_v \left(P_v - P_{vap}\right)}{\sqrt{RT/2\pi M}} \qquad (3\text{-}18)$$

where α is a numerical factor which includes the probability of condensation of a vapor molecule and the surface roughness of the miniscus. The value of α is very nearly unity.

Cotter next considered the conservation principle of energy and by neglecting radiative and conductive contributions he arrived at

$$Q(z) = h_{fg}\, \dot{m}_v(z) \qquad (3\text{-}19)$$

Finally, Cotter coupled the heat pipe to the surrounding environment by expressions accounting for heat fluxes or imposed temperature conditions respectively

$$\frac{dQ(z)}{dz} = - 2\pi\ r_p q_r(z, r_p) = H(z, T_p, Q) \qquad (3\text{-}20)$$

and

$$T(z, r_p) = T(z, r_v) + \frac{H}{2\pi} \left(\frac{1}{k_p} \ln \frac{r_p}{r_w} + \frac{1}{k_w} \ln \frac{r_w}{r_v} \right) \qquad (3\text{-}21)$$

where equation (3-21) relates the temperature on the outer surface of the heat pipe to the temperature at the liquid vapor meniscus.

Equations (3-10) through (3-21) are generalized heat pipe relations as presented by Cotter. These equations can be solved if the vapor has a nearly uniform temperature, T_0, throughout the vapor space. If equation (3-21) is solved for $T_p\left[T(z,r_p)\right]$, then H in equation (3-20) may be expressed as a function of length, z, temperature distribution in the vapor $T_v\left[T(z,r_v)\right]$, and the heat flow, Q. Also, if the heat flow through the pipe ends is denoted by $F_0(T_v)$ and $F_1(T_v)$, then the average vapor temperature, T_0, and the corresponding axial heat flux distribution, $Q_0(z)$ are determined from the relations

$$\frac{dQ_0}{dz} = H(z,T_0,Q_0)$$

$$Q_0(0) = F_0(T_0) \; ; \; Q_0(1) = F_1(T_0) \tag{3-22}$$

With this approximation for the heat flux, the mass flow rates may be determined from equations (3-12) and (3-19). The vapor mass flow rate can then be used in the appropriate equation, (3-15), (3-16), or (3-17) to determine the pressure distribution in the vapor. Also equation (3-13) may be integrated to yield the axial pressure distribution in the liquid. Finally, equation (3-18) can be solved for the vapor pressure of the liquid to within an additive constant. Cotter recommends using $P(T_0)$ for this constant. Since the vapor pressure is a known function of liquid surface temperature, $T_v(z)$ may be determined. The

consistency of this procedure can be verified if the axial variation of T_v is small compared to T_0.

Cotter used this procedure for the special case of constant heat addition along the evaporator and constant heat removal along the condenser. Thus he obtained

$$Q_0(z) = h_{fg}\dot{m}_v(z) = \begin{cases} zQ_c/l_e & ; \quad 0 \le z \le l_e \\ (1-z)Q_c/1-l_e & ; \quad l_e \le z \le 1 \end{cases} \tag{3-23}$$

where Q_e is the total heat input to the evaporator. By employing equations (3-23) in (3-15) and (3-16) and neglecting the term Re_r^2 in the former, and assuming the vapor density, ρ_v, to be constant in both, a straightforward integration yields

$$\Delta P_v = P_v(1) - P_v(0) = \begin{cases} -\dfrac{4\mu_v\, lQ_e}{\pi\rho_v\, r_v^4\, h_{fg}} & ; \quad Re_r << 1 \\ -\dfrac{(1-4/\pi^2)Q_c^2}{8\rho_v\, r_v^4\, h_{fg}^2} & ; \quad Re_r >> 1 \end{cases} \tag{3-24}$$

Likewise, integration of equation (3-13) yields

$$\Delta P_\ell = P_\ell(1) - P_\ell(0) = \rho_\ell g l \cos\beta + \frac{b\,\mu_\ell\, Q_e l}{2\pi\left(r_w^2 - r_v^2\right)\rho_\ell \varepsilon r_c^2\, h_{fg}} \tag{3-25}$$

The temperature difference in the vapor space can be obtained from equation (3-18) leading to

$$\Delta P_{vap} = \Delta P_v - \frac{lQ_e\sqrt{RT_0/2\pi M}}{l_e(1-l_e)\, h_{fg}\, \alpha r_v} \tag{3-26}$$

And finally by considering the vapor as an ideal gas, application of the Clapeyron - Clausius equation and neglecting the volume of the liquid phase results in

$$\Delta T_v = \frac{RT_0^2 \, \Delta P_{vap}}{\gamma h_{fg} \, P(T_0)} \tag{3-27}$$

The preceding equations were applied to a horizontal sodium heat pipe and the results of these calculations are listed below. The left hand column indicates the pertinent values used and the right hand column shows the calculated parameters.

Q_e = 500 watts	$\dot{m}_v(l_e)$ = .1 gm/sec
T_0 = 920°K	$P_{vap}(T_0)$ = 50 mm Hg
l = 90 cm	ΔP_v = -.2 mm Hg
l_e = 15 cm	ΔP_{vap} = -.5 mm Hg
r_v = .64 cm	ΔP_ℓ = 2 mm Hg
r_w = .80 cm	ΔT_v = -.7°K
r_c = .012 cm	

An inspection of the computed values explains why the heat pipe has generated so much enthusiasm among thermal engineers. A relatively large energy transport is accomplished with an almost negligible temperature drop.

Cotter next considered the maximum heat transport which is possible in a heat pipe which is limited only by the pumping ability of a wick in association with a given working fluid. The maximum pressure difference which can be

supported between the liquid and vapor is achieved when the meniscus radius in the evaporator achieves a minimum value, i.e., equal to r_c. Therefore equation (3-10) becomes

$$P_v(z) - P_\ell(z) \overset{\bullet}{\leq} \frac{2\sigma\cos\theta}{r_c} \qquad (3\text{-}28)$$

which must be satisfied for all positions, z. In particular, for z = 0, equation (3-28) may be rewritten with the aid of equations (3-24) and (3-25) to give the capillary limiting condition for the total axial heat flux

$$\left.\begin{matrix}\dfrac{4\mu_v}{\pi\rho_v r_v^4 h_{fg}}\dfrac{lQ_e}{} \\ \dfrac{(1-4/\pi^2)Q_c^2}{8\rho_v r_v^4 h_{fg}^2}\end{matrix}\right\} + \left[\rho_\ell g l\cos\beta + \frac{b\,\mu_\ell\,Q_e l}{2\pi\left(r_w^2-r_v^2\right)\rho_\ell\varepsilon r_c^2 h_{fg}}\right] \leq \frac{2\sigma\cos\theta}{r_c} \begin{cases} Re_r << 1 \\ Re_r >> 1 \end{cases} \qquad (3\text{-}29)$$

where

$$P_v(0) - P_\ell(0) = P_v(1) - \Delta P_v + \Delta P_\ell - P_\ell(1) = \Delta P_\ell - \Delta P_v \qquad (3\text{-}30)$$

has been used to simplify the left hand side of (3-28) prior to the substitution of equations (3-24) and (3-25).

Cotter next determined the optimum capillary pore radius, r_c, in terms of Q_e by considering equation (3-29) where the equality sign is used and the first term is simply $-\Delta P_v$. Now since ΔP_v is directly proportional to Q_e (or Q_e^2), the heat transported is a maximum if ΔP_v is a maximum. Thus equation (3-29) becomes

$$\Delta P_v = \rho_\ell l g \cos\beta + \frac{b\,\mu_\ell\,1Q_e}{2\pi\left(r_w^2 - r_v^2\right)\rho_\ell \varepsilon h_{fg} r_c^2} \qquad (3\text{-}31)$$

With equation (3-31), the pressure drop, ΔP_v, becomes a maximum when

$$r_c = \frac{b\,\mu_\ell\,1Q_c}{2\pi\left(r_w^2 - r_v^2\right)\rho_\ell \varepsilon h_{fg}\,\sigma\cos\theta} \qquad (3\text{-}32)$$

The maximum heat transport is determined by converting equation (3-28) to the form

$$\Delta P_\ell - \Delta P_v - \frac{2\sigma\cos\theta}{r_c} = 0 \qquad (3\text{-}33)$$

Now for $Re_r << 1$, and with no hydrostatic contribution to ΔP_ℓ, equation (3-33) is used in conjunction with equations (3-24), (3-25), and (3-32) to solve for Q_e, leading to

$$Q_e^2 = \frac{-\sigma^2\cos^2\theta\; r_v^4 \left(r_w^2 - r_v^2\right)}{\left(\frac{-2\,bl^2\,\mu_v\,\mu_\ell}{\pi^2 h_{fg}^2\,\varepsilon\rho_v\rho_\ell}\right)} \qquad (3\text{-}34)$$

Obviously Q_e becomes a maximum when the term $r_v^4\left(r_w^2 - r_v^2\right)$ assumes a maximum. Simple calculus shows that this situation is achieved when

$$\frac{r_v}{r_w} = \frac{2}{3} \qquad (3\text{-}35)$$

Substituting equation (3-35) into (3-34) finally yields

$$Q_e = \frac{\pi r_w^3\, h_{fg}\,\sigma\cos\theta}{3l}\left(\frac{2\rho_v\rho_\ell\varepsilon}{3h\mu_v\mu_\ell}\right)^{1/2} \qquad (3\text{-}36)$$

Inserting equations (3-36) and (3-35) into (3-32) yields for the optimum pore size for $Re_r << 1$

$$r_c = r_w \left[\frac{b\mu_\ell \rho_v}{6\rho_\ell \mu_v \epsilon}\right]^{1/2} \qquad (3\text{-}37)$$

The analogous expressions to equations (3-36) and (3-37) for $Re >> 1$ are

$$Q_c = \frac{4r_w \pi h_{fg}}{s} \left[\frac{\rho_v \rho_\ell \epsilon \sigma^2 \cos^2\theta}{(\pi^2-4)b\ l\mu_\ell}\right]^{1/3} \qquad (3\text{-}38)$$

and

$$r_c = \left[\frac{8\rho_v\ b^2\mu_\ell^2\ l^2}{(\pi^2-4)\rho_\ell^2 \epsilon^2 g \cos\theta}\right]^{1/3} \qquad (3\text{-}39)$$

Cotter's model for $Re_r >> 1$ predicts that the maximum extent of pressure recovery is fixed at $4/\pi^2$ corresponding to 40.5 percent of the drop that occurs in the evaporator regardless of the amount of heat transferred. Therefore, the profile illustrated in Figure 3.29 represents the vapor pressure distribution for any case which is dominated by inertial forces. It should be recalled that the profile in Figure 3.29 is dependent on all the assumptions made by Cotter in his analysis and in particular, on the assumption that the vapor is incompressible. Parker and Hanson [24] have written a computer code in which they consider the vapor to be compressible, and consequently, treats the vapor density as a variable. A comparison of their results with Cotter's predictions demonstrates excellent agreement for

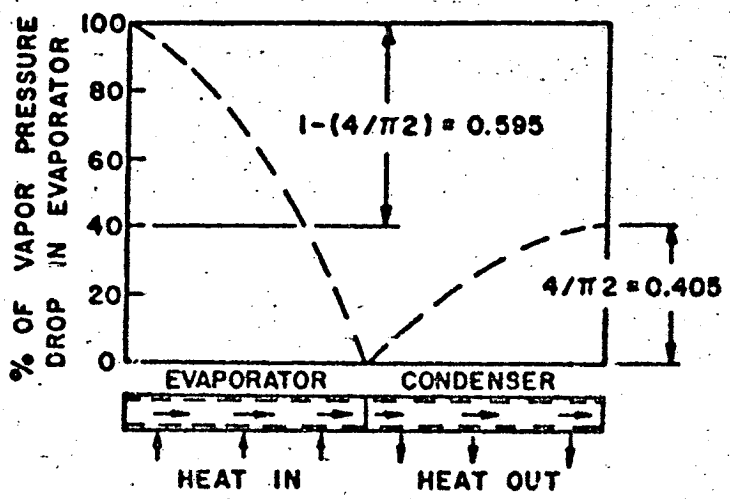

Figure 3.29 Theoretical Axial Profile of Pressure in Vapor, Cotter [4]

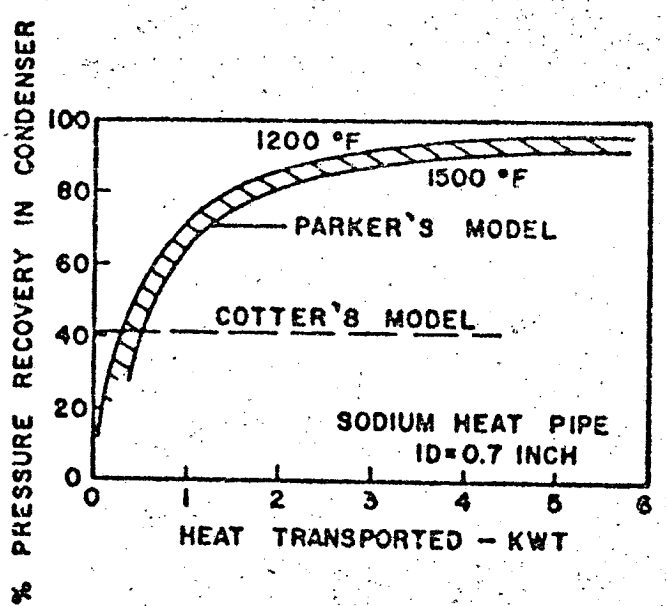

Figure 3.30 Condenser Pressure Recovery vs. Heat Transported, Parker and Hanson [24]

the pressure profile in the evaporator section. However, a significant departure from Cotter's prediction was found to exist in the condenser section. Here, the extent of pressure recovery was dependent on the heat transported by the pipe. Figure 3.30 illustrates the predicted pressure recovery as a function of the heat transported for a particular sodium heat pipe. The extent of pressure recovery is seen to be considerably larger than that predicted by Cotter for large heat transport rates and hence the net end to end pressure drop in the heat pipe will be smaller. When compressibility effects are important, Cotter's analysis underpredicts the maximum heat transfer capability of the heat pipe, and it may be used to provide a conservative estimate of the capability of the pipe. Of course, an even more conservative estimate could be obtained by neglecting pressure recovery altogether.

Ernst [54] has disputed the validity of the meniscus boundary conditions employed by Cotter for the special case of large radial Reynolds numbers, zero gravity, and incompressible vapor flow. It should be recalled that Cotter assumed a meniscus profile of the type shown in Figure 3.31. Using this profile, he went on to optimize the capillary radius and heat transfer rate and arrived at equations (3-29), (3-38), and (3-39). Ernst has calculated the pressure profiles based on these equations for the special case of a sodium heat pipe operated at 700°C with r_w = 1 cm,

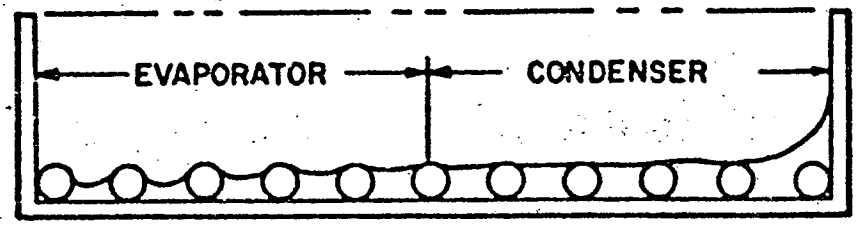

Figure 3.31 Liquid Profile for Non-Optimized Capillary at Maximum Q, Ernst [54]

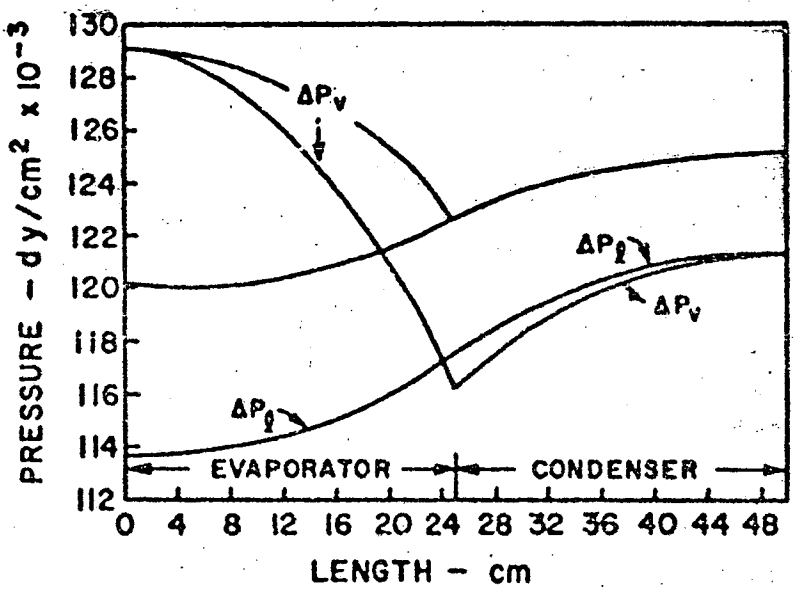

Figure 3.32 Pressure Profile for 700°C Sodium Heat Pipe, Ernst [54]

l_e = 50 cm, and l_a = 50 cm. His profiles are illustrated in Figure 3.32 by the lower set of curves. Figure 3.32 shows that at the condition of maximum heat transfer predicted by Cotter, the pressure gradient in the liquid is smaller than that in the vapor. Consequently, the pressure of the liquid in the condenser is greater than the pressure in the vapor. Ernst has concluded that for such a situation, a meniscus profile of the type illustrated in Figure 3.33 must exist. However, he regarded this meniscus profile as unrealistic and instead proposed the profile illustrated in Figure 3.34 for the non-optimized capillary case. In this revised profile, pressure equality between the liquid and the vapor is assumed to occur at the interface between the condenser and the evaporator instead of at the condenser end as assumed by Cotter. For the special case of a wire screen capillary structure, Ernst has derived the following equations for the pressure balance in the evaporator and condenser, the optimum mesh opening half-width, and the maximum heat transfer capability, respectively.

Evaporator:

$$\frac{Q^2}{8\rho_v r_v^4 h_{fg}^2} + \frac{b\,\mu_\ell\,Ql_c}{2\pi\left(r_w^2-r_v^2\right)\rho_\ell \varepsilon d^2 h_{fg}} \leq \frac{2\sigma\cos\theta}{d(1+K)} \qquad (3\text{-}40)$$

Condenser:

$$\frac{4Q^2}{8\pi^2\rho_v r_v^4 h_{fg}^2} = \frac{b\,\mu_\ell\,Ql_c}{2\pi\left(r_w^2-r_v^2\right)\rho_\ell \varepsilon d^2 h_{fg}} \qquad (3\text{-}41)$$

Optimum mesh opening half-width:

$$d = \left[(1+K)\left(\frac{\pi^2}{4} + \frac{l_e}{l_c}\right)\left(\frac{b^2\rho_v\mu_\ell^2 l_c^2}{\rho_\ell^2\varepsilon\sigma\cos\theta}\right)\right]^{1/3} \qquad (3\text{-}42)$$

Maximum heat transfer:

$$Q_m = \frac{4\mu r_w^2 h_{fg}}{3}\left[\frac{1}{(1+K)^2\left(\frac{\pi^2}{4} + \frac{l_e}{l_c}\right)^2} \cdot \frac{\rho_v\rho_\ell\varepsilon\sigma^2\cos^2\theta}{b\,\mu_\ell\, l_c}\right]^{1/3} \qquad (3\text{-}43)$$

where $r_c = d(1+K)$ and $K = d_1/d$ has been used in deriving equations (3-40) through (3-43) and $r_v^2 = (2/3)r_w^2$ has been applied to the derivation of equations (3-42) and (3-43). Ernst also applied equations (3-40) through (3-43) to the same 700°C sodium heat pipe discussed earlier. His pressure profiles are illustrated by the upper set of curves in Figure 3.32. The pressure equality between the liquid and vapor in the condenser implies a meniscus profile of the type shown in Figure 3.35. A comparison of the revised maximum heat transport equation (3-43), with the expression derived by Cotter, equation (3-38), lead Ernst to believe that Cotter's expression tends to over-predict the maximum heat transfer capability of the heat pipe. In particular, for the 700°C sodium heat pipe for which the pressure profiles in Figure 3.32 were calculated; this over-prediction is approximately 40%. The extent of over-prediction, of course, will vary for different heat pipe geometries. Ernst also claimed that the maximum heat transfer capability

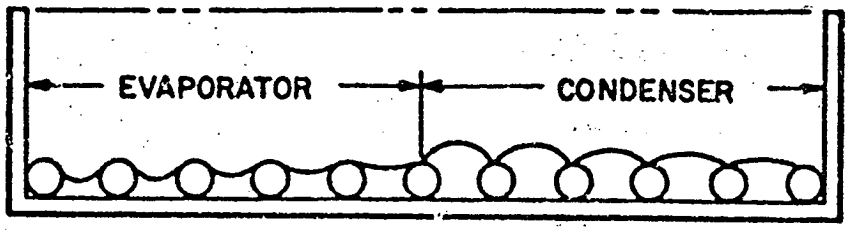

Figure 3.33 Interpretation by Ernst of Cotter's Liquid Profile for Optimized Capillary at Maximum Q, Ernst [54]

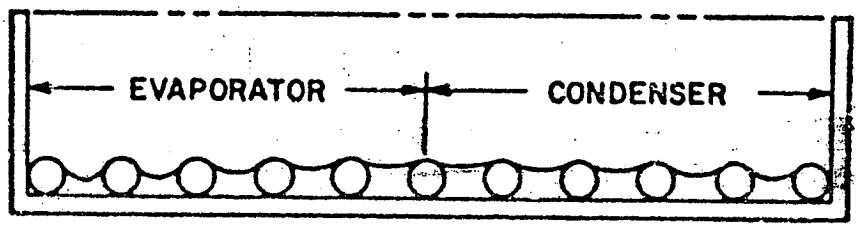

Figure 3.34 Revised Liquid Profile for Maximum Q, Non-Optimized Capillary, Ernst [54]

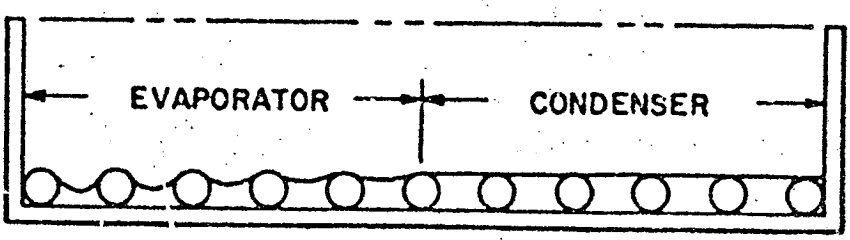

Figure 3.35 Revised Liquid Profile for Maximum Q, Optimized Capillary, Ernst [54]

of a heat pipe can be increased if the wick in the evaporator is different from the wick in the condenser. If the optimum mesh half-width in the evaporator and condenser are respectively

$$d_e = \left[(1+K)\frac{8b^2\rho\,\mu_\ell^2\,l_e^2}{\pi^2\rho_\ell^2\varepsilon^2\sigma\cos\theta}\right]^{1/3} \qquad (3\text{-}44)$$

and

$$d_c = \left[\frac{4\pi}{3}\frac{b\mu_\ell l_c\rho_v\,r_w^2\,h_{fg}}{\rho_\ell\,\varepsilon\,Q_m}\right]^{1/2} \qquad (3\text{-}45)$$

then the expression for the maximum heat transfer, given previously by equation (3-43), becomes

$$Q_m = \frac{4\pi\,r_w^2\,h_{fg}}{3}\left[\frac{1}{\pi^2(1+K)^2}\cdot\frac{\rho_v\rho_\ell\sigma^2\cos^2\theta}{b\,\mu_\ell\,l_c}\right]^{1/3} \qquad (3\text{-}46)$$

A comparison of equations (3-43) and (3-46) for a typical case where $\varepsilon = .8$ and $l_c = l_e$ accompanied by some calculations shows that the use of different wicks in the evaporator and condenser may increase the maximum heat transport capability of heat pipes by over 15%. The percentage increase varies from pipe to pipe depending on the evaporator and condenser lengths, and on the porosity of the capillary structure.

Many investigators have suggested various alternative expressions for the pressure drop in the gas and liquid for different heat pipe configurations which may be used in equation (3-29) instead of the pressure drops predicted by

Cotter as given by equations (3-24) and (3-25). Bohdansky et al. [46], for instance, recommended the following expressions for a heat pipe which employs axial channels for the liquid return and for which zero g, laminar, incompressible flow is assumed in both the liquid and the vapor:

$$\Delta P_v = \frac{8\dot{m}_v \mu_v l}{\pi \rho_v r_v^4} \qquad (3\text{-}47)$$

and

$$\Delta P_\ell = \frac{8\dot{m}_\ell \mu_\ell l}{\pi n K^4 r_{ch}^4 \rho_\ell} \qquad (3\text{-}48)$$

where K is a channel shape correction term which is approximately 1.3 for channels of rectangular cross section and depth equal to twice the width. Equations (3-47) and (3-48) were used to derive the following relations for the maximum heat transfer rate:

$$Q_{max} = \frac{\pi}{6} \frac{r_v^3 h_{fg}}{a l} \left[\frac{K^4 A}{2\nu_v^2 \nu_\ell}\right]^{1/3} \qquad (3\text{-}49)$$

where 'a' is a channel shape factor which has a value of about 2 for the channel discussed above, and 'A' is another dimensionless number defined by

$$n = \frac{A r_v}{r_{ch}} \qquad (3\text{-}50)$$

Notice that A is dependent on the number and spacing of the axial channels and has a maximum value of π. Equation (3-49) is of limited importance to the design engineer, because of the large number of dimensionless constants which must be employed, and the lack of a method for the

determination of these constants. Busse et al. [47] modified equation (3-49) so that all the dimensionless parameters are incorporated into one constant. His equation for the maximum heat flux is

$$q_{max} = \frac{.13\ \delta\ r_v \sigma h_{fg} \cos\theta}{l_{eff}} \cdot \frac{1}{\nu_v^{2/3}\ \nu_\ell^{1/3}} \qquad (3\text{-}51)$$

where δ is this dimensionless constant. If the channel depth is l_1, the channel width is l_2, and the dimension between channels is l_3, then δ is approximately .9 for $l_1 = 2l_2 = 2l_3$ and is approximately .5 for $l_1 = l_2 = l_3$. The term l_{eff} is defined by Busse as

$$l_{eff} = \frac{1}{q_{max}} \int \bar{q}(z)dz \qquad (3\text{-}52)$$

and is the so-called effective length of the heat pipe where $\bar{q}(z)$ is the average axial heat flux at any position, z, averaged over the pipe cross section. The inclusion of equation (3-52) into equation (3-51) would, however, cause the term of interest, i.e., q_{max}, to cancel. A more straightforward approach is to simply replace l_{eff} in (3-51) by l, the total heat pipe length.

Bohdansky and Schins [90] recommended the following expressions for the vapor and liquid pressure drop for turbulent flow:

$$\Delta P_v = \frac{.065}{\pi^{7/4}} \left(\frac{Q}{h_{fg}}\right)^{7/4} \frac{\mu_v^{1/4}\ l_{eff}}{\rho_v\ r_v^{19/4}} \qquad (3\text{-}53)$$

and

$$\Delta P_\ell = \frac{.065}{\pi^{7/4}} \left(\frac{Q}{nh_{fg}}\right)^{7/4} \frac{\mu_\ell^{1/4} l_{eff}}{\rho_\ell (Kr_{ch})^{19/4}} \qquad (3\text{-}54)$$

Equation (3-53) is obtained by a straightforward integration of equation (3-17). The expression for ΔP_ℓ is obtained in a similar manner but has been modified to account for channel shape by the dimensionless K term. As suggested above, l_{eff} should perhaps be replaced by the total heat pipe length. Equation (3-54) is very likely of limited value because the liquid flow will generally be laminar even for very high heat transfer rates.

Busse [123] considered laminar vapor flow in a cylindrical heat pipe which had an adiabatic section separating the evaporator from the condenser. For the case of constant heat addition and removal the vapor flow was described by the Navier-Stokes equation which was solved by approximating the axial velocity profile by a fourth power polynomial of the radius. The analysis furnished a velocity profile which was relatively constant along the evaporator; that is, it approached the Poiseiulle profile in the adiabatic section, and deviated considerably from the Poiseiulle profile in the condenser. The pressure drop in the evaporator is given by

$$P_v(z) - P_v(0) = \frac{-4\mu_v V_m l_e}{r_v^2} \left[1 + Re_r\left(\frac{7}{9} - \frac{8A}{27} + \frac{23A^2}{405}\right)\right] \frac{z^2}{\ell_e^2} \qquad (3\text{-}55)$$

where V_m is the axial velocity averaged over the cross section in the evaporator, and A is given by

$$A = \frac{15}{22}\left\{5 + \frac{18}{Re_r} - \left[\left(5 + \frac{18}{Re_r}\right)^2 - \frac{44}{5}\right]^{1/2}\right\} \qquad (3\text{-}56)$$

Equation (3-55) may be approximated with an error of less than 1% by

$$P_v(z) - P_v(0) = \frac{-4\mu_v V_m l_c}{r_v^2}\left[1 + .61Re_r + \frac{.61Re_r}{3.6+Re_r}\right]\frac{z^2}{l_c^2} \qquad (3\text{-}57)$$

The pressure drop in the adiabatic section is given by

$$P_v(z) - P_v(0) = \frac{-8\mu_v V_m z}{r_v^2}\left\{1 + \frac{r_v Re}{8z}\left[\frac{8}{27}(A-a) - \frac{23}{405}(A^2-a^2)\right]\right\} \qquad (3\text{-}58)$$

where Re is the axial Reynolds number defined by $Re = 2r_v V_m \rho_v/\mu_v$ and 'a' is a correction to the Poiseiulle velocity profile defined by

$$a\exp(-22a/75) = A\exp(-22A/75)\exp(-144z/5r_v Re) \qquad (3\text{-}59)$$

Typical values of 'a' are illustrated in Figure 3.36 for several radial Reynolds numbers. Equation (3-58) can be approximated with an error of about 1% by

$$P_v(z) - P_v(0) = \frac{-8\mu_v V_m z}{r_v^2}\left[1 + \frac{.106Re_r}{18+5Re_r} \cdot \frac{1-\exp(-30z/r_v Re)}{z/r_v Re}\right] \qquad (3\text{-}60)$$

The pressure distribution in the condenser section is given by

$$P_v(z) - P_v(z=l_c) = \frac{4\mu_v V_m l_c}{r_v^2}\left[1 - Re_r\left(\frac{7}{9} - \frac{8a}{27} + \frac{23a^2}{405}\right)\right]\left[1 - \frac{z}{l_c}\right]^2 \qquad (3\text{-}61)$$

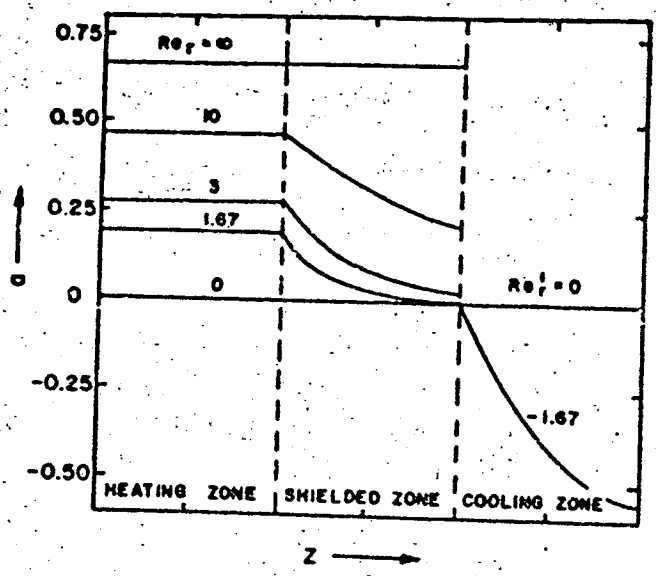

Figure 3.36 Velocity Profile Correction vs. Position in Heat Pipe, Busse [123]

where now 'a' is found by the solution of

$$\left[\frac{a_o - A}{a - A}\right]^{75/(22-A)} \left[\frac{a - B}{a_o - B}\right]^{75/(22-B)} = \left[1 - \frac{z}{I_c}\right]^{B-A} \qquad (3\text{-}62)$$

and

$$B = \frac{15}{22}\left\{5 + \frac{18}{Re_r} + \left[\left(5 + \frac{18}{Re_r}\right)^2 - \frac{44}{5}\right]^{1/2}\right\} \qquad (3\text{-}63)$$

Here a_o is the velocity profile correction at the beginning of the condenser section. From Figure 3.36 it is seen that $0 \leq a_o \leq .655$. Busse plotted the dimensionless pressure distribution in the condenser section as a function of dimensionless length as illustrated in Figure 3.37. Figure

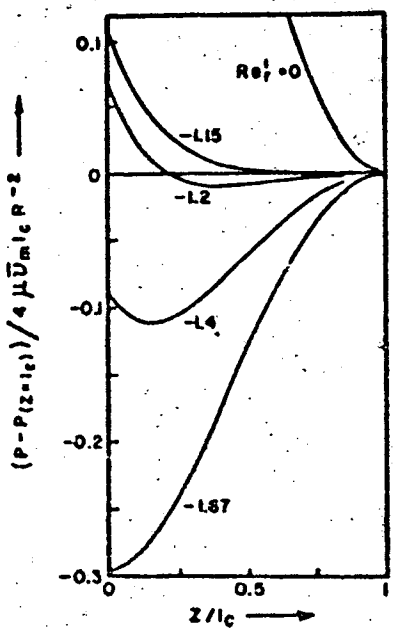

Figure 3.37 Pressure Profiles in Condenser, Busse [123]

3.37 represents the special case where the adiabatic section is so long that the flow at the beginning of the condenser has assumed a Poiseuille velocity profile, i.e., $a_o = 0$. It also shows that up to a certain radial Reynolds number a pressure minimum occurs at the end of the condenser and that increasing condensation rates tend to move this minimum toward the beginning of the condenser. The dislocation of this minimum indicates a partial pressure recovery. The pressure drop of the vapor which should be employed in an overall pressure balance equation, such as equation (3-29), depends on the net heat transfer of the heat pipe. Busse has mentioned that for strong heating and cooling rates a pressure equality exists in the vapor and the liquid phase

in the proximity of the beginning of the condenser. The observation was substantiated by Bohdansky et al.[76]; recall that Ernst also had noted this equality in pressures. For such a situation, only the vapor pressure drop in the evaporator and adiabatic section has to be taken into account for the calculation of the maximum heat flow. Thus a combination of equations (3-55) and (3-58) yields the total pressure drop in the vapor expressed by Busse as

$$\Delta P_v = \frac{4\mu_v V_m}{r_v^2}\left[l_e\left(1 + FRe_r\right) + 2\,l_a\right] \qquad (3\text{-}64)$$

where

$$F = \frac{7}{9} - \frac{8a_o}{27} + \frac{23a_o^2}{405} \qquad (3\text{-}65)$$

The factor F can be approximated with an error of less than 1% by

$$F = \frac{7}{9} - \frac{1.7Re_r}{36 + 10Re_r}\exp\left(\frac{-7.5\,l_a}{Re_r\,l_e}\right) \qquad (3\text{-}66)$$

and has values ranging from .61 to .81. On the other hand, for low heating and cooling rates, i.e., small Re_r, the pressure equality between the vapor and liquid will generally exist at the far end of the condenser. For this case knowledge of the pressure drop in the entire vapor space is required and Busse combined equations (3-55), (3-58), and (3-61) to arrive at the simple result

$$\Delta P_v = \frac{4\mu_v V_m}{r_v^2}\left(l_e + 2l_a + l_c\right) \qquad (3\text{-}67)$$

The relation was previously obtained by Cotter, equation (3-24), for a heat pipe with no adiabatic section, i.e., $l_a = 0$, where the bracketed lengths in equation (3-67) were replaced by the total heat pipe length. It is interesting to note that the length of the adiabatic section has more influence on the pressure drop than the contributions caused by the lengths of the evaporator or condenser.

Haskin [25] has dealt with a heat pipe containing an adiabatic section. He transformed equation (3-23) into

$$Q_o(z) = h_{fg}\dot{m}_v(z) = \begin{cases} zQ_e/l_e & ; \quad 0 \le z \le l_e \\ Q_e & ; \quad l_e \le z \le l_c \\ (1-z)Q_c/l_c & ; \quad l_c \le z \le 1 \end{cases} \qquad (3\text{-}68)$$

The pressure drop in the evaporator and condenser was obtained by substituting equation (3-68) into equation (3-15) and its subsequent integration. The pressure drop in the adiabatic section was found by assuming the existence of Poiseuille flow. The net end to end pressure drop for $Re_r << 1$ is given by the sum of the individual contributions

$$P_v = \frac{-4\mu_v Q_e \left(1 + l_a\right)}{\pi \rho_v r_v^4 h_{fg}} \qquad (3\text{-}69)$$

This expression is identical to equation (3-67) which was derived by Busse. For the case of $Re_r >> 1$, Haskin used equations (3-68) and (3-16) for the condenser and evaporator and applied equation (3-17) to the adiabatic section and obtained

$$\Delta P_v = \frac{-(1-4/\pi^2)Q_c^2}{8\rho_v r_v^4 h_{fg}^2} - \frac{.0655\,\mu_v^{1/4} l_a}{\rho_v r_v^3}\left(\frac{Q}{\pi h_{fg} r_v}\right)^{7/4} \qquad (3\text{-}70)$$

Notice that both equations (3-69) and (3-70) reduce to Cotter's results, equation (3-24), for the special case of $l_a = 0$. The equation for the pressure drop in the liquid was found to be identical to that obtained by Cotter, equation (3-25), with the exception that the length, l, in the viscous term is replaced by $\left(l + l_a\right)$.

Schwartz [58] has used Cotter's analysis and its extension by Haskin to display the liquid and vapor velocity and the vapor mass flow rate as a function of the heat load for a water-stainless steel heat pipe. The wick consisted of two layers of 100 mesh screen and the pertinent dimensions of the pipe were; $l_e = 3$ in., $l_c = 3$ in., $l_a = 8.5$ in., and $r_v = .189$ in. The results are presented in Figure 3.38, and are typical for a low temperature heat pipe. The vapor velocity decreases with increasing heat load due to the large vapor density variation in the temperature range of interest.

Werner [118] has employed Cotter's pressure balance, equation (3-29), for $Re_r >> 1$, and obtained in a computer calculation the axial heat flux and Mach number as a function of length for a 1500°K lithium heat pipe with $r_p = .5$ cm and $r_v = .4$ cm. The results of these computations are shown in Figure 3.39 illustrating the high

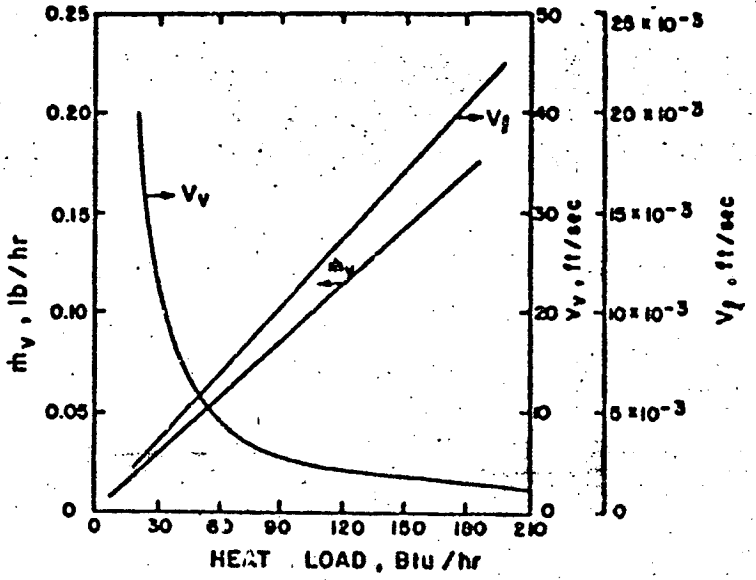

Figure 3.38 Calculated Heat Pipe Parameters vs. Heat Transport Rate, Schwartz [58]

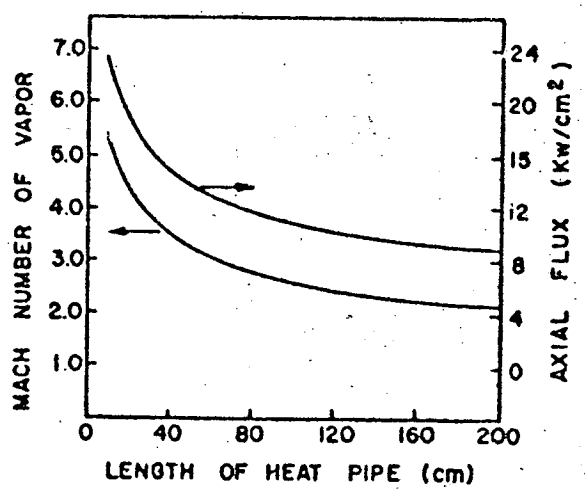

Figure 3.39 Calculated Axial Heat Flux and Mach Number vs. Length for Lithium Heat Pipe at 1500°K, Werner [118]

velocities and fluxes which may be obtained in a high temperature heat pipe. Figure 3.39, of course, is based on the equations for a capillary limited heat pipe and thus the flux rates may well exceed other heat pipe limits such as the entrainment or boiling limit. Werner and Carlson [105] modified equation (3-29) for the special case of a heat pipe with a capillary structure consisting of axial grooves covered by a single layer of screen material. If the intervening wall between grooves is negligibly thin at the inner radius, then the pressure drop in the liquid may be written as

$$\Delta P_\ell = \rho_\ell g l \cos\beta + \frac{3\mu_\ell Q l}{4(r_w - r_v)\pi h_{fg}\rho_\ell r_v r_c^2} \qquad (3\text{-}71)$$

where $(r_w - r_v)$ is the groove depth and r_c is the capillary radius (groove half width). Following a procedure identical to Cotter's and assuming no gravity effect, Werner inserted equation (3-71) into equation (3-29) and arrived at the following expressions for the optimum capillary radius and the maximum heat transfer rate:

$$r_{c,opt} = \frac{2B}{AC} \qquad (3\text{-}72)$$

and

$$Q_{max} = \frac{B}{A(r_{c,opt})^2} \qquad (3\text{-}73)$$

where

$$A = \frac{(1-4/\pi^2)}{8\rho_v r_v^4 h_{fg}^2}, \quad B = \frac{3\mu_\ell l}{4\pi(r_w - r_v)h_{fg}\rho_\ell r_v}, \quad C = 2\sigma\cos\theta.$$

In addition, he found that the maximum axial heat flux is obtained when $r_v/r_w = 5/6$ a value approximately 2.3% higher than the one found by Cotter ($\sqrt{2/3}$). Notice that Werner assumed the same size for the capillary radius and the groove half-width. Consequently the screen mesh size and the groove width can not be selected independently Hampel and Koopman [32] rectified this limitation by decoupling the channel dimension from the pressure supporting mesh dimension. The liquid flow in the channels was treated simply as flow through an annulus and corrected adequately to account for the actual area available to the flow. In addition, a scaling factor 'a' was introduced to account for the additional pressure drop induced by the channel configuration. For the case of $Re_r \gg 1$ and zero gravity effect, Hampel derived an equation similar to equation (3-29):

$$\frac{(1-4/\pi^2)Q^2}{8\rho_v r_v^4 h_{fg}^2} + \frac{2a\,\mu_\ell\, Q\, l}{e\rho_\ell \pi\, h_{fg} r_v \left(r_w - r_v\right)\left[r_w^2 + r_v^2 - \left(\frac{r_w - r_v^2}{\ln\left(r_w/r_v\right)}\right)\right]} \leq \frac{2\sigma\cos\theta}{d} \tag{3-74}$$

where 'd' is the screen mesh opening half-width and 'e' is the ratio of the active channel area to the total circumferential area of r_v. By differentiating equation (3-74) with respect to r_v, the resulting ratio, r_v/r_w, was found to no longer be a constant, i.e., $\sqrt{2/3}$ or 5/6, but to depend on the heat flux, the operating temperature, and the

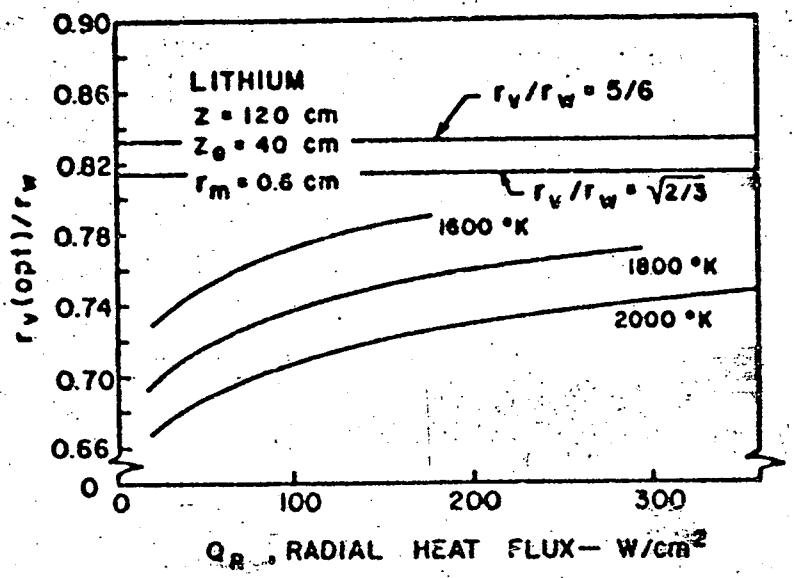

Figure 3.40 Optimized Relationship Between Vapor Radius and Wall Radius for Lithium Heat Pipe, Hampel and Koopman [32]

thermodynamic properties of the working fluid. Typical values for this ratio, r_v/r_w, are illustrated in Figure 3.40 for a high temperature lithium heat pipe.

Anand et al. [14] and Anand [96] employed advantageously, equation (3-56). The total length, l, was replaced by $\left(l_e + l_c\right)$ and the condenser length, l_c, was replaced by Q_e/C where C is a condenser parameter defined by

$$C = 2\pi \frac{k_w \left(T_v - T_w\right)}{\ln \left(r_p/r_v\right)} \qquad (3\text{-}75)$$

This procedure led to a quadratic term in Q with the solution

$$Q_{opt} = \left[\frac{1}{3} C\pi r_w^3 h_{fg} \sigma \cos\theta \left(\frac{2}{3} \frac{\rho_v \rho_\ell}{\mu_v \mu_\ell} \frac{\varepsilon}{b}\right)^{1/2} + \frac{C^2 l_e^2}{4}\right]^{1/2} - \frac{C l_e}{2} \qquad (3\text{-}76)$$

Equation (3-76) illustrates how a restraint on the axial heat transport capability is imposed by the radial heat flow in the condenser section. The condenser parameter, C, may be varied by wick flooding, introduction of noncondensable gases, or by manually changing the surface area. Equation (3-76) reveals the possible applicability of these techniques for heat pipe control.

Brosens [110] started with equation (3-19) and considered both the liquid and the vapor flows as laminar, steady and incompressible, i.e., Poiseuille flow. The wick structure was thought to consist of 'n' cylindrical capillary tubes and pressure equality was assumed at the far end of the condenser. For the case of zero gravity and perfect wetting of the wick, the expression for the maximum heat transfer was found to be

$$Q_{max} = \left[\frac{\sigma \pi h_{fg}}{4 \left[\frac{2}{r_c}\right]}\right] \Bigg/ \left[\frac{\nu_\ell}{n r_c^4} + \frac{\nu_v}{r_v^4}\right] \qquad (3\text{-}77)$$

The same result was independently arrived at by Schlinder and Wassner [124]. Brosens optimized equation (3-77) with respect to the capillary radius and obtained

$$r_{c,opt} = r_v \left(\frac{3\,\nu_\ell}{n\,\nu_v}\right)^{1/4} \qquad (3\text{-}78)$$

from which resulted

$$Q_{max,opt} = \frac{3\pi\,\sigma\,r_v^4\,h_{fg}}{16\,[2]\,\nu_v\,r_{c,opt}} \qquad (3\text{-}79)$$

The values predicted by equations (3-77) and (3-79) tend to be much larger than those measured experimentally. The deviations are caused by the many simplifying assumptions made during the derivation of these equations.

Frank et al.[30] used Poiseuille flow for the liquid and a modified Poiseuille flow for the vapor. He gave the vapor pressure drop as

$$\Delta P_v = \Phi_v \frac{8\mu_v l_f \dot{m}_v}{\pi r_v^4 \rho_v} \tag{3-80}$$

where l_f is the effective flow length and extends from the mid-point of the evaporator to the mid-point of the condenser, and the function, Φ, is given by

$$\Phi_v = \begin{cases} 1 & ; \quad Re \leq 2200 \\ .00494\ Re^{3/4} & ; \quad Re > 2200 \end{cases} \tag{3-81}$$

Notice that Φ_v is a discontinuous function at Re = 2200 (by approximately 50%), so some reservations as to its applicability in this range are indeed justified. Frank made use of equation (3-80) to derive an expression for the maximum heat transfer capability of a horizontal heat pipe:

$$Q_{max} = A_w \left[\frac{a\ \epsilon\ F_L}{32}\right] \left[\frac{D_1^2}{r_f^1}\right] N \tag{3-82}$$

where

$$a = \left(1 + \frac{r_1}{r_2}\right) \cos\theta \tag{3-83}$$

and

$$F_L = \left[1 + \Phi_v \left(\frac{\nu_v}{\nu_\ell}\right) \left(\frac{D_1}{2r_v}\right)^2 \left(\frac{\epsilon A_w}{\pi r_v^2}\right)\right]^{-1} \tag{3-84}$$

D_1 in the preceding expression is the hydraulic diameter of the capillary pores. Frank [26] next discussed the application of equation (3-82) for a grooved heat pipe and by assuming perfect wetting, i.e., a = 1, and by replacing by A_L/A_w, obtained for maximum heat flow

$$Q_{max} = \frac{F_L}{32 l_f} \cdot \frac{D_1^2 A_L N}{r} \qquad (3\text{-}85)$$

Referring to Figure 3.41, a number of auxiliary variables are defined. The mean radius of the grooves is

$$r_m = r_w - \frac{\delta}{2} = r_v + \frac{\delta}{2} \qquad (3\text{-}86)$$

while the dimensionless pitch of the grooves is given by

$$\beta = \frac{w + w'}{w} \qquad (3\text{-}87)$$

and the number of grooves is

$$n = \frac{2 \pi r_m}{\beta w} \qquad (3\text{-}88)$$

The aspect ratio of the grooves is defined by

$$\alpha = \frac{\delta}{w} \qquad (3\text{-}89)$$

and finally a depth ratio is given as

$$\psi = \frac{\delta/2}{r_m} \qquad (3\text{-}90)$$

By inserting equations (3-86) through (3-90) into (3-85) the following expression is obtained:

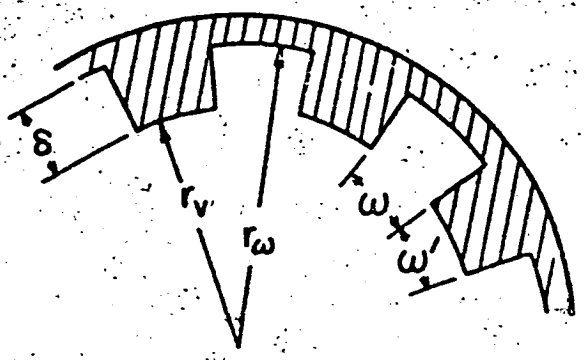

Figure 3.41 Sketch Illustrating Design Variables in Grooved Heat Pipe, Frank et al. [30]

$$\frac{Q_{max}}{r_w^3} = \frac{\delta C}{1+S} \cdot \frac{\alpha \psi^2}{(1+2\alpha)^2 (1+\psi)^3} \qquad (3\text{-}91)$$

where

$$C = \pi N/\beta l_f \qquad (3\text{-}92)$$

and

$$S = \frac{1}{F_L} - 1 \qquad (3\text{-}93)$$

Equation (3-91) was next extremized to yield the optimum value of Q_{max}/r_w^3 and if a bar is used to denote the optimum value, then the result is

$$\frac{\bar{Q}_{max}}{r_w^3} = C \frac{\bar{\psi}^2}{(1+\bar{\psi})^3} \cdot \frac{10\bar{\psi} - 1 - \bar{\psi}^2}{1 + 7\bar{\psi}} \qquad (3\text{-}94)$$

where $\bar{\psi}$ is given implicitly by:

$$\frac{(1-\bar{\psi})^5 (2-\bar{\psi})(1+7\bar{\psi})}{\bar{\psi}^3 (10\bar{\psi} - 1 - \bar{\psi}^2)^2} = \frac{16}{\beta} \left(\frac{\nu_v}{\nu_\ell}\right) \bar{\Phi}_v \qquad (3\text{-}95)$$

and $\bar{\alpha}$ is given by

$$\bar{\alpha} = \frac{(3+\bar{\psi})(1+\bar{\psi})}{2(10\bar{\psi} - 1 - \bar{\psi}^2)} \qquad (3\text{-}96)$$

In addition, since the optimum heat flow generally occurs when the vapor flow is turbulent, Φ_v may be written as

$$\Phi_v = .00494 Re^{3/4} = .00494 \left[\frac{2}{\bar{n}h_{fg}\mu_v}\left(\frac{Q_{max}}{r_w}\right)\left(\frac{1+\psi}{1-\psi}\right)\right]^{3/4} \qquad (3\text{-}97)$$

The solutions of equations (3-94), (3-95), (3-96), and (3-97) were obtained by Frank and are reproduced in Figures 3.42, 3.43, 3.44 and 3.45, respectively. The procedure for optimizing the ratio Q_{max}/r_w^3 is an iterative one. First, the effective flow length, l_f, the operating temperature, the working fluid, and the pitch, β, are selected. The pitch has a minimum value of unity and it is advisable to make it as small as possible. In general, the minimum value of the pitch will be imposed by machining and strength requirements. Once these values have been selected, an initial value of $\Phi_v = 1$ is assumed and $\bar{\psi}$ may be found from Figure 3.44. Using this value of $\bar{\psi}$, the optimum value of Q_{max}/r_w^3 can be taken from Figure 3.42 and Φ_v from Figure 3.45. If $\Phi_v \leq 1$, the vapor flow is laminar and no further iterations are required. If, on the other hand, $\Phi_v > 1$, then the prevailing vapor flow regime is turbulent and the procedure should be repeated using the new value of Φ_v to enter Figure 3.44. The optimum value of α can be found

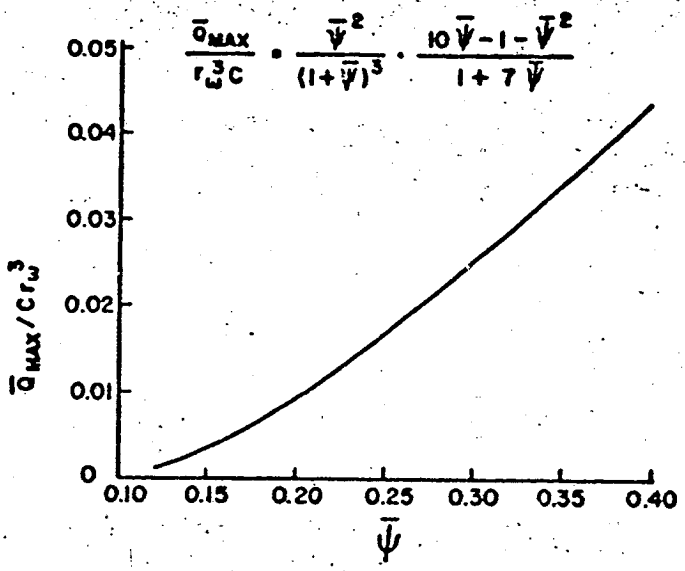

Figure 3.42 Optimum Value of Q_{max}/r_w^3, Franket al. [30]

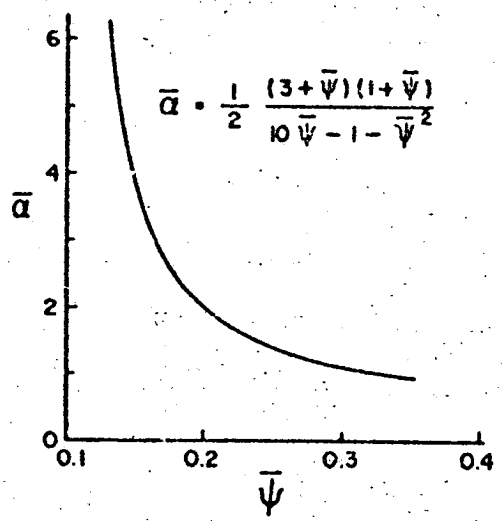

Figure 3.43 Optimum Value of α, Frank et al. [30]

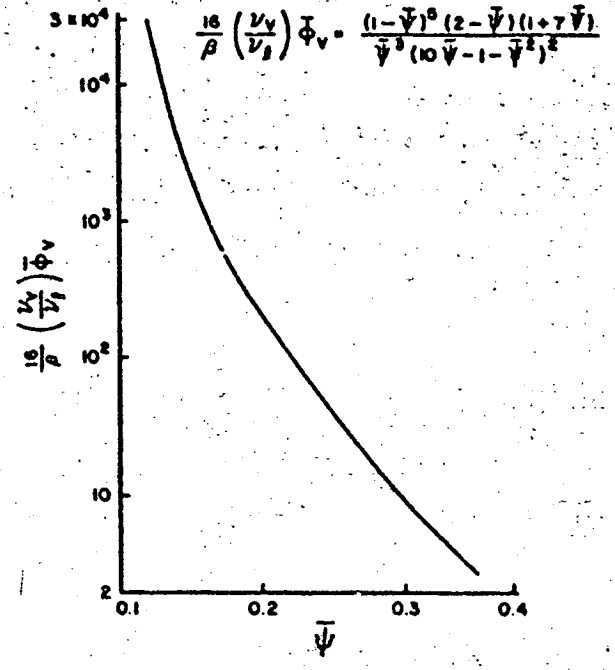

Figure 3.44 Optimum Value of ψ, Frank et al. [30]

from Figure 3.43 once the iteration procedure has converged to constant values of Φ_v. Frank claims that this convergence is rapid and may generally be accomplished by approximately three iterations. Completion of this procedure finally yields the optimum values of Q_{max}/r_w^2 and the aspect ratio, α. This implies that for a given heat pipe radius the maximum heat flow may be found, or conversely, for a given heat flow, the minimum pipe radius may be determined and, moreover, for both situations, the optimum groove shape (as given by the aspect ratio). Only the capillary limit to the maximum heat flow has been taken into account in the iteration procedure and other limits, such as the entrainment

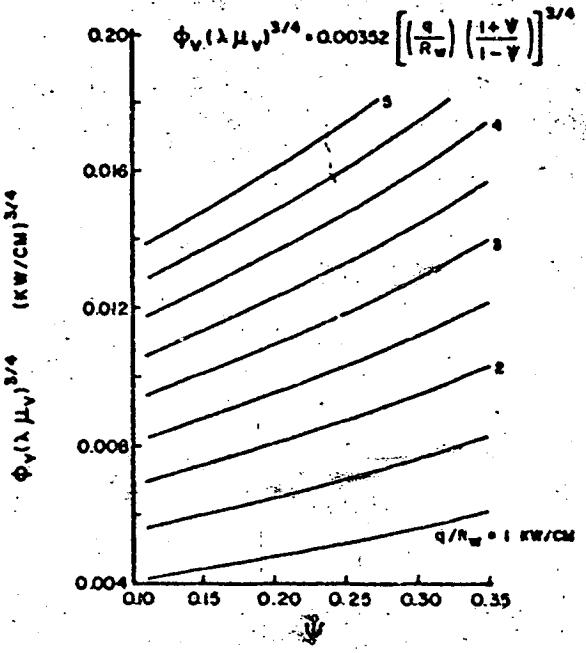

Figure 3.45 Graph for Determining ϕ_v, Frank et al. [30]

limit which is especially important for open grooves, may well pose additional restrictions and warrants further consideration.

McKinney [35, 91] discussed a heat pipe having an adiabatic section. He found for $Re_r \ll 1$ the pressure drop in the vapor to be identical to that reported by Haskin, equation (3-69). The resulting expression for the maximum heat transport rate was given as

$$Q_{max} = \left[\frac{2\sigma\cos\theta}{r_c} - \rho_\ell g l \cos\beta\right]\left[\frac{r_w^2 - r_v^2}{A\left[\frac{r_w^2 - r_v^2}{r_v^2}\right] + B}\right] \qquad (3\text{-}98)$$

where

$$A = \frac{4\mu_v\left(1+1_a\right)}{\pi\,\rho_v\,h_{fg}}, \qquad B = \frac{\mu_\ell\left(1+1_a\right)}{2\pi K\rho_\ell h_{fg}} \qquad (3\text{-}99)$$

For the case of $Re_r >> 1$, McKinney employed Cotter's results for the evaporator and condenser and assumed Poiseuille flow in the adiabatic section finding the heat flow

$$Q_{max} = \frac{-E + \left[E^2 - 4D\left(\rho_\ell 1\cos\beta - \frac{2\sigma\cos\theta}{r_c}\right)\right]^{1/2}}{2D} \qquad (3\text{-}100)$$

where

$$D = \frac{(1-4/\pi^2)}{8\rho_v h_{fg}^2\, r_v^4} \qquad (3\text{-}101)$$

and

$$E = \frac{8\mu_v\, 1_a}{\pi\rho_v h_{fg} r_v^4} + \frac{\mu_\ell\left(1+1_a\right)}{2K\,\rho_\ell\, h_{fg}\,\pi\left(r_w^2 - r_v^2\right)} \qquad (3\text{-}102)$$

Notice that for $Re_r >> 1$; McKinney worked with the Poiseuille flow assumption for the vapor in the adiabatic pipe section whereas Haskin assumed fully developed turbulent flow for the evaluation of the pressure drop. For intermediate axial Reynolds numbers, therefore, these two techniques may both be employed to encompass the actual pressure drop and the resultant heat transfer limit. McKinney with the aid of equations (3-98) and (3-100) developed a computer program for the graphical display of Q_{max} versus the ratio r_v/r_w for various adiabatic lengths, permeabilities, wetting angles, and temperatures. In all cases, the maximum heat transfer tended to maximize in the neighborhood of $r_v/r_w = .3$.

The reason for the large deviation of his value from the values obtained by Cotter and Werner, i.e., $\sqrt{2/3}$ and 5/6 respectively, cannot be explained without a more detailed study of the problem.

In all of the preceding analyses the pressure drop in the vapor space in one way or another was considered. Since for low temperature heat pipes this pressure drop may generally be assumed negligible, a quick estimate of the capillary limited heat flux can be obtained by regarding only the pressure drop in the liquid. Several authors whose results are discussed below have used this simplification. Phillips [29] and Phillips and Hindermann [53] applied Darcy's law to the liquid flow and arrived at equation (3-25) where 1 is replaced by $\left(l_e + 2l_a + l_c\right)$ from which he obtained for $l_a = 0$:

$$Q_{max} = 4\left[\frac{\sigma h_{fg}}{\nu_\ell}\right]\frac{KA_w}{r_c l} - 2\left[\frac{\rho_\ell h_{fg}}{\nu_\ell}\right] KA_w\, g\cos\beta \qquad (3\text{-}103)$$

In addition, he recommended the use of the following expression for heat pipes which employ a bypass or arterial type of wick:

$$\Delta P_\ell = \frac{8\pi\,\nu_\ell}{A_a^2}\frac{Q}{h_{fg}}\left[\frac{l_c}{2} + l_a + \frac{l_c}{2}\right] + \frac{\pi}{16}\frac{\nu_\ell}{K}\frac{\left(r_v + r_w\right)^2}{r_v\left(r_w - r_v\right)}\frac{Q}{h_{fg}}\left(\frac{l_c + l_e}{l_c - l_e}\right) \qquad (3\text{-}104)$$

The first term in equation (3-104) represents the pressure drop in the artery while the second term pertains to the pressure drop associated with the flow of liquid to and from

the artery in the circumferential direction. It is noteworthy that the effective length utilized in the pressure drop calculation equation (3-25), is essentially $l_e/2 + l_a + l_c/2$ and that $l_a = 0$, which reduces it to half of the total heat pipe length. Feldman [8] and Streckert and Chato [125, 126] have used the entire heat pipe length in their pressure drop calculations; consequently their resultant maximum heat transfer rate is one half of that calculated with equation (3-103). A similar analysis has been performed by Neal [28]. Langston and Kunz [13, 55] considered mass, momentum, and energy balances based on an elemental thickness of wick in the condenser. By assuming an infinite meniscus radius at the far end of the condenser and a minimum value at the condenser-evaporator interface, he obtained the limiting heat flux

$$Q_{max} = h_{max} K \left[\left(\frac{2\rho_\ell h_{fg} \sigma}{\mu_\ell} \right) \frac{A_w}{l_c} \left(\frac{g}{g_o} \frac{\rho_\ell}{\sigma} \right)_{WR} - \left(\frac{2\rho_\ell^2 h_{fg}}{\mu_\ell} \right) \frac{g}{g_o} \left(\frac{A_w}{h_{max}} \right) \cos\beta \right] \tag{3-105}$$

where the minimum meniscus radius has been evaluated from

$$r_{min} = \left(\frac{2\, g_o\, \sigma}{\rho_\ell\, g\, h_{max}} \right)_{WR} \tag{3-106}$$

The subscript, WR, refers to the temperature conditions at which the maximum wicking rise is measured. Implicit in the derivation of equation (3-105) is the assumption that

$\epsilon = 1$. Cosgrove et al.[37,38] extended the analysis of Langston and Kunz to include the effect caused by an adiabatic heat pipe section and the temperature variation of the fluid properties. The maximum heat transfer is then given by

$$Q_{max} = \frac{2K \epsilon A_w h_{fg}}{\left[\nu_\ell(T_c) l_c + 2\nu_\ell(T_a) l_a\right]} \left[\frac{g}{g_o} \frac{\sigma(T_a) \rho_{\ell WR} h_{max}}{\sigma_{WR}} - \frac{g}{g_o} \left[\rho_\ell(T_c) l_c + \rho_\ell(T_a) l_a\right] \cos\beta\right] \quad (3\text{-}107)$$

where T_a is the temperature of the adiabatic section and is equal to the saturation temperature of the fluid, and T_c is the condenser temperature and is taken as the average of the saturation and sink temperatures. Notice that for the special case of $l_a = 0$ equation (3-107) reduces to equation (3-105).

The above discussion has dealt solely with the capillary limit to heat pipe operation. As mentioned earlier this type of limit is especially important for low temperature applications where relatively low vapor velocities and heat fluxes prevail. For high vapor velocities, on the other hand, the sonic and entrainment limits become important. Levy [127] performed a one-dimensional compressible vapor flow analysis on a control volume basis restricted

to the vapor space. Two models were used to relate the thermodynamic properties in the vapor. First by treating the vapor as a perfect gas, the sonic limiting heat transfer rate was found to be

$$Q_{max} = \frac{\rho_v \pi r_v^2 V_a h_{fg}}{\sqrt{2(K+1)}} \qquad (3\text{-}108)$$

This condition is reached when the vapor flow chokes at the downstream side of the evaporator. The second model described a single-component equilibrium two-phase saturated vapor and the analysis to which it was applied yielded a complex trancendental equation for the limiting heat transfer rate. Equation (3-108) therefore may be used to obtain the theoretical limiting curves which were illustrated earlier in Figure 3.17. Levy compared the limiting heat transfer rates predicted with both models for a particular sodium heat pipe. These limiting rates are illustrated in Figure 3.46 as a function of temperature. Curve A was obtained with equation (3-108) while curves B and C represent the two phase model solutions. Curve B was calculated using the temperature at the upstream end of the evaporator and curve C was obtained using the temperature at the downstream end. Also displayed are the wicking limit derived from Cotter's fundamental equations and experimental data provided by Kemme [85]. Relatively good agreement is discernible between the sonic limiting curves and the experimental data for temperature less than 600°C. Above that

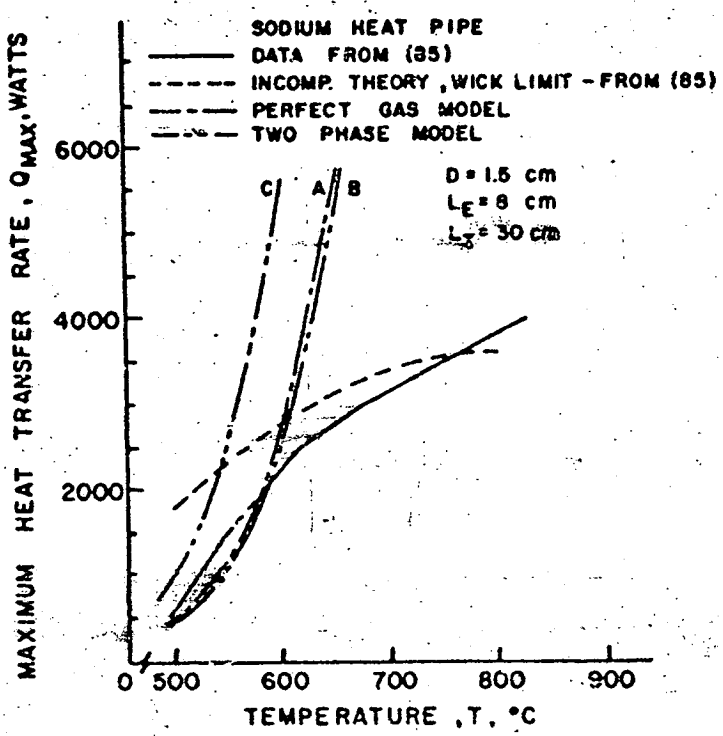

Figure 3.46 Comparison of Perfect Gas Model and Two Phase Model for Sonic Limit to Experimental Data, Levy [127]

temperature the sonic limit curve greatly overpredicts the measured maximum heat transfer rates and, in fact, the measured rates were probably limited by the pumping ability of the capillary system. It becomes also apparent from the agreement between curves A and B that the perfect gas model (equation (3-108)) is useful to estimate the heat transfer rate required to achieve choking within the evaporator section.

The theory of the entrainment limit has received little attention, the reason being the dependency of this limit on

the details of the geometry and the interfacial shear stress distribution. Cotter [19] and Kemme [86] claim that, for Weber numbers greater than unity, the possibility of entrainment exists. The Weber number is the ratio of inertial force to surface tension force written as

$$\text{Weber Number} = \frac{\rho_v V_v^2 \ell'}{\sigma} \qquad (3\text{-}109)$$

where ℓ' is a characteristic dimension associated with the wick surface. An estimate of the entrainment limited heat flux may be established by equating the Weber number to unity. This assumption, together with the energy equation (equation (3-19)), yields

$$\frac{Q_{max}}{A_v} = \left[\frac{\rho_v \sigma h_{fg}^2}{\ell'}\right]^{1/2} \qquad (3\text{-}110)$$

Kemme claimed that for screen wicks, the characteristic length, ℓ', is very nearly equal to the screen wire diameter and that it probably depends to some extent on the wire spacing.

The heat transfer limit associated with boiling within the wick did not receive much attention either. This type of limit is difficult to predict since it requires, among other properties, a thorough knowledge of the cavity dimensions in the wick and of the effective thermal conductivity of the saturated wick. The boiling limit was illustrated in Figure 2.7 and has to be considered as qualitative in

nature according to Deverall [18]. Notice that the limiting heat flux decreases with increasing temperature. Neal [28] took the superheat which is necessary for the incipience of nucleation in the wicking into consideration and related the superheat to the temperature difference existing across the wick in the evaporator and obtained for the boiling limited heat flux:

$$Q_{max} = \frac{2\pi\, l_e k_w}{\ln r_w/r_v} \frac{\sigma\, T_{sat}}{\rho_v\, h_{fg}} \left[\frac{2}{r_b} - \frac{\cos\theta_c}{2\pi\, \epsilon\, r_v}\right] \qquad (3\text{-}111)$$

Marcus [128] contributed yet another relation for the boiling heat transfer limit

$$Q_{max} = \pi\left(r_v+r_w\right)\left[\frac{T_{sat}\sigma\rho_\ell K l_e k_w \left(\frac{2}{r_b} - \frac{1}{2\pi\epsilon r_v}\right)\left(\frac{\sigma}{2\pi\epsilon r_v} - \rho_\ell g l\cos\beta\right)}{\mu_\ell\, l\, \rho_v}\right]^{1/2}$$

(3-112)

He further recommended to evaluate the effective wick conductivity with

$$k_w = \epsilon k_\ell + (1-\epsilon)k_{wick} \qquad (3\text{-}113)$$

Obviously the above expressions are quite different from the qualitative limit given by Deverall since both Neal and Marcus conclude that the limiting heat transfer increases with increasing vapor temperature. Hence the boiling limit curve, depicted in Figure 2.7, should have a positive slope instead of a negative one. A great deal more experimental

and theoretical effort must be expended before the boiling limit can be treated with sufficient confidence.

The foregoing discussions pertained to the numerous predictions of the maximum heat transport capability of heat pipes in view of the wicking, sonic, entrainment, and boiling limit respectively. Only a few analyses have been undertaken on other aspects of heat pipe technology.

Lyman and Huang [129] studied two dimensional liquid flow and heat conduction within the wick near the condenser entrance. Assuming constant pressure and a constant rate of condensation in the condenser he computed the temperature distribution in the wick. The results of his analysis are displayed in Figures 3.47 and 3.48. The numbers on the isotherms represent the temperature above the coolant temperature, T_c, in units of $\left(Q/bk_w\right)$ while the numbers on the adiabatic curves give the fraction of the heat flow, Q, which passes through the portion of the wick to the left of the curve. Figure 3.48 illustrates the dimensionless temperature distribution in the midplane and at the surface of the wick. For wick matrices of low conductivity large temperature gradients are possible in the wick at the junction between the adiabatic section and the condenser. Such temperature gradients have been observed qualitatively in several experiments with low temperature water heat pipes. Unfortunately in general, the thermocouples were not placed sufficiently close to accurately

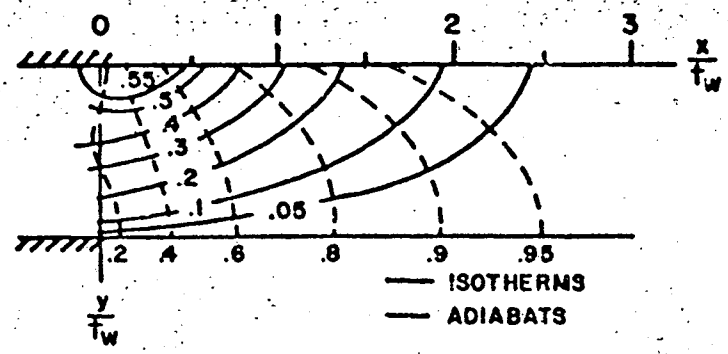

Figure 3.47 Isothermal and Adiabatic Curves in Condenser Wick, Lyman and Huang [129]

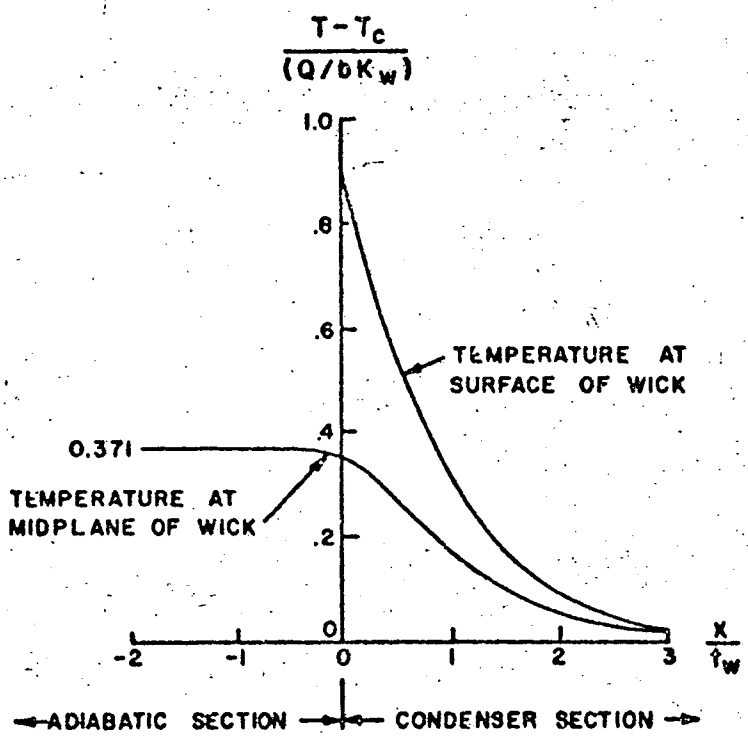

Figure 3.48 Temperature Distributions on Midplane and Surface of Wick, Lyman and Huang [129]

verify the steepness of the gradient. It should be emphasized that this analytical solution is applicable only to condensers with a fixed temperature boundary condition, e.g., calorimeter cooling. It is also evident that major condensation and the associated heat flow into the wick occur very near the entrance to the condenser section. The effective wick conductivity was calculated by assuming parallel heat conduction through the liquid and wick material as described by equation (3-113). Gorring and Churchill [130] and Nissan et al. [131] have suggested various techniques for the measurement and the computation of the effective thermal conductivity of other wick materials.

Bressler and Wyatt [132] solved the differential equation for the velocity during the transient capillary rise of a liquid in grooves of various geometries. The mean velocity is plotted in terms of dimensionless groups shown in Figure 3.49. The constant C equals $[2\ \csc^3(\beta/2) - 2\ \csc^2(\beta/2)]$, [2], $[8(\pi - 2)/\pi^2]$ and D is $[-\csc^2(\beta/2)]$, [2], [2], for triangular, semicircular, and square cross section grooves, respectively. For a given groove geometry, fluid properties, and temperature difference between the wall and liquid surface, $\left(T_w - T_s\right)$, the mean velocity $\bar{v}$ may be determined from Figure 3.49. The total heat flux at steady state can then be calculated from

$$Q = \rho_\ell \bar{v} A_L h_{fg} \qquad (3\text{-}114)$$

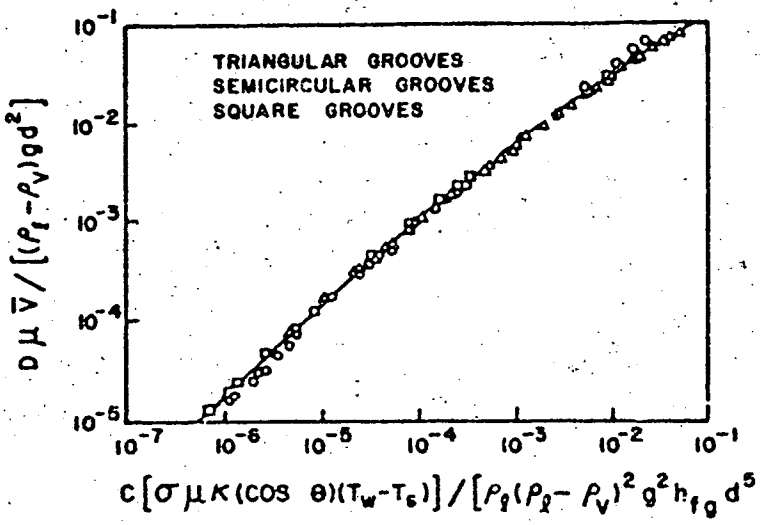

Figure 3.49 Calculated Mean Velocity in Grooves, Bressler and Wyatt [132]

Bressler used the above method to investigate the effect which groove geometry has on the maximum heat transfer. He found that a vertex angle of approximately 30° led to the highest heat transfer rates among triangular grooves. Furthermore, it was found that square grooves are characterized by the highest heat transfer rates per unit groove width when all grooves have an optimized depth. The results were different, however, when all grooves were compared at the same depth. Many more comparisons of groove characteristics may be made depending on the specific requirements to be evaluated.

In another study, Galowin and Barker [133] employed a two parameter, fourth order velocity profile in the Karman - Pohlhausen boundary layer integral method to determine

velocity and pressure fields in a two-dimensional heat pipe. The vapor was assumed to be incompressible while the injection and suction velocities at the wick surface were considered as small. For the case of $l_e = l_c = L$ and uniform injection and suction rates with a velocity V_w, the velocity and pressure distributions were found to be:

For $0 \leq z \leq L$:

$$V_m(z) = \frac{3V_w}{2} \left(\frac{L}{R}\right) \left(\frac{z}{L}\right) \qquad (3\text{-}115)$$

$$P(z) - P(0) = \frac{-3\mu_v V_w}{2R} \left(\frac{L}{R}\right)^2 \left(\frac{z}{L}\right)^2 \qquad (3\text{-}116)$$

For $L \leq z \leq 2L$:

$$V_m(z) = \frac{3V_w}{2} \left(\frac{L}{R}\right) \left(2 - \frac{z}{L}\right) \qquad (3\text{-}117)$$

$$P(z) - P(0) = \frac{3\mu_v V_w}{2R} \left(\frac{L}{R}\right)^2 \left[\left(\frac{z}{L}\right)^2 - 4\left(\frac{z}{L}\right) + 2\right] \qquad (3\text{-}118)$$

Approximate solutions were also obtained for the case where the injection velocity obeys a ramp function.

Miller and Holm [134] considered the possibility of using model heat pipes to predict the performance of different prototype heat pipes. A material preservation scheme was employed in which the same working fluid and wick material was used in both the model and the prototype. This implies that the thermal conductivities of the wall and wick, the emittance of the condenser surface, and the

permeability of the wick have to be preserved. With a starred quantity representing the model to prototype ratio of that quantity, the modeling equations are

$$\left(T_v - T_o\right)^* = q^*/\ell^* \qquad (3\text{-}119)$$

$$T_o^* = (q^*)^{1/4}/(\ell^*)^{1/2} \qquad (3\text{-}120)$$

and

$$q^* = N^* \ell^* \qquad (3\text{-}121)$$

Experimental verification of the above equations showed that prototype thermal behavior could be predicted from the model behavior to within 10°F over a temperature range of 140 to 330°F for a pair of water heat pipes. Modeling equations for another scheme which preserves the heat flux from model to prototype were also presented but an experimental verification was not attempted.

CHAPTER IV: THEORETICAL CONSIDERATIONS OF A TWO COMPONENT HEAT PIPE

The processes which take place within a two component heat pipe are considerably more complex than those encountered in a more conventional single component heat pipe. In addition to variations in velocity, pressure and temperature, concentration changes may occur throughout both the vapor and liquid phases. If it is assumed that local equilibrium conditions are present between the liquid and vapor, then the addition of a second component, in effect, provides an extra degree of thermodynamic freedom in the pipe; thus both the pressure and temperature must be specified to completely determine the state of the mixture at a given location. Additional modes of mass transport, such as diffusion, must also be taken into consideration.

The phenomena which occur in the vapor core of a two component heat pipe are described by a set of eight coupled, nonlinear, second order, partial differential equations. If the vapor behavior may be regarded as two dimensional, then these equations include the momentum equations in each coordinate direction, the energy equation, two mass flux equations, an equation of state, and two continuity equations.

The latter two equations are required because the total mass and the mass of each component must be conserved which leads to three continuity equations, however, only two are independent. The eight equations mentioned above represent the relationship between the eight unknowns:

$u(x, y)$	$\rho_1(x, y)$
$v(x, y)$	$\rho(x, y)$
$j_{1x}(x, y)$	$T(x, y)$
$j_{1y}(x, y)$	$P(x, y)$

The solution of these equations requires a complete specification of the physical properties as well as a sufficient number of boundary conditions to define the problem. A consideration of the equations indicates that twenty boundary conditions are necessary. The velocity boundary conditions are easily specified by applying the no-slip condition at the end walls and wicks and by assuming some sort of injection velocity distribution at the wick surface. This injection velocity distribution is of course coupled to the external conditions applied on the container wall; e.g. it depends on whether constant temperature or flux conditions are utilized for the ultimate source and sink. The temperature gradients normal to the end walls may also be assumed to be zero if the end walls are treated as adiabatic surfaces. The commonly applied condition of symmetry

about the pipe centerline is not applicable due to the presence of the body force term which tends to produce an asymmetric density and temperature distribution depending on the pipe's orientation with respect to gravity. Moreover, the density boundary conditions at the wick surface are not uniquely determined. In fact, to establish only the ratio of component density to mixture density (or mass fraction) at the wick surface requires a prior knowledge of both the local temperature and pressure as well as an experimentally determined equilibrium curve relating pressure, temperature, and mass fraction. Considering the above difficulties, it is not surprising that the equations have not been solved.

The prediction of complete component separation as presented by Cotter [4] is based on the assumption that only axial variations of temperature and concentration occur. His prediction is based solely on the criteria of mass conservation and a consideration of the equilibrium curve for the binary two phase mixture. The characteristics of binary equilibrium curves are discussed in great detail by Bosnjakovic and Blackshear [135]. A typical set of such curves for the binary system water-methanol is illustrated in Figure 4.1 using data from references [136, 137]. Each enclosed curve represents the temperature and concentration characteristics at a liquid vapor interface for a given pressure. For a particular pressure, any point below the closed curve represents a liquid phase only, while any point above the closed curve indicates that only the vapor phase

exists. For points which fall inside of the curves, however, both phases are present. The compositions in the liquid and vapor are now determined by the intersection of the prevailing temperature line with the lower and upper branches of the curve, respectively. This implies that whenever a two component, two phase mixture with an equilibrium diagram of the type illustrated in Figure 4.1 exists, the vapor phase is always richer in the more volatile component than the liquid phase. If this is the case, then Cotter argued as follows. The same total amount of mass must be moving in opposite directions in the vapor core and in the liquid saturated wick at any given axial position to satisfy continuity. However, if the vapor is richer in one component, then more of that component is entering the condenser end of the pipe than is leaving. The net transfer of the more volatile component to the condenser end would continue until the two components are completely separated. Since the pressure in the vapor core is nearly constant, a complete separation into pure components would manifest itself by significant temperature variations from one end of the pipe to the other. In fact, where each pure component exists, the temperature would tend toward the saturation temperature of that component as determined by the prevailing pressure. The result would be a temperature distribution along the pipe that consists of two plateaus with some transition region between them.

The one dimensional argument discussed above appears to be highly idealistic. Since the velocity and pressure fields

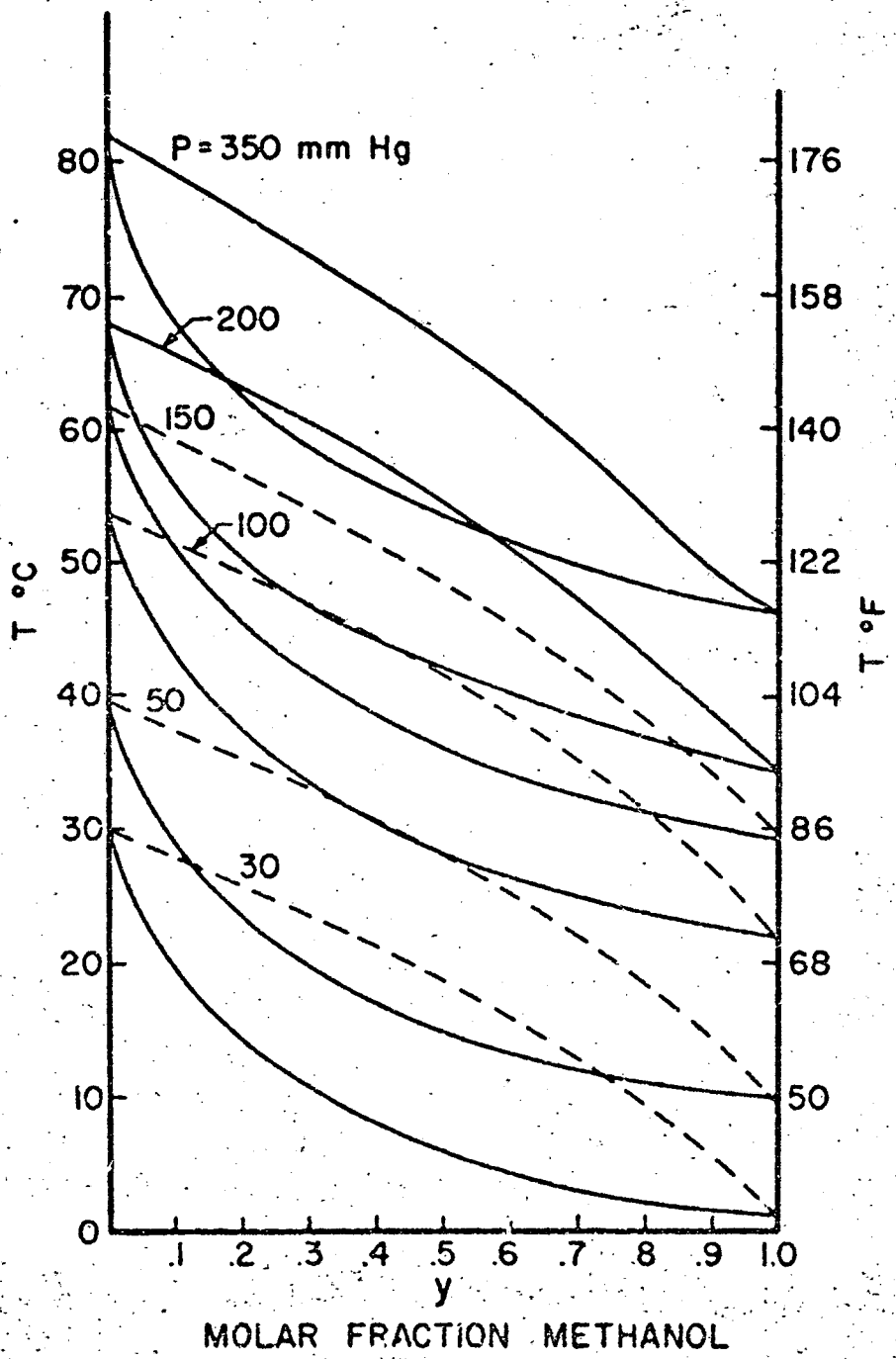

Figure 4.1 Equilibrium Diagram for Water-Methanol

are obviously two dimensional (due to the injection and suction at the wick interfaces), there would seem to be no logical reason to assume that the concentration distribution is also not two dimensional. If this is the case then the vapor must be richer in the more volatile component only in the immediate vicinity of the liquid vapor interface. The conservation of species requirement would then mean that at each axial position the following condition must be satisfied.

$$\int_{\text{vapor}} \rho_{1v}(y)u_v(y)dy = \int_{\text{wick}} \epsilon\rho_{1\ell}(y)u_\ell(y)dy \qquad (4\text{-}14)$$

An infinite number of component density and velocity distributions exists which satisfy the above equation. It is readily apparent that situations may exist where a partial separation of components is possible. The exact nature of the resulting component distribution, however, must be determined either experimentally or from the solution of the eight equations mentioned earlier.

Since a solution to the equations is virtually impossible due to an insufficient number of boundary conditions, an experimental solution to the problem was instigated. The experimental apparatus employed and the results obtained with it in the investigation are described in subsequent chapters.

CHAPTER V: EXPERIMENTAL APPARATUS

Introduction

The experimental program consisted of three phases. During the early stages of the investigation it was decided that some effort should be committed to the study of wicking materials. It was felt that an adequate knowledge of various types of wicks was a prerequisite to the design of heat pipes. Of special interest was the maximum height to which liquids could be raised by capillary forces. Of equal importance was the magnitude of the velocity at which fluid could be delivered at any chosen height in the wick. This velocity can then be used to calculate a conservative limiting mass circulation rate assuming that all of the liquid is removed from the wick at a particular height. The product of this mass circulation rate and the latent heat of vaporization provides a measure for the maximum heat transport capability of a heat pipe. The validity of using a dynamic velocity measurement technique to predict the steady state mass flow within a saturated capillary structure is somewhat questionable. Wetting difficulties associated with the moving liquid interface most certainly impede the flow. The difference between the rising and falling equilibrium heights discussed earlier in the literature survey was also

attributed to such wetting problems. However, a qualitative comparison of capillary induced mass flow rates may certainly be made using this technique.

Hence an apparatus was designed and constructed which allowed in one experiment the measurement of both the maximum wicking height and the liquid velocity as a function of height. Later a conventional cylindrical heat pipe was constructed and operated with a single component fluid. The construction of and experimentation with a co-planar heat pipe concluded the experimental phase of the investigation. The dimensions of this rectangular heat pipe were such that it should, however, be referred to as a vapor chamber. Two side walls were made transparent to allow visual and optical observations of the wick and the vapor core. Experiments in this heat pipe were performed with both single and two component working fluids.

Wick Investigation

For this phase of the investigation an apparatus was developed which allowed the advancing liquid front in a porous sample to be continuously monitored. The apparatus consisted of a rigid balance beam to which the test specimen was attached at one end and compensating balance weights at the other (see Figure 5.1). The beam was supported on a sharpened tool steel fulcrum which could be adjusted according to the weight of the test specimen. Once the dry specimen was balanced with the compensating weights, a Daytronic

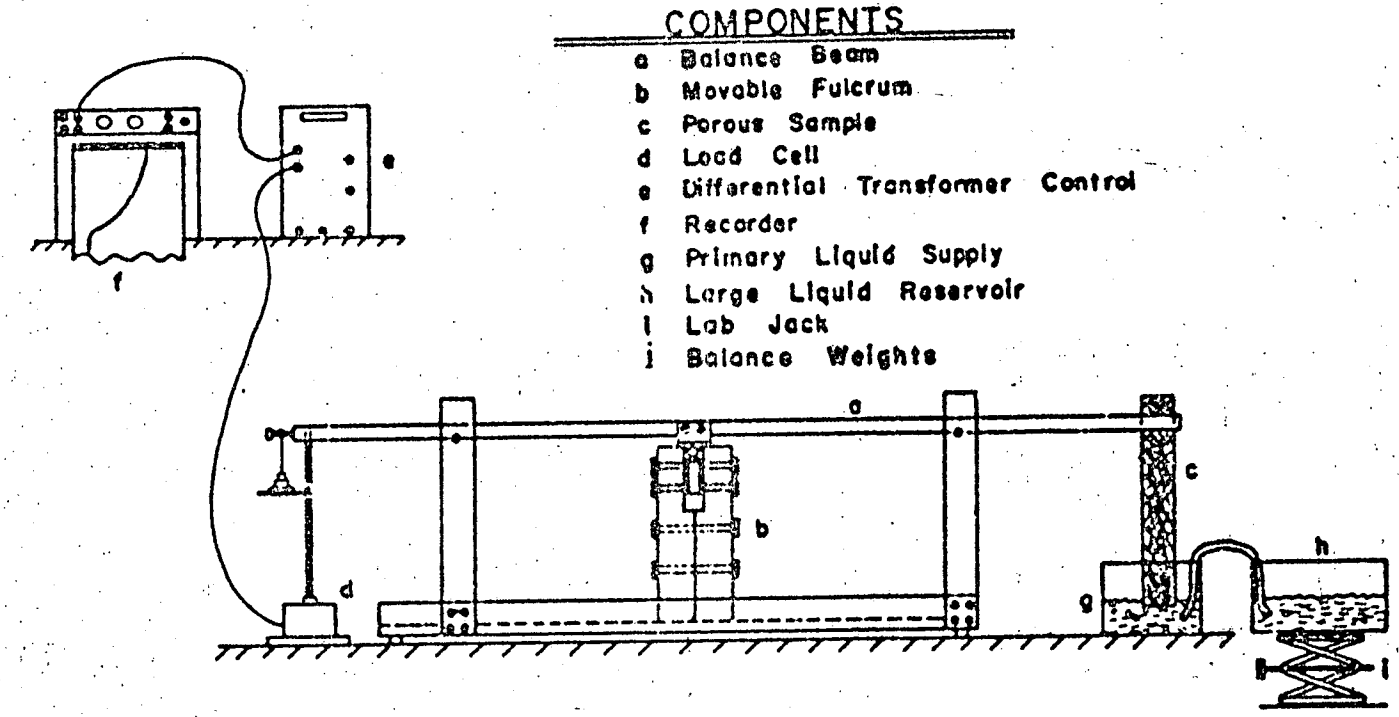

Figure 5.1 Diagram of Balance Beam Apparatus

(152A-1) load cell was rigidly attached adjacent to the compensating weights. The liquid level in the pan beneath the specimen was then slowly raised by adjusting the height of a larger liquid reservoir which was connected to the pan with a flexible syphon tube. This method of liquid height control eliminated any surface disturbances in the pan beneath the specimen and also guaranteed a constant liquid level as the specimen began to transport liquid from the pan. The rising liquid exerted a force on the beam which was sensed by the load cell and converted into an electrical signal which was suitably amplified and finally recorded with a Honeywell strip chart recorder. With known porosities of the test specimens and measured distances between fulcrum and the supporting point of the specimen and between fulcrum and the attachment of the load cell respectively, the strip chart recording could easily be converted to a transient liquid height versus time graph. The maximum wicking height was simply the height at which no further variation of the signal could be detected.

Eleven porous metal specimens acquired from the General Electric Company were tested. The porous metals are marketed under the trade name of "Foam Metal". They had various porosities and were fabricated from two different materials, nickel and copper. Of the eleven specimens, only the two nickel samples of the highest density yielded repeatable data. It is believed that the copper specimens oxidized

and that their wetting properties decreased to such an extent that essentially no water could be "wicked". The maximum wicking height obtained with one of the nickel samples was 16.5 cm.

Cylindrical Heat Pipe

Next a conventional cylindrical heat pipe was constructed. The heat pipe was composed of three sections bolted together resulting in an overall length of 71.1 cm (see Figure 5.2). The two end sections were made of 2.54 cm O.D. brass tubing while the center section was made of 2.54 cm O.D. stainless steel tubing. The lengths of the evaporator, adiabatic, and condenser sections were respectively 24.1 cm, 20.3 cm, and 26.7 cm. The sections were separated from each other by bakelite rings which were sealed with sheared annealed copper gaskets. The bakelite rings as well as the low thermal conductivity stainless steel adiabatic section reduced the axial heat conduction through the container walls. The brass walls of the condenser and the evaporator tended to reduce the radial temperature drop.

The condenser was surrounded by a 5.08 cm O.D. stainless steel tube. Cooling water supplied from a constant head supply tank was pumped through the annulus (see Figure 5.3). Since the pump was a constant displacement pump, a bypass line to the condenser was required to regulate the water flow through the condenser annulus. By observing the

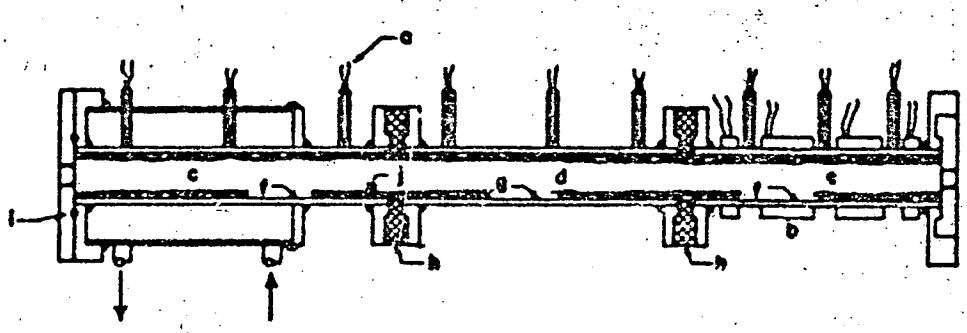

COMPONENTS

a	Thermocouple Junctions	f	Brass Tube
b	Band Heaters	g	Stainless Steel Tube
c	Condenser Section	h	Bakelite
d	Adiabatic Section	i	"O" Ring
e	Evaporator Section	j	Wick

Figure 5.2 Cylindrical Heat Pipe

flow meter in the main line and by adjusting the valves in both lines, any given flow rate from 8.7 liters per minute to 178 liters per minute could be easily maintained.

Nine chromel-alumel thermocouples were placed firmly against the exterior of the container wall at various axial positions. Thermocouple potentials were measured with a potentiometer by selecting any desired thermocouple with an isothermal switch. The reference junction was immersed in a distilled water-ice bath.

Four Ogden hose clamp type band heaters were installed firmly around the evaporator. The power input was controlled with a Powerstat and monitored with a wattmeter. The maximum power input was 1000 watts.

Small access tubes were provided on both ends of the heat pipe. The tube at the condenser was utilized for

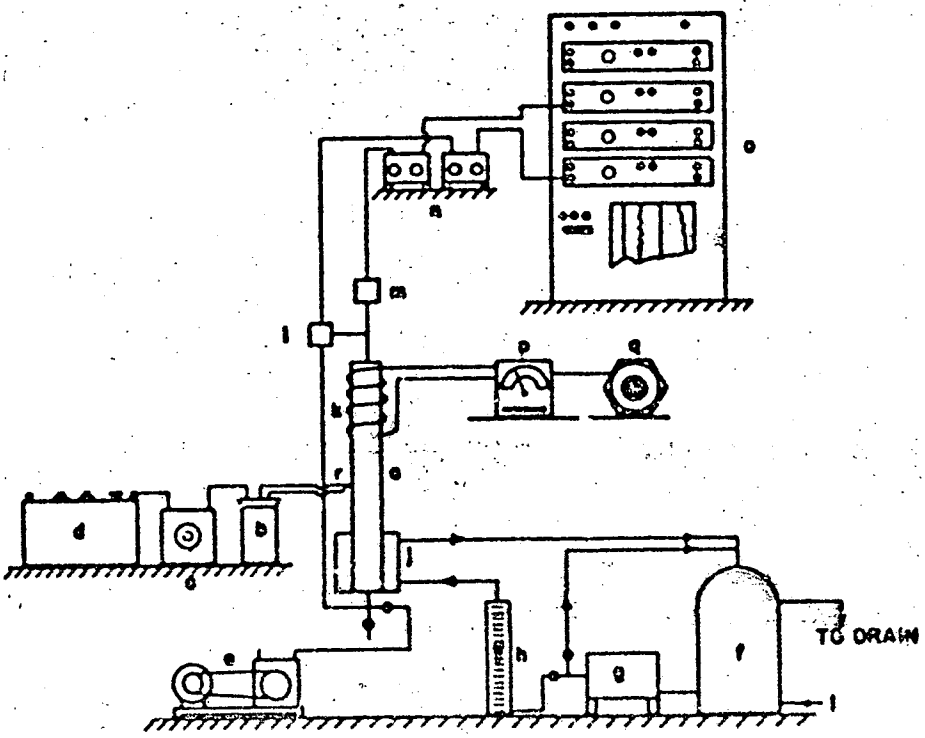

COMPONENTS

a	Cylindrical Heat Pipe	j	Condenser
b	Ice Bath	k	Resistance Heater
c	Isothermal Switch	l	Differential Pressure Transducer
d	Potentiometer	m	Absolute Pressure Transducer
e	Vacuum Pump	n	Carrier Demodulators
f	Constant Head Tank	o	Recorder
g	Pump	p	Watt Meter
h	Flow Meter	q	AC Power Variac
i	Building Water Supply	r	Thermocouple Junctions

Figure 5.3 Schematic Diagram of Cylindrical Heat Pipe Facility

fluid addition or removal, and if desired, for the evacuation of the pipe with a mechanical vacuum pump. In operation it also served as a pressure tap connection to a differential pressure transducer. The access tube on the evaporator was connected to the other side of the differential pressure transducer and also to an absolute pressure transducer, both manufactured by the Pace Engineering Company. The pressure signals were amplified with a Pace carrier demodulator, model CD-10, and finally recorded with a four channel Sanborn recorder. Prior to operation the differential transducer was calibrated against different heads of water acting on one side of the diaphragm, while the other side remained exposed to the atmosphere. Full scale deflection on the Sanborn recorder was obtained for pressure differentials ranging from +1 psi in the evaporator to +1 psi in the condenser. Based on repeated calibrations, the accuracy obtained was ± .02 psi for any given pen position. The absolute pressure transducer was calibrated with a Heise pressure gauge and full scale pen deflection was obtained for absolute pressures ranging from 0 to 45 psia. The accuracy for any given pen deflection was ± .4 psia.

The heat pipe was mounted on a pivot which allowed the pipe to be operated in any orientation with respect to gravity. Although two wicks were employed during the experiments, for the majority of the experiments a wick consisting of four layers of 150 mesh stainless steel screen with a

wire diameter of .0026 inches was used. The screen was held firmly against the interior of the container wall by a coiled steel spring. Prior to assembly, the pipe interior, as well as the screen wick and spring were thoroughly degreased by repeated rinses with trichlorethylene, ethanol, and distilled water. In addition, the stainless steel screen was passivated with a dilute nitric acid solution. The other wick used consisted of a silicon oxide cloth which is marketed under the trade name of Refrasil by the Hitco Company. The particular form of this cloth used was a braided tubular sleeving with a nominal inner diameter of 1.91 cm. The sleeving was retained in the heat pipe in an annulus between the container wall and a smaller diameter perforated teflon tube.

The pipe was primarily operated in the horizontal or near horizontal orientation both with and without insulation. The insulation consisted of approximately 3 inches of vermiculite which completely surrounded the entire pipe. This insulation material was chosen because it could be simply poured into a retaining structure which surrounded the heat pipe and was likewise, easily removable.

The energy transported from the evaporator to the condenser was calculated in the following manner. The pipe was first evacuated and if desired, insulated. The power input was selected, and once steady state operating conditions were achieved nine axial temperatures were recorded. This

procedure was repeated for several power inputs. The heat pipe was divided into nine segments, each segment containing one of the thermocouples. The initial evacuation of the pipe insured that all energy added was either lost from the surface of a particular segment, or conducted to the next segment, i.e. no energy was transferred through the vapor core. Energy balances were made for each segment and the heat loss from each segment was computed. This loss and the measured temperatures were then used to calculate the thermal resistance between each segment and the surrounding environment. Since the pipe was run at various power levels, and consequently various temperatures, these thermal resistances were established as a function of temperature in each segment. For the actual heat pipe test, the temperatures were again measured and again an energy balance was made, this time however including energy transfer within the vapor space. The heat loss from each segment was found by employing the temperature dependent thermal resistances obtained with the evacuated pipe. The heat transfer rate due to heat pipe action was considered to be the sum of the energy transfers to the vapor core in the evaporator. For the uninsulated case, the accuracy of the above method was very good. During the determination of the external thermal resistances as a function of temperature, a minimum of 95.4% of the energy input could be accounted for, while for the insulated cases, a minimum of 87.4% could be accounted for.

The working fluid in all tests was distilled water. The pipe was charged initially with a measured quantity of water after which it was placed in a vertical position with the evaporator below the condenser. The heaters were turned on and steam and air were ejected from the pipe at the top where the steam was condensed, collected and measured. When the collected condensate indicated that the desired amount of water remained in the pipe, a valve was shut and the pipe was ready for operation. The vacuum pump was employed to periodically withdraw noncondensable gases which occasionally accumulated in the pipe. The experimental data obtained with this heat pipe will be presented and discussed in chapter VI.

Rectangular Heat Pipe

A rectangular geometry was employed so that two sides could be made of glass, allowing visual observations of the wick, and possible optical measurements of phenomena occurring in the vapor core. The dimensions of the vapor space were 35 cm from end to end, by 22.7 cm from window to window, by 14 cm from wick to wick (see Figure 5.4). The entire structure was made of stainless steel with .635 cm plates used for the longer side walls and 2.54 cm plates employed for the ends. The plates were welded together and the sides for the mounting of the windows were machined and ground flat and parallel. The windows were 1.43 cm thick and were held in place with two brackets which fastened to

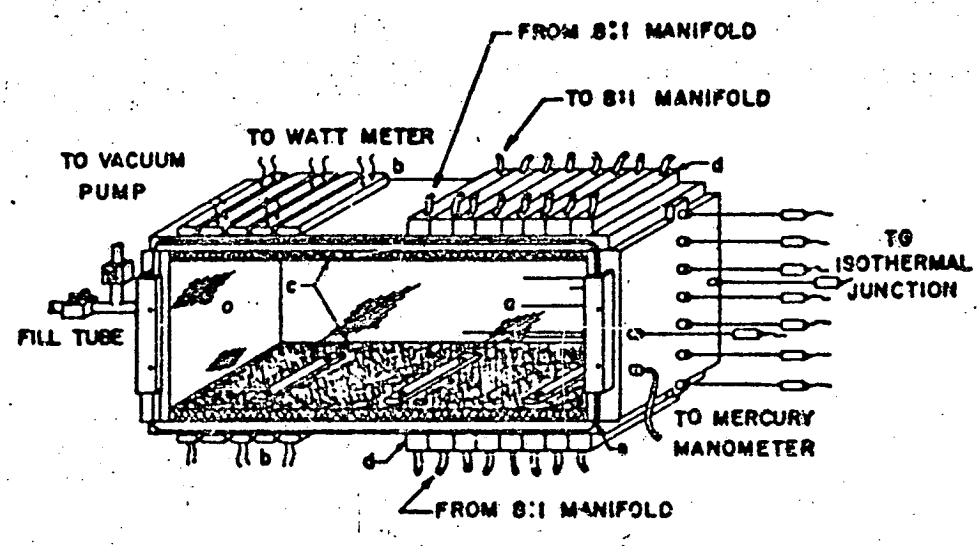

Figure 5.4 Rectangular Heat Pipe

the end plates. Natural rubber gaskets together with a thin film of vacuum grease provided the seal between the windows and the stainless steel walls. The structure was mounted on a stand which permitted the pipe to be positioned in any orientation with respect to gravity.

The wick consisted of two porous .635 cm thick sheets of sintered nickel fiber. These were manufactured by the Huyck Metals Company under the trade name of "Feltmetal" and the particular form employed was FM315. The porosity was given as 85% and the average pore size was 74 microns. The wicks were held firmly against the interior walls of

the pipe with three brass strips which were screwed against the .635 cm stainless steel plates.

Packing glands were provided on the condenser wall for nine thermocouple probes. Seven were symmetrically placed on the centerline between the two windows and two were placed close to the windows to check the two-dimensionality of the device. Two types of probes were used. The uppermost and lowermost probes on the centerline were purchased from the Conax Corporation and were 1 mm in diameter. The other probes were made "in house" and were 1.8 mm diameter and 40 cm long, and were of the copper-constantan type. The packing glands contained a teflon bushing which was compressed against the probe shaft to provide a leak proof seal and yet permitted movement of the probes to any desired location. The two smaller diameter probes were located in thin grooves cut into the underside of the wick material.

The thermocouple probes were calibrated against a mercury in glass thermometer which could be read to the nearest .2 °F. A thermostatically controlled bath provided constant temperatures for calibration from 55 °F to 151 °F. For convenience, a least square fit straight line was fit through the calibration points and extended for all temperatures measured during the experiments. The accuracy of this technique within the calibration range was ± .5 °F. For temperatures considerably in excess of 151 °F, the error was estimated to be somewhat greater due to the nonlinearity

of the thermocouples; however, it was anticipated, and later justified, that such high temperatures occurred only under dry out conditions in the wick and hence an accuracy of ± 1 1/2 - 2 °F was adequate.

The wiring diagram for the temperature measurement system is illustrated in Figure 5.5. Eleven thermocouple junctions were used in the experiments. During the early tests two dimensionality of the device was ascertained and subsequently only seven thermocouples were employed in the heat pipe, all located midway between the windows. The remaining thermocouples were used to measure the ambient air temperature, thermostat bath temperature, and the inlet and outlet temperatures of the condenser coolant. All thermocouple voltages were measured against a single reference junction which was immersed in a distilled water-ice mixture. All wire connections were made in an isothermal enclosure, and solid copper wires housed in a shielded cable led to an isothermal switch and ultimately to a digital volt meter of the type Vidar 510 Integrating Digital Voltmeter (DVM). The inaccuracy of this instrument according to the Vidar Manual is "typically less than ± .07% at full scale including the effects of non-linearity, 24-hour drift, 5 °C temperature change, 10% line voltage change and attenuator inaccuracy all added in rms fashion". The drift problem was reduced by re-calibration of the DVM which was done immediately prior to any data acquisition.

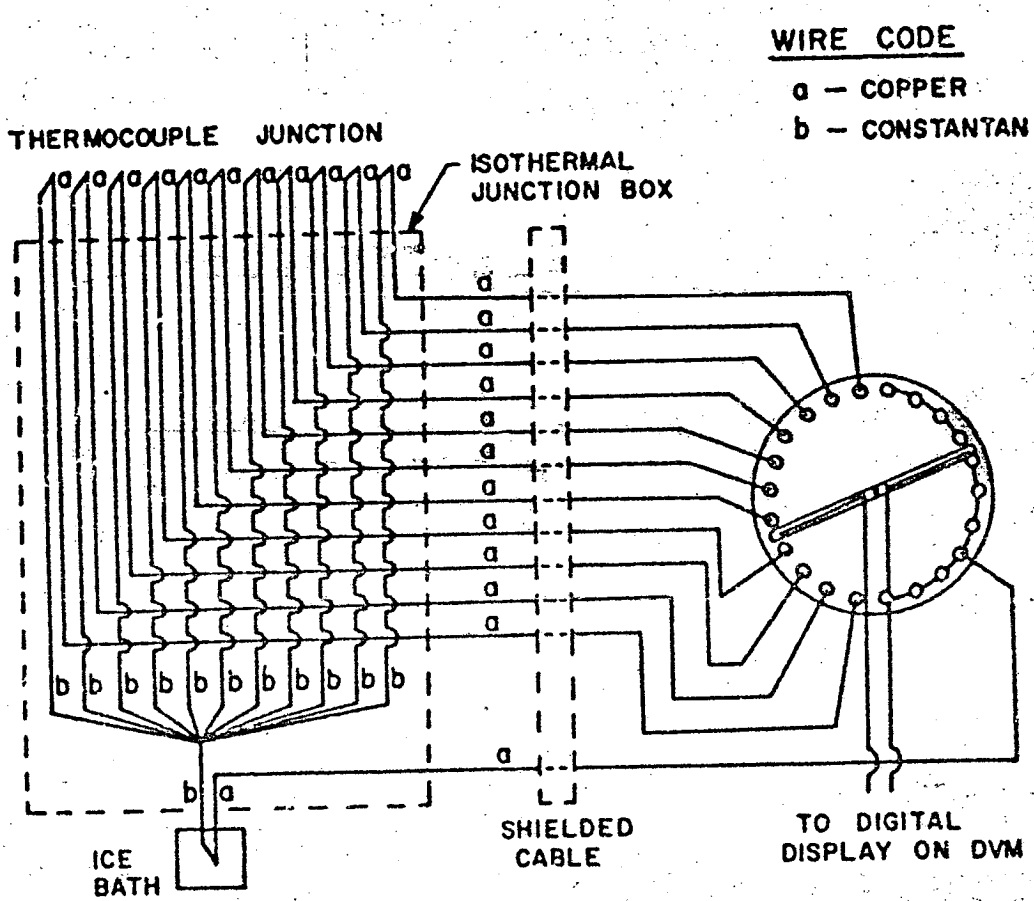

Figure 5.5 Wiring Diagram of Temperature Measurement System

The condenser surface of the heat pipe (vapor chamber) was maintained at a constant temperature by circulating cooling water through a bank of two times eight thin walled brass tubes, shown in Figure 5.4. This particular design was selected because it allowed the condenser area to be easily controlled by merely interrupting the flow in any number of tubes. The water was supplied from a constant temperature bath and the flow rate was measured with a flow meter as depicted in Figure 5.6. Between the flow meter and the actual condenser surface the flow was divided into sixteen currents by two manifolds placed in series. The first manifold divided the flow into two streams, one for each side of the heat pipe, and the second manifold which was mounted on the heat pipe support subdivided the two flows into eight parts each. The opposite manifold arrangement was used to recombine the flows after they had passed through the condenser tubes. The two thermocouple probes used to measure the condenser inlet and outlet temperatures were placed inside of the "one to two" manifolds. For the purpose of clarity the "one to eight" manifolds as well as the sixteen individual condenser tubes are not shown in Figure 5.6. The constant temperature bath which supplied the condenser coolant fluid was a Lauda NBSD Thermostat. The thermostat consisted of a reservoir, circulating pump, and a temperature control unit. The reservoir was filled with distilled water and connected to the manifolds forming

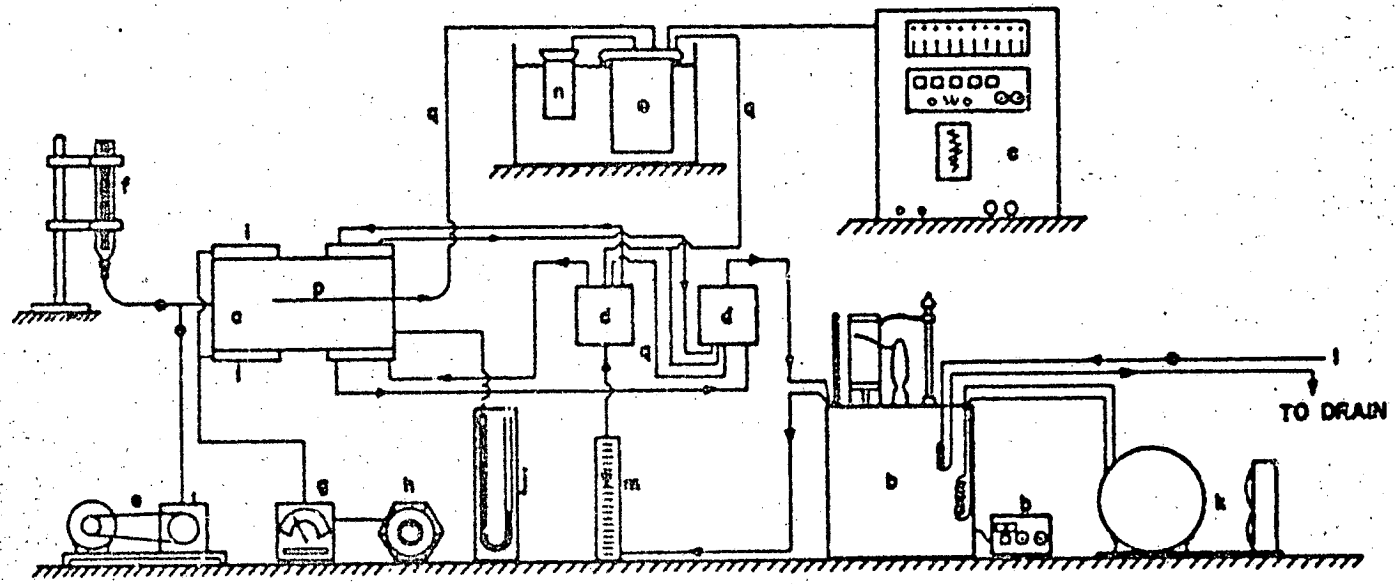

COMPONENTS

a	Rectangular Heat Pipe	j	Mercury Manometer
b	Thermostat & Control	k	Auxiliary Freon Refrigeration Unit
c	Digital Volt Meter	l	Building Water Supply
d	Calorimeter	m	Flow Meter
e	Vacuum Pump	n	Ice Bath
f	Graduated Buret	o	Isothermal Junction
g	Watt Meter	p	Thermocouple Probes
h	AC Power Variac	q	Thermocouple Cable
i	Resistance Heaters		

Figure 5.6 Schematic Diagram of Rectangular Heat Pipe Facility

a closed loop, through which the fluid was circulated by a Duplex pump. The reservoir temperature was maintained constant by bucking the heat losses with an adequate heat input. The heat loss was controlled either by a continuous flow of cold tap water or by an auxiliary Freon refrigeration unit while the heat was supplied by an electrical resistance heater installed inside the bath. This type of temperature control avoids the fluctuations normally encountered when the resistance heater is periodically cycled to maintain a desired temperature. Such temperature fluctuations were easily sensed by the thermocouples in the manifolds and since the fluctuations were out of phase with one another (due to the different positions in the flow path), an accurate determination of the inlet and outlet condenser temperatures was difficult when the on-off temperature controlling mode was used.

The evaporator was heated with ten Ogden strip resistance heaters. Five heaters were located on each side of the pipe as shown in Figure 5.4. All heaters were connected in parallel and the power input was controlled and measured by an AC variac and a wattmeter, respectively. Each heater had a maximum power rating of 150 watts at 120 volts, hence limiting the maximum power input to the heat pipe to 1500 watts. As with the condenser, this design was considered desirable since the evaporator area could be varied simply by disconnecting the leads to various heaters.

The gage pressure in the test section was measured with a mercury manometer which was connected to the condenser for horizontal operation of the pipe and to the evaporator for vertical operation. The pressure could be read within ± .5 mm Hg. A mercury barometer located near the test section indicated the prevailing atmospheric pressure so that the absolute pressure in the test section could be easily determined.

Access tubes were installed in the evaporator end wall for the charging of fluid to the pipe and for a pipe connection to a mechanical vacuum pump. The procedures used to charge and operate the pipe were as follows. The pipe was first evacuated to remove as much air as possible. It was then placed at a moderate angle from the horizontal with the evaporator on top. About 800 cm^3 of fluid was forced into the pipe from a buret by atmospheric pressure resulting in a pool of liquid at the bottom. The top wick was saturated by rotating the condenser into a top position and applying power to the lower bank of resistance heaters while only the top bank of condenser tubes was cooled. This caused a preferred condensation on the upper wick and resulted in total saturation of both wicks. Enough fluid was added so that a slight amount of excess liquid remained on the lower wick after both wicks had been saturated. This procedure was repeated occasionally during the experiments and especially after a relatively high heat flux test

for which a partial drying of the top wick was often experienced. The majority of cases investigated were steady state, although several tests were made for which transient temperatures were recorded in response to a step change in power input to the evaporator.

For the steady state modes, the temperatures were measured at 3 cm intervals starting 1 cm from the evaporator end wall. The condenser inlet and outlet temperature, as well as the room and bath temperature were recorded every time the thermocouples in the pipe were read, and the average values were used in subsequent data reductions. The gage pressure in the test section and the atmospheric pressure were read midway through the temperature readings so that an average value could be used if these values changed. A complete set of data required approximately one hour of time due to the repeated movement of the probes by 3 cm increments and the subsequent waiting period for the temperature readings to stabilize.

The energy transported by the heat pipe was determined calorimetrically. However, because of the presence of heat losses from both the pipe and the calorimeter tubing and the effect of heat conduction along the walls, the following reasoning in ascertaining these losses was used. When the coolant flow is at a temperature different from room temperature, the outlet temperature, T_{out}, will be different from the inlet temperature, T_{in}, due to the heat exchange with

room air. As shown in Figure 5.7, if the ambient temperature is less than the coolant temperature (given by T_{in}) and the power input to the heaters is zero, then T_{out} is less than T_{in} and vice versa. In addition, if for a particular difference in coolant and ambient temperatures the power input is greater than zero, then the additional energy conducted along the heat pipe wall will further increase $(T_{out} - T_{in})$.

The procedure adhered to for the calibration consisted of the evacuation of the pipe, and the subsequent measuring of the calorimeter temperature difference, $(T_{out} - T_{in})$, for various coolant temperatures and heat additions. The coolant flow rate was maintained constant at 200 Kgm/hr. The resultant curves which are illustrated in Figure 5.7 were used as reference curves in the experiments. That is, any increase in temperature difference $(T_{out} - T_{in})$ above these curves was considered to be due to the mass transfer and phase change process taking place inside of the heat pipe. For example, if the coolant temperature was 25 °C above room temperature and the heat input to the evaporator was 300 watts, the calorimeter temperature difference expected would be approximately -1.5 °C. However, if a temperature difference of -.5 °C was measured during the experiment, then a difference of +1 °C would be used in the calorimetric equation to calculate the energy transport in the heat pipe. Since during normal heat pipe operation the presence of fluid in the evaporator wick caused a lower

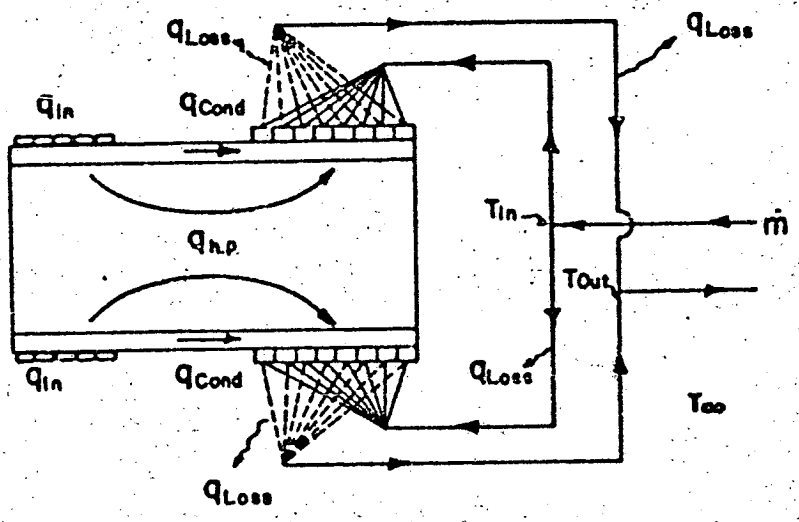

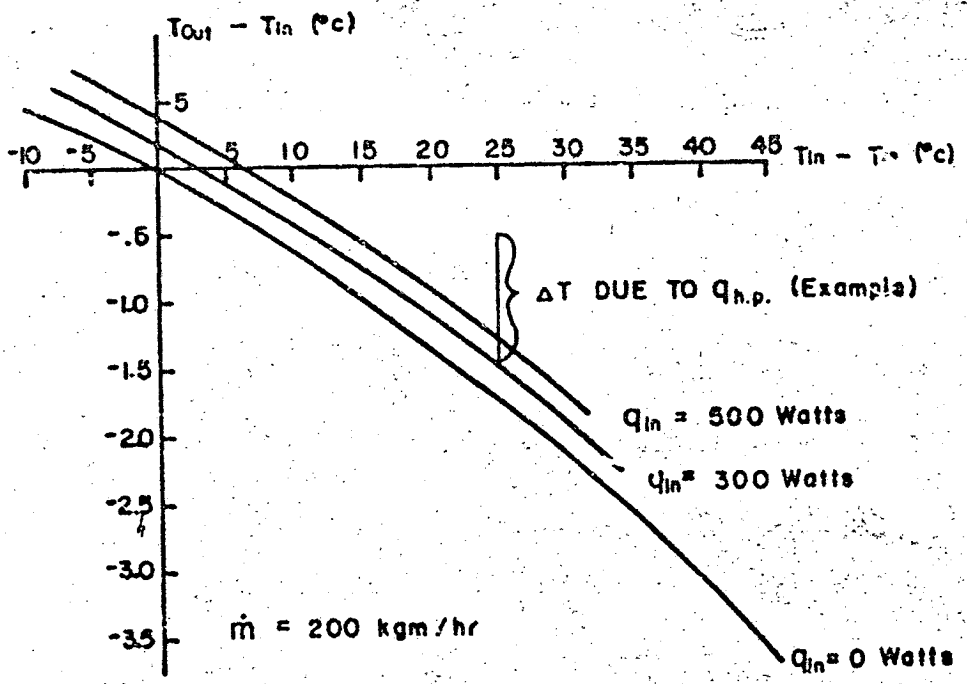

Figure 5.7 Calorimeter Calibration Procedure

temperature there than in the absence of fluid (such as was the case during calibration), the reference lines in Figure 5.7 would probably be situated somewhat lower and consequently the actual heat pipe energy transfer was somewhat greater than predicted by this technique.

Experimental data obtained with the rectangular heat pipe will be presented and discussed in chapter VI.

CHAPTER VI: EXPERIMENTAL RESULTS

Balance Beam

The balance beam described in chapter V was used to measure the transient wicking characteristics of eleven porous "Foam Metal" specimens. A particular test was initiated by allowing the lower surface of the sample to touch a liquid pool which was slowly elevated beneath it. The sample weight, and hence the liquid height, was continuously monitored for approximately thirty minutes. The sample surface was left exposed to the environment so that a small amount of liquid evaporation undoubtedly took place. However, for runs of relatively short duration this effect may be neglected. This, of course, is not the case for long duration runs; for example, up to 2 months have been reported in other studies where a saturated environment must be employed.

Of all the specimens tested, the best wicking rate was obtained with a 40% dense nickel sample. The transient height versus time curve for this sample with water as test fluid is presented in Figure 6.1. Also illustrated is the curve for 85% dense nickel "Feltmetal" as supplied by the manufacturer. The curves illustrated in Figure 6.2 were obtained by numerically differentiating the height versus

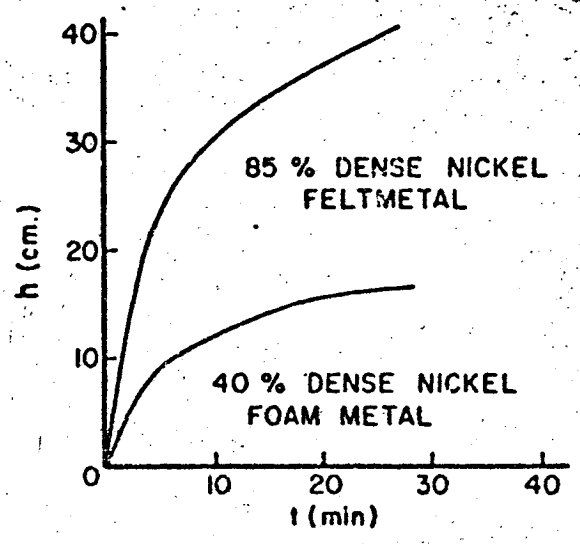

Figure 6.1 Transient Wicking Height

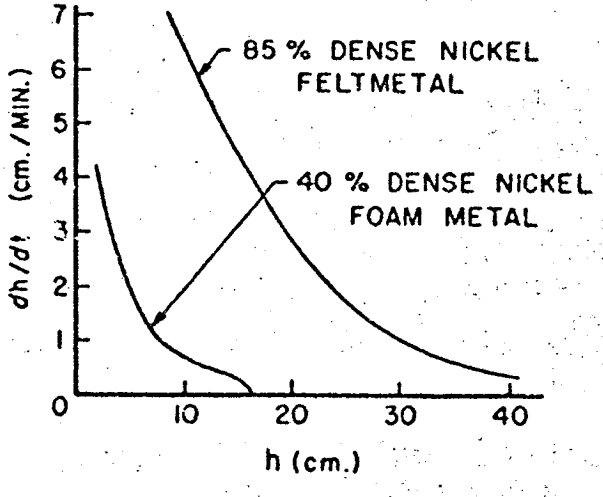

Figure 6.2 Wicking Velocity vs. Height

time curves and replotting as a function of height. These curves are useful in comparing the relative merit of various wicks for potential heat pipe use. From these curves it is easy to see why the "Feltmetal" was ultimately chosen for use in the coplanar heat pipe.

For all nickel samples tested, the data were repeatable over a time span of approximately one month. For the copper samples, however, the wicking performance decreased with increasing time. The transient rise of water in a 45% dense copper sample is illustrated in Figure 6.3. The higher curve was measured shortly after the sample was received from the manufacturer while the lower curve was measured twenty-five days later. The change in performance was attributed to oxidation of the wick which was readily apparent from the discoloration of the copper.

The significance of the data obtained with this device lies not in the actual values measured since none of the samples tested were used in subsequent heat pipe designs, but in the method used to measure them. A device has been designed and tested which continuously and accurately monitors an advancing liquid front within a porous sample. This is a distinct improvement over spaced visual sightings of the advancing liquid since often the liquid line in the wick is difficult to see. To overcome such difficulties organic dyes are often added to the liquid, or litmus strips are taped to the sample surface. Such techniques often influence the data to such an extent as to make it almost

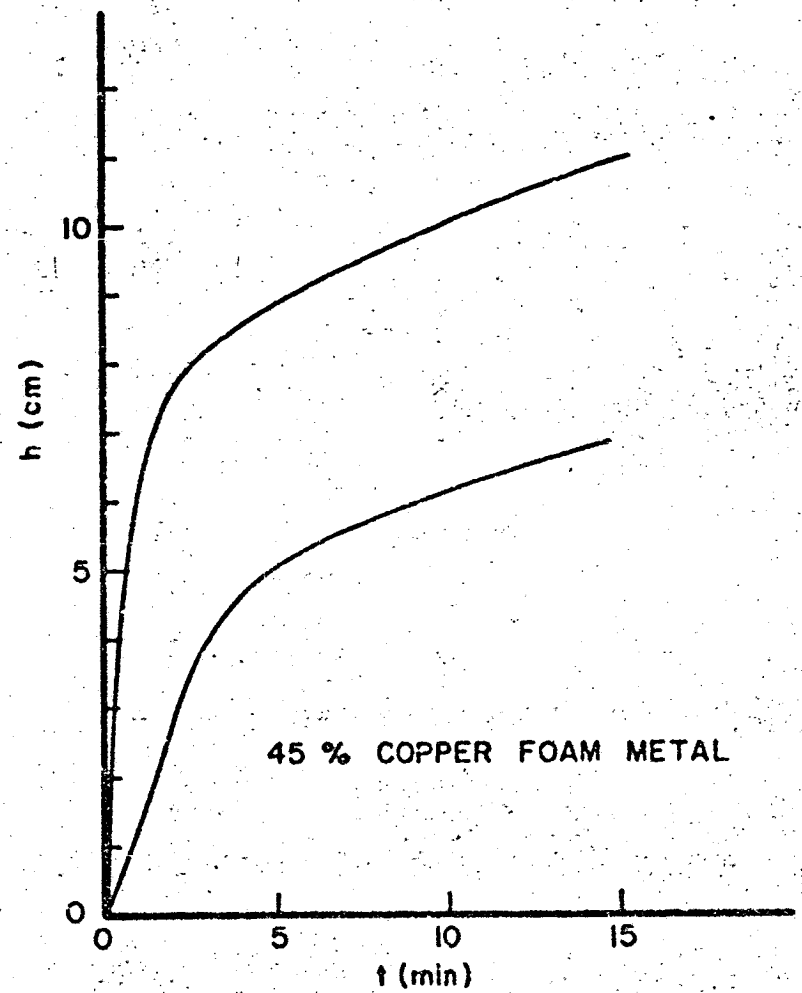

Figure 6.3 Transient Wicking Height

meaningless. The balance beam, moreover, may be easily adjusted to different sensitivities by simply moving the fulcrum. For long duration runs the device may be adapted to provide a saturated environment around the sample by enclosing the entire beam within a plexiglas box.

Cylindrical Heat Pipe

In all of the tests with the cylindrical heat pipe distilled water was used as a working fluid. Prior to the actual heat pipe tests, the pipe was operated dry at several power inputs. This, in effect, calibrated the pipe so that for subsequent tests with a fluid in the pipe, the actual heat transport of the pipe could be determined using the method discussed in chapter V. With a stainless steel screen as wick, and water as a working fluid, several tests were conducted at different power inputs with the pipe oriented horizontally ($\theta = 0°$), and insulated. The measured axial wall temperature distributions are presented in Figure 6.4 as a function of power input. The power values in parentheses indicate the power actually transferred by the heat pipe while the first value represents the power input. Temperature profiles for the insulated case were quite similar even though the losses from the surface of the pipe were much smaller. The rather abrupt temperature change at the condenser entrance is probably due to the presence of a noncondensable gas. Carnesale, et al. [36] and Marto and Mosteller [80] also observed this behavior in their low

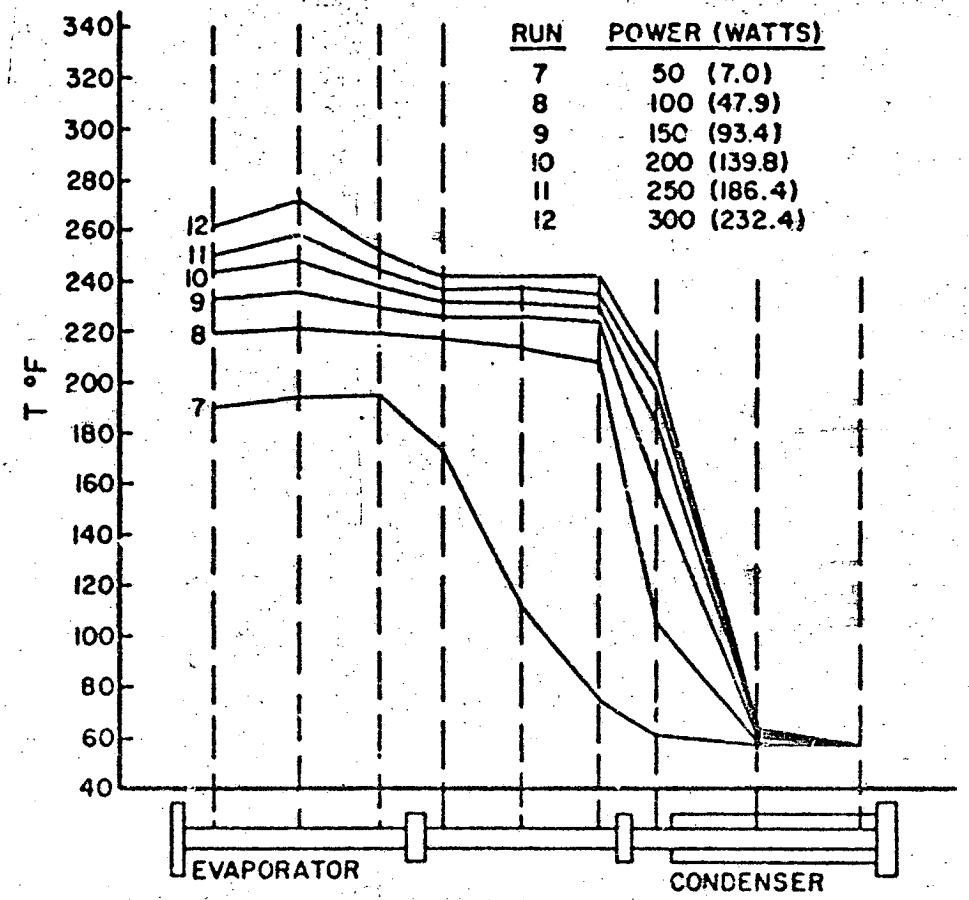

Figure 6.4 Axial Temperature Distribution as Function of Power Input

temperature water heat pipes. As with the other experimental investigations, the thermocouples were not placed close enough together to verify Lyman and Huang's [129] theory which predicts large temperature gradients in the wick at the junction between the adiabatic section and the condenser for wick matrices of low thermal conductivity. It is interesting to note that the wall temperature behaves as expected for a pipe with a floating temperature source and a fixed temperature sink. For the tests depicted in Figure 6.4 the absolute pressure within the pipe varied from 11 to 28.5 lbs/in^2 and closely paralleled the saturation curve as expected. The differential pressures indicated that the evaporator pressure was above the condenser pressure but all values were very nearly zero and no trend could be detected.

In Figure 6.5 the effect of pipe orientation at a constant power input is presented. The power actually transferred as indicated by the values in parentheses, however, was not constant. It is evident that the temperature in the evaporator begins to increase for angles from the horizontal as small as 3 degrees. When the angle was increased to 8 degrees (corresponding to approximately a 11.5 cm difference in elevation between the evaporator and condenser) the evaporator temperature began to approach that obtained for a completely dry pipe, hence indicating almost complete wick dryout. This apparent dryout was caused by the inability of the screen wick to supply fluid to the evaporator at a rate equal to that of the evaporation process.

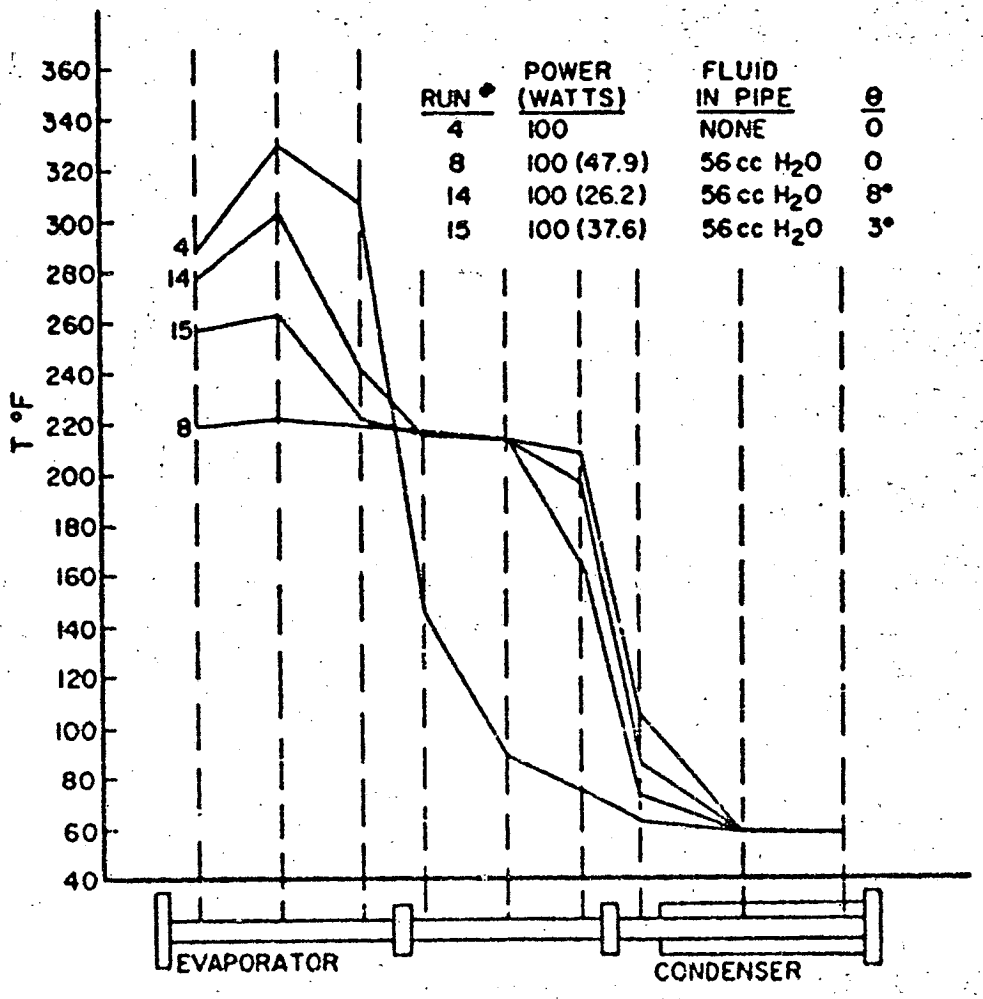

Figure 6.5 Axial Temperature Distribution as Function of Inclination

The heat pipe was also operated with a Refrasil wick. Several tests were made and temperature profiles qualitatively similar to those of Figure 6.4 were obtained. Continued testing, however, indicated a significant decline in heat pipe performance as evidenced by the high temperatures measured in the evaporator for even relatively low heat flux tests. Subsequent inspection of the wick indicated a high degree of deterioration. The fiber was semi-dissolved and when squeezed produced a gritty milky white fluid which seemed to contain many fine fibers and powder. It was concluded that Refrasil cloth is not a desirable heat pipe wick.

Coplanar Heat Pipe

The experimental program utilizing the coplanar heat pipe consisted of 67 tests. Either pure water or pure methanol or some mixture of water and methanol was used as a working fluid in all tests. This combination of fluids was chosen because 1) they were easily attainable, 2) they are completely miscible, 3) their vapor pressure characteristics are such that a large temperature difference could be expected if the components completely separated at constant pressure, and 4) their binary equilibrium curves do not exhibit an azeotropic point. Of the 67 tests, all but 6 utilized a relatively cool condenser sink temperature of approximately 63°F. This temperature varied about 3 degrees in either direction depending on the ambient and tap water temperatures. The remaining 6 tests were conducted with

elevated sink temperatures (as high as 145°F). For the tests with the "cool" sink temperature, 45 were conducted with "normal" heat pipe orientations, i.e., either horizontal or with the evaporator above the condenser. Five different mass fractions of methanol (0.0, 0.25,0.50, 0.75, 1.00) were employed at each of three orientations, i.e., horizontal ($\theta = 0°$), $\theta = 45°$, and vertical ($\theta = 90°$), for each of 3 power inputs to the evaporator (50, 100, 250 watts). All of these experiments were conducted under steady state operating conditions in the pipe. In addition to these tests, 2 trials were conducted with the evaporator below the condenser (i.e., as a reflux condenser), 10 trials were performed to determine the influence that stratification had on the steady state temperature profiles, and 4 tests were conducted to study the transient behavior of the pipe after a step change in power input to the evaporator. The effect of stratification and the procedures adhered to for data reduction is discussed in Appendix A.

For a series of constant composition tests, the pipe was charged in the following manner. First it was evacuated and then approximately 800 cm^3 of the desired mixture were pressure fed into the pipe. A vacuum was again applied until vigorous boiling of the excess liquid took place. This assured that saturation conditions were present in the pipe. The pipe was then sealed and the upper wick was saturated as explained in chapter V. The amount of fluid added allowed for complete saturation of both wicks as well

as some excess fluid which resided on the lower wick. Each of the 45 "normal" tests were begun by setting the power input and pipe orientation to the desired values. All thermocouple probes were positioned so that the probe tips were 1 cm away from the evaporator end wall ($x/L = 1/35$). Steady state conditions were considered present when the measured temperatures varied less than .1°F per hour. The achievement of steady state usually took between 5 and 8 hours after the operating conditions were changed. For a particular test, the temperature field within the pipe was determined by measuring the output signal of each of the 5 probes in the vapor space as well as of the 2 probes under the wicks at 3 cm intervals along the pipe axis. In addition, the room, thermostatic bath, and calorimeter inlet and outlet temperatures were recorded for each axial position of the probes. The temperatures were made nondimensional by subtracting the calorimeter inlet temperature and dividing by the difference between the maximum temperature and the calorimeter inlet temperature. This procedure was performed twice, once using the maximum temperature measured in the vapor space only, and once including the temperatures under the wicks. The resulting dimensionless profiles were plotted by a Calcomp Plotter as a function of the dimensionless axial distance, x/L.

Several typical temperature profiles for $\theta = 0°$, $\theta = 45°$, and $\theta = 90°$ are illustrated in Figures 6.6, 6.7, 6.8 respectively. These curves have in common a methanol mass fraction

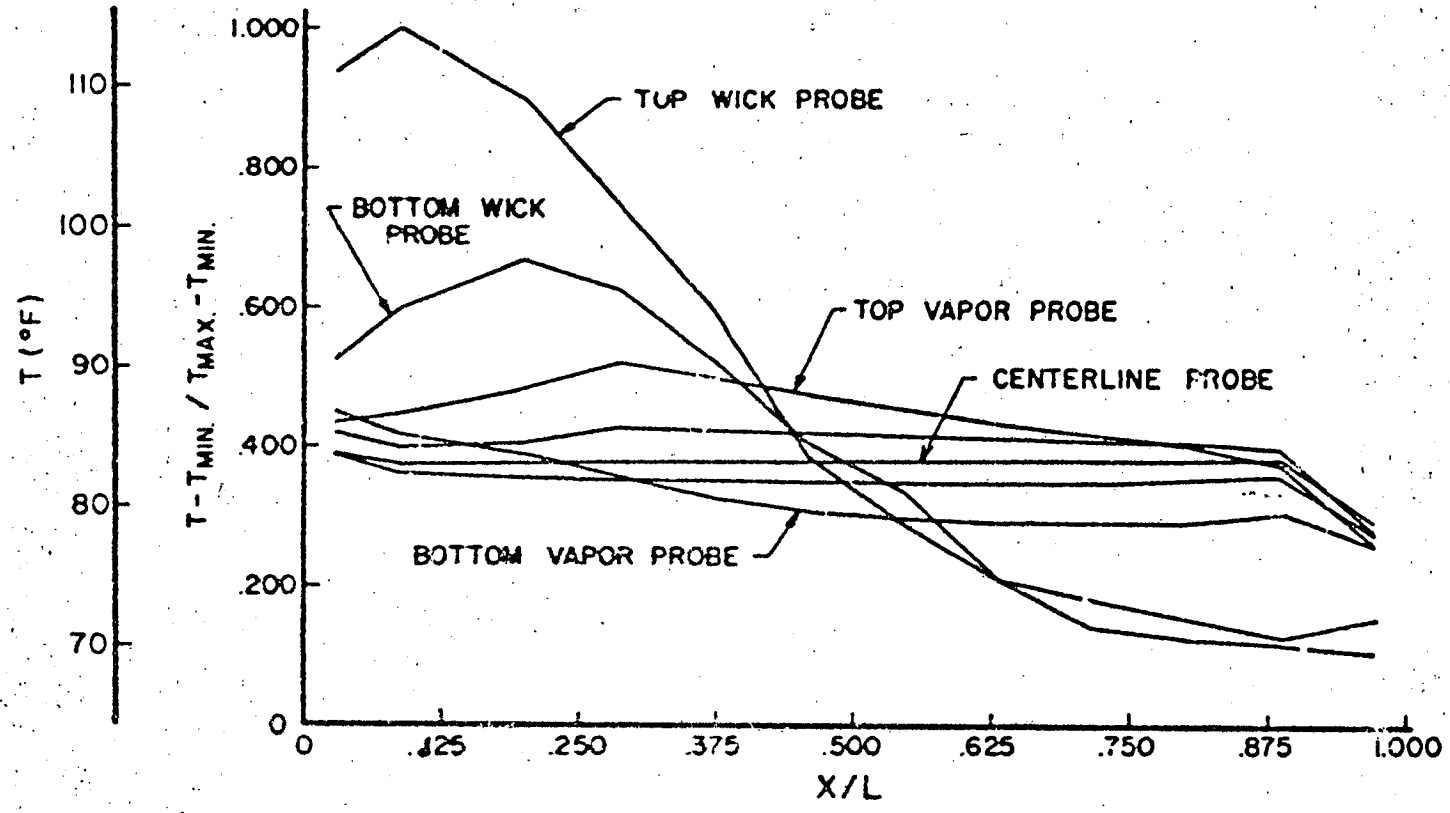

Figure 6.6 Axial Temperature Distribution, θ = 0°

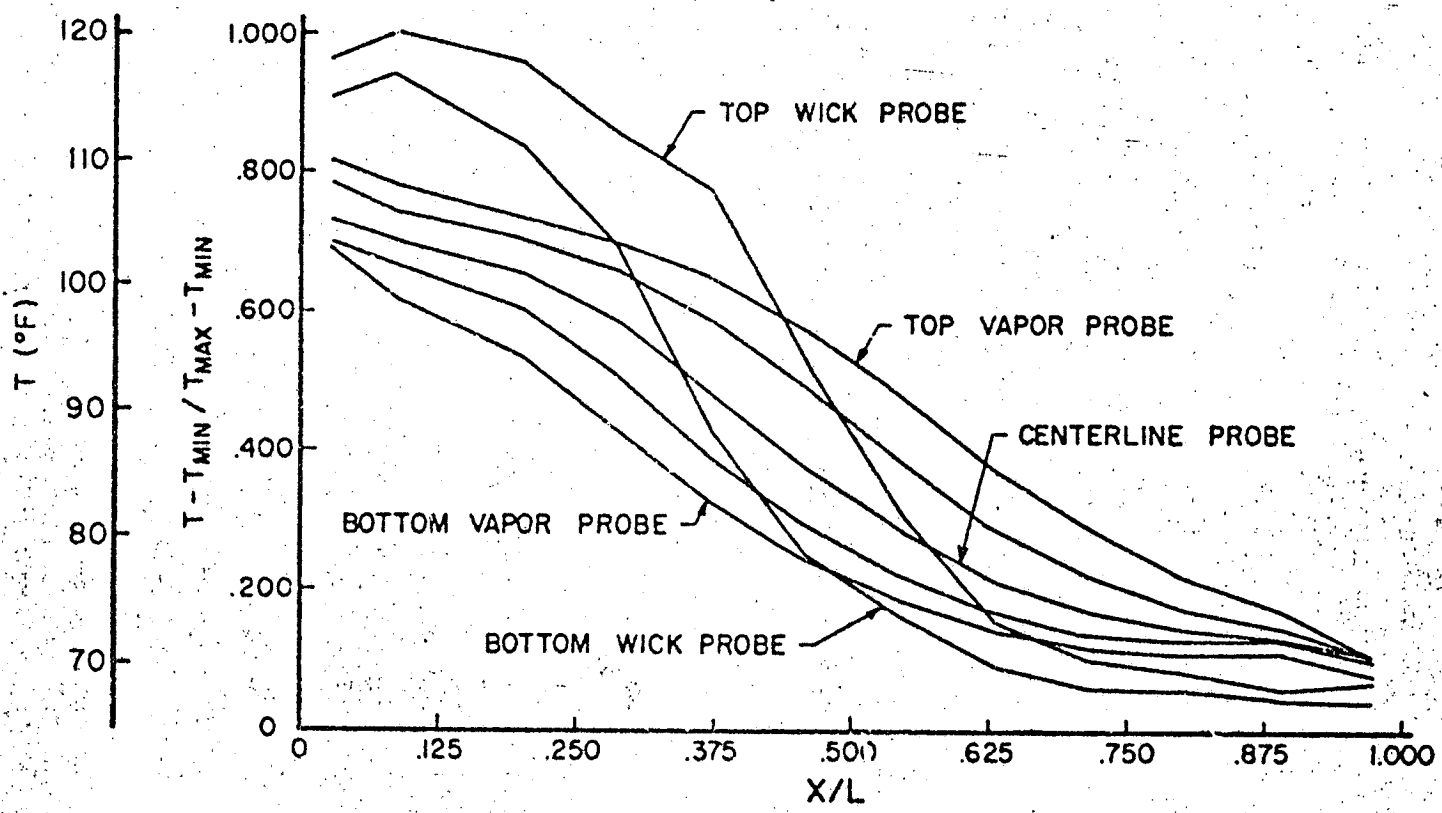

Figure 6.7 Axial Temperature Distribution, θ = 45°

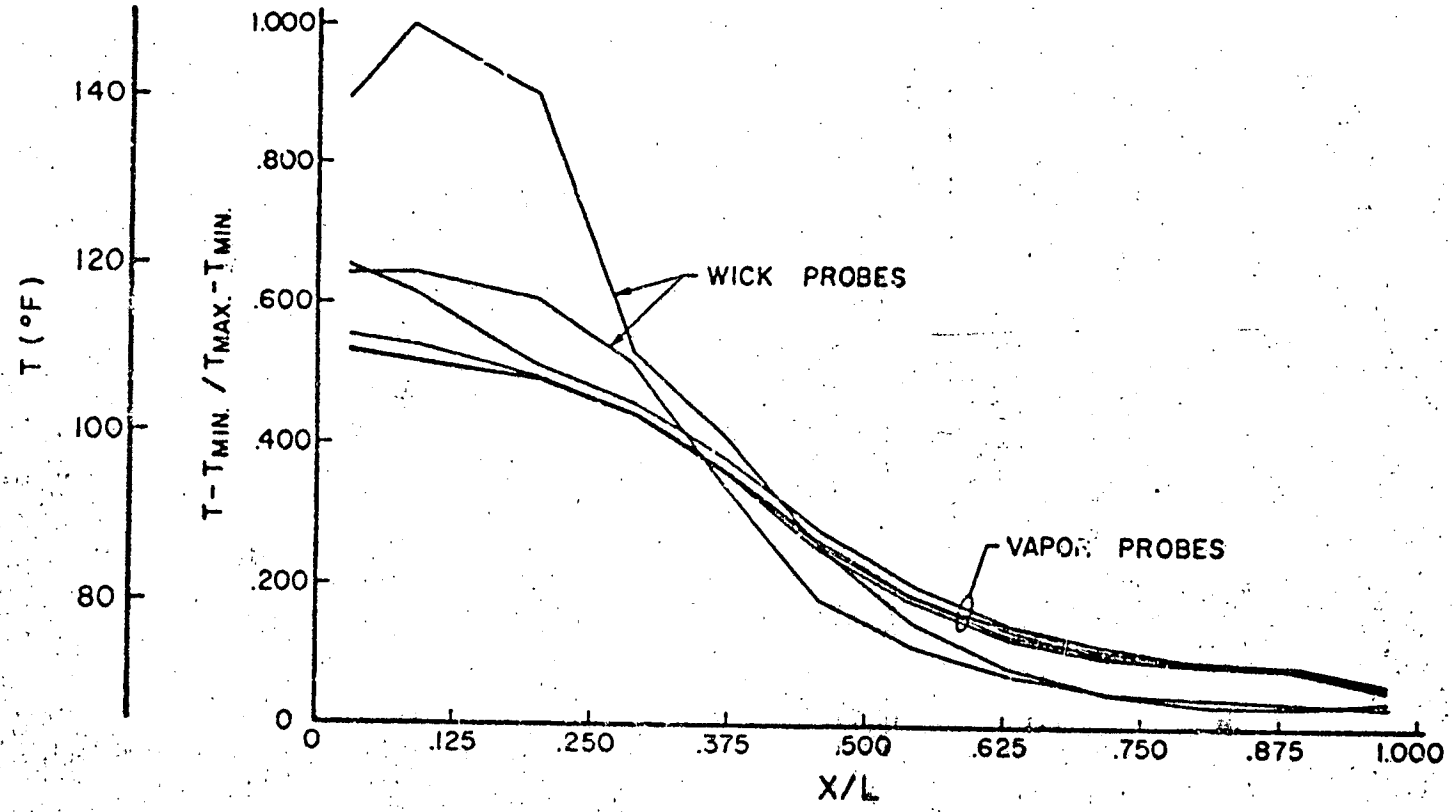

Figure 6.8 Axial Temperature Distribution, θ = 90°

of 50% and a power input to the evaporator of 100 watts. The profiles for the horizontal case (Figure 6.6) indicate that the vapor temperature changed very little in the axial direction. In fact for the centerline probe, with the exception of the extreme right hand point the temperature range was between 82.6°F and 83.3°F. The temperature difference between the top and bottom vapor probes averages approximately 7°F and is due to stratification. As expected, the wick temperatures are higher in the evaporator and lower in the condenser. In addition, the top wick temperature in the evaporator is hotter than the lower wick temperature. This is to be expected because any condensation on the end walls or the windows is gravity fed to the lower wick while the upper wick may not be totally saturated. In addition, the upper wick is in contact with a higher temperature vapor than the lower wick. For the case where the angle of inclination $\theta = 45°$ (Figure 6.7), the same trends are evident with one exception; now the vapor temperatures exhibit a definite variation along the pipe axis. This phenomenon is again caused to some extent by the occurrence of stratification. The curves illustrated in Figure 6.8 are for a vertical orientation of the heat pipe and again display some degree of stratification in the axial direction. The vapor temperatures at any particular cross-section are now nearly constant with slight deviations occurring in the evaporator section. The wick temperatures follow the same trend as observed for the other pipe orientations. The highest curve

in the evaporator section indicates a semi-dryout condition for one of the wicks. This particular curve was measured under the wick which was designated as the bottom wick in Figures 6.6 and 6.7. This asymmetric condition was noted several times and means that one wick operated more effectively than the other.

The data obtained for other mass fractions and power inputs were qualitatively though not quantitatively similar. The phenomenon of wick dryout was observed several times and was especially prevalent for high methanol content and high heat input tests.

An evaluation of the measured heat transfer rates leads to several conclusions. The average heat transferred for all tests was greatest for horizontal pipe orientations, less for 45° inclinations, and the smallest for vertical orientations. In addition, the pipe efficiencies (as determined by the ratio of the energy transferred to the energy input) exhibited the same trend as a function or orientation. These average efficiencies were 40%, 22%, and 15.3% for horizontal, 45°, and vertical orientations, respectively. For the horizontal case, no correlation appeared to exist between the pipe efficiencies (averaged over the three power inputs) and the mass fraction of methanol in the pipe. For the 45° case, however, the average efficiencies were greater for the pure component tests than for the two component tests with the minimum efficiency occurring at a methanol mass fraction of 0.5. The vertical tests indicated the same

behavior as the 45° tests with the exception of the pure methanol experiments where dryout often took place.

When the heat pipe was operated as a reflux condenser, i.e., with the evaporator located below the condenser, no significant temperature variations were measured at different positions in the vapor core. The temperatures for a particular location, however, fluctuated up to 1°F. These fluctuations were probably caused by the presence of strong convection currents. The temperature profiles under the wicks were qualitatively similar to those obtained for horizontal heat pipe operation.

The temperature profiles measured in the heat pipe when an elevated sink temperature was employed were similar qualitatively to those obtained for lower sink temperatures. The higher temperatures, however, contributed to wick dryout as was evidenced by the lower heat transfer rates which were measured.

The pressures for the single component tests were found to be the saturation pressures corresponding to the wick temperatures in the adiabatic section. For a majority of tests, moreover, the pressure was determined by the wick temperature at the location where the temperature profile in the vapor crossed the temperature profile in the wick, i.e., where the vapor and wick temperatures were identical.

The basic question as to whether or not the components in a two component heat pipe separate will now be considered. A conclusive verification of separation (or the lack of it)

was attempted using a Mach-Zehnder interferometer. The combination of the measured index of refraction changes and the temperature field would then have indicated concentration changes. This technique, however, was not successful due to the inhomogeneity of the vapor condensation on the optical windows in all tests which made the attainment of reasonable interference patterns impossible. A referral to the multicomponent, multiphase literature, e.g. Bosnjakovic and Blackshear [135], nevertheless indicates that due to the isobaric nature of the vapor core, any separation must manifest itself in temperature changes. Moreover, these temperature changes should be dependent primarly on the difference in component concentrations between locations and should not be evident for heat pipes employing only single component working fluids. The behavior of two component heat pipes can thus be ascertained qualitatively by comparing their characteristics with those obtained for pure component heat pipes.

As evident from the raw data, the temperatures within the vapor space for both single and two component fluids were dependent to a large degree on the vertical direction. This behavior is explained by the fact that the vapor velocities (on the order of 2 cm/sec) were insufficient to completely overcome buoyancy effects which tended to form a stable stratified vapor. The resulting temperature distributions within the vapor are thus a result of both the stratification effect and the operational characteristics

of the heat pipe. The stratification effect is essentially a pure conduction process and may be accounted for using the technique described in Appendix A. The dimensionless temperature profiles illustrated in Figure 6.9 were obtained by subtracting the stratification profiles from the dimensionless temperature distributions which were measured when the heat pipe employed pure water as a working fluid. The resulting curves indicate the behavior of the temperature field within the vapor as compared to the behavior experienced for pure stratification. Several trends are discernible from the figure. The corrected profiles for the pure water tests are consistently negative in the evaporator and positive in the condenser. This means that the centerline temperatures in an operating single component heat pipe are cooler in the evaporator and warmer in the condenser than the temperatures which would be observed if only pure stratification accounted for the entire temperature field. Such a behavior indicates that the axial temperature distribution within the vapor space is tending toward an isothermal condition as is to be expected for a single component heat pipe. The higher temperatures in the condenser may be attributed to the forced flow of the hot vapor from the evaporator which tended to heat the vapor in the condenser. A similar trend was observed for the pure methanol tests for the orientation where $\theta = 45°$, although the behavior was not as clearly pronounced. For the vertical tests the tendency toward isothermalization for methanol was very slight,

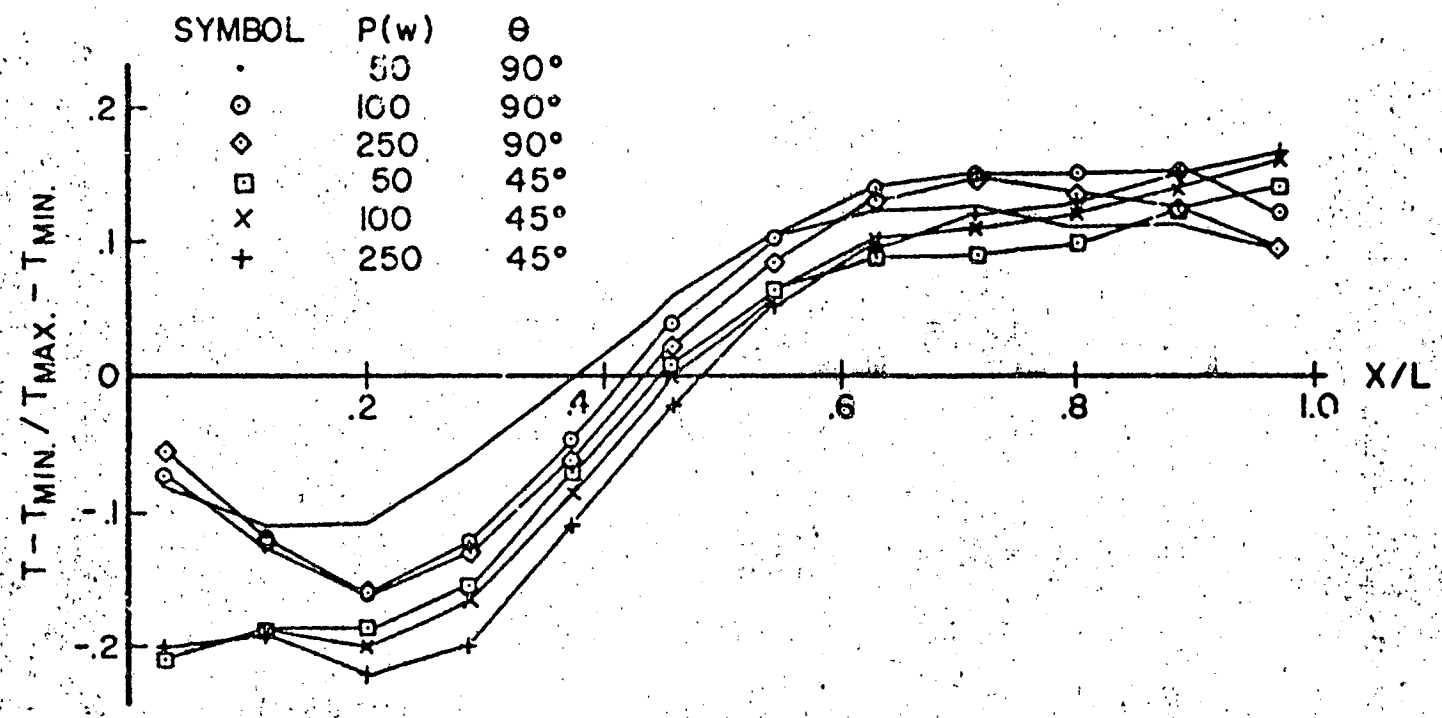

Figure 6.9 Centerline Temperature Distribution for Pure Water Normalized with Respect to Stratification Profile

especially in the evaporator where dryout often occurred. However, the behavior in the condenser qualitatively matched that obtained for pure water. The behavior of the corrected profiles for the probes nearer to the wick exhibited the same behavior as the centerline probes for both pure water and pure methanol.

The conduct of the two component tests may now be compared to that obtained for pure water. To account for the pressure differences between various tests, the temperatures are made nondimensional by subtracting the saturation temperature of methanol and dividing by the difference in the saturation temperatures of water and methanol. The saturation temperatures are evaluated at the measured pressure for each particular test situation.

The dimensionless temperature profiles for the two component tests are plotted in Figures 6.10 through 6.13. The curves in each figure are for a common power input and pipe orientation. In addition, the profiles are normalized with respect to the corresponding profile which was obtained for pure water. This means that the temperature distribution for pure water is represented in these figures by a horizontal straight line where the ordinate has a value of one. This normalization technique is used so that the behavior of the two component temperature profiles with respect to those for pure water are more vividly illustrated. It is not meant to imply that the pure water heat pipe operated in a completely isothermal manner.

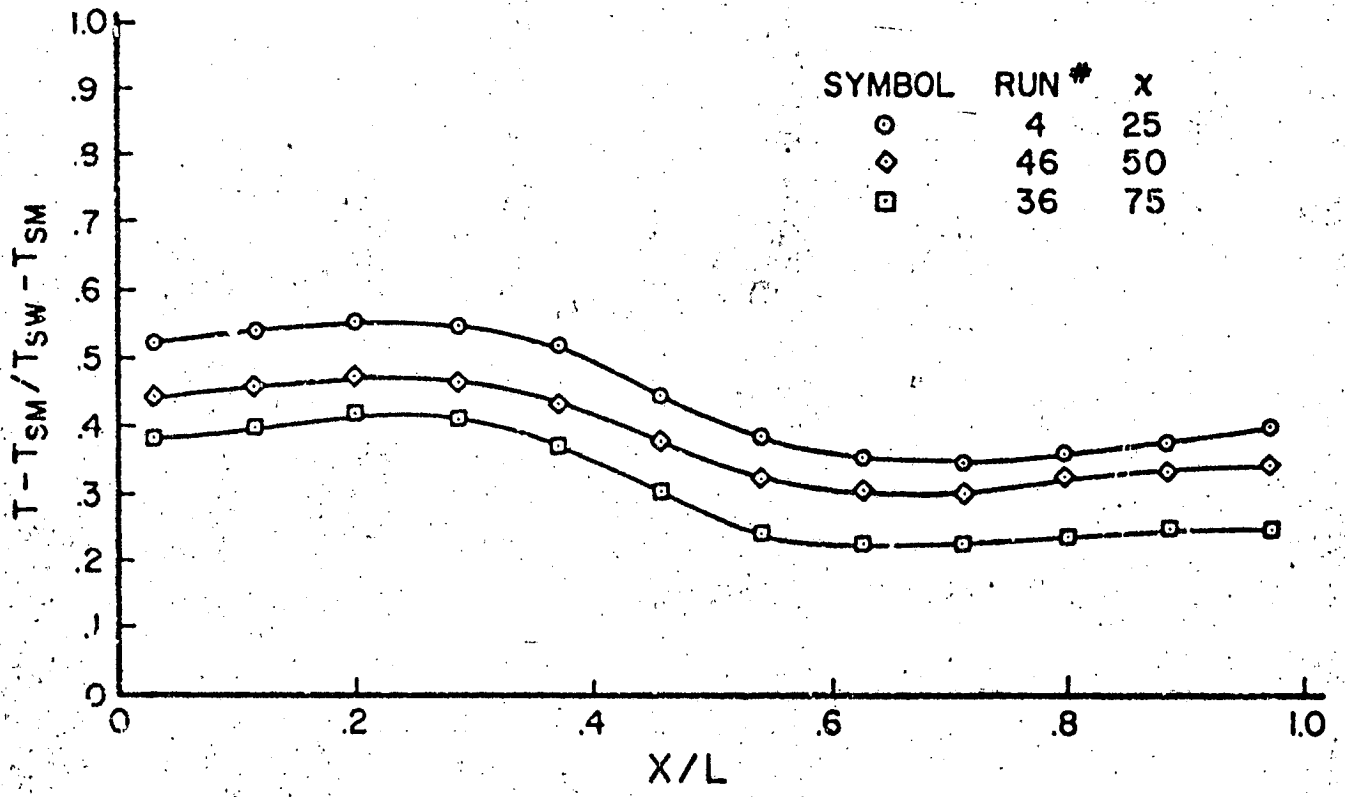

Figure 6.10 Centerline Temperature Distribution for Water-Methanol Mixtures Normalized with Respect to Pure Water Test, θ = 90°, P = 50w

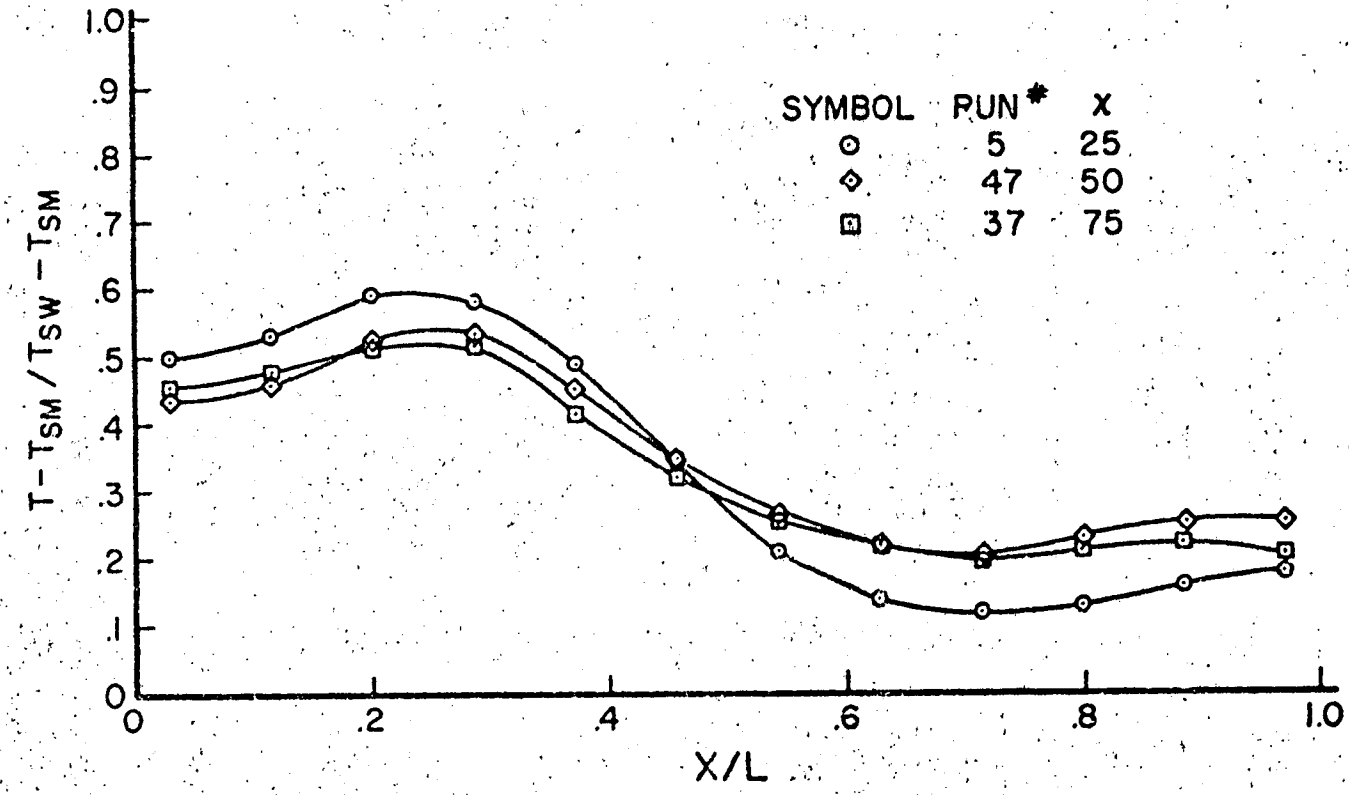

Figure 6.11 Centerline Temperature Distribution for Water-Methanol Mixtures Normalized with Respect to Pure Water Test, θ = 90°, P = 100w

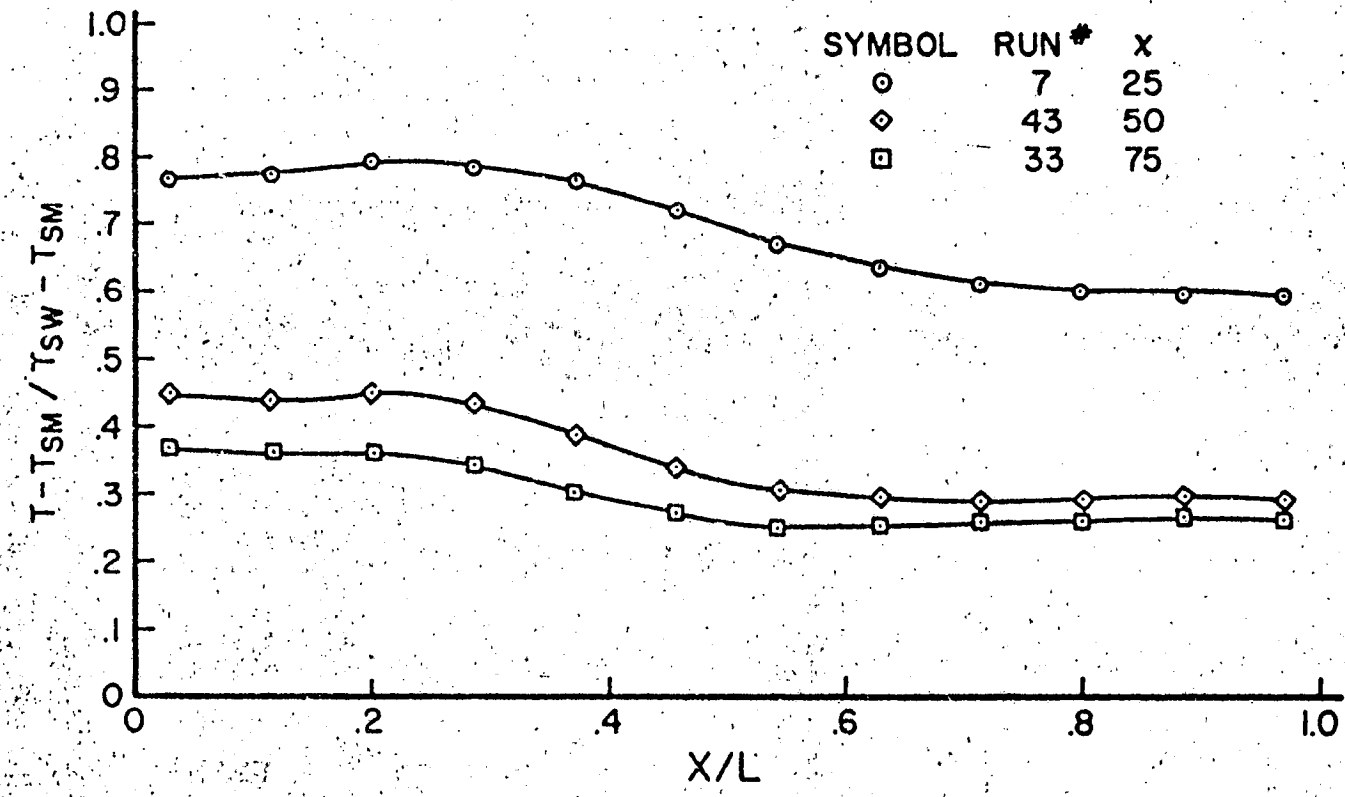

Figure 6.12 Centerline Temperature Distribution for Water-Methanol Mixtures Normalized with Respect to Pure Water Test, θ = 45°, P = 50w

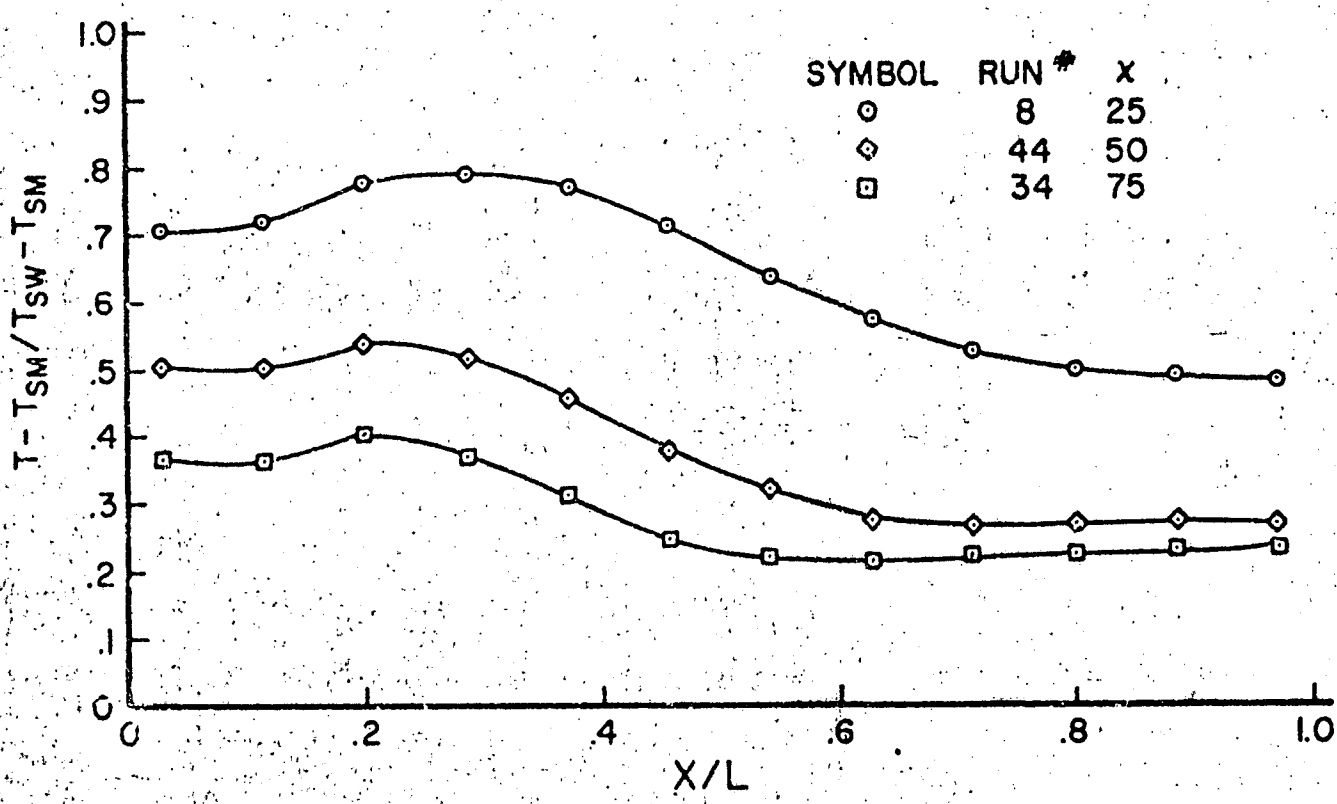

Figure 6.13 Centerline Temperature Distribution for Water-Methanol Mixtures Normalized with Respect to Pure Water Test, θ = 45°, P = 100w

In regards to Figures 6.10 through 6.13, several observations may be made. In all cases the temperature profiles indicate a consistent behavior. That is, the temperatures are always higher in the evaporator and lower in the condenser. Moreover, with the exception of Figure 6.11, where the profiles are very close and even overlap, the tests with the higher water content working fluids exhibit higher temperatures.

The data (not shown) for a power input of 250 watts showed somewhat the same trends. However, the occurrence of dryout in the evaporator wick produced some deviations from the above profile shapes. This, of course, was due to the fact that there was no heat pipe action occurring in the dried out evaporator.

The effect of cross axial temperature variations for $\theta = 90°$ and $\theta = 45°$ are illustrated in Figures 6.14 and 6.15 respectively. These curves are plotted with respect to the stratification profile as measured for each particular probe. Each figure presents three sets of curves corresponding to each of the two component mixtures. The two profiles in each set compare the corrected temperature profile near the wick with that obtained at the pipe centerline. It is clear from the figures that the centerline temperatures are higher than the near wick temperatures in the evaporator and the difference becomes much smaller as the condenser section is approached.

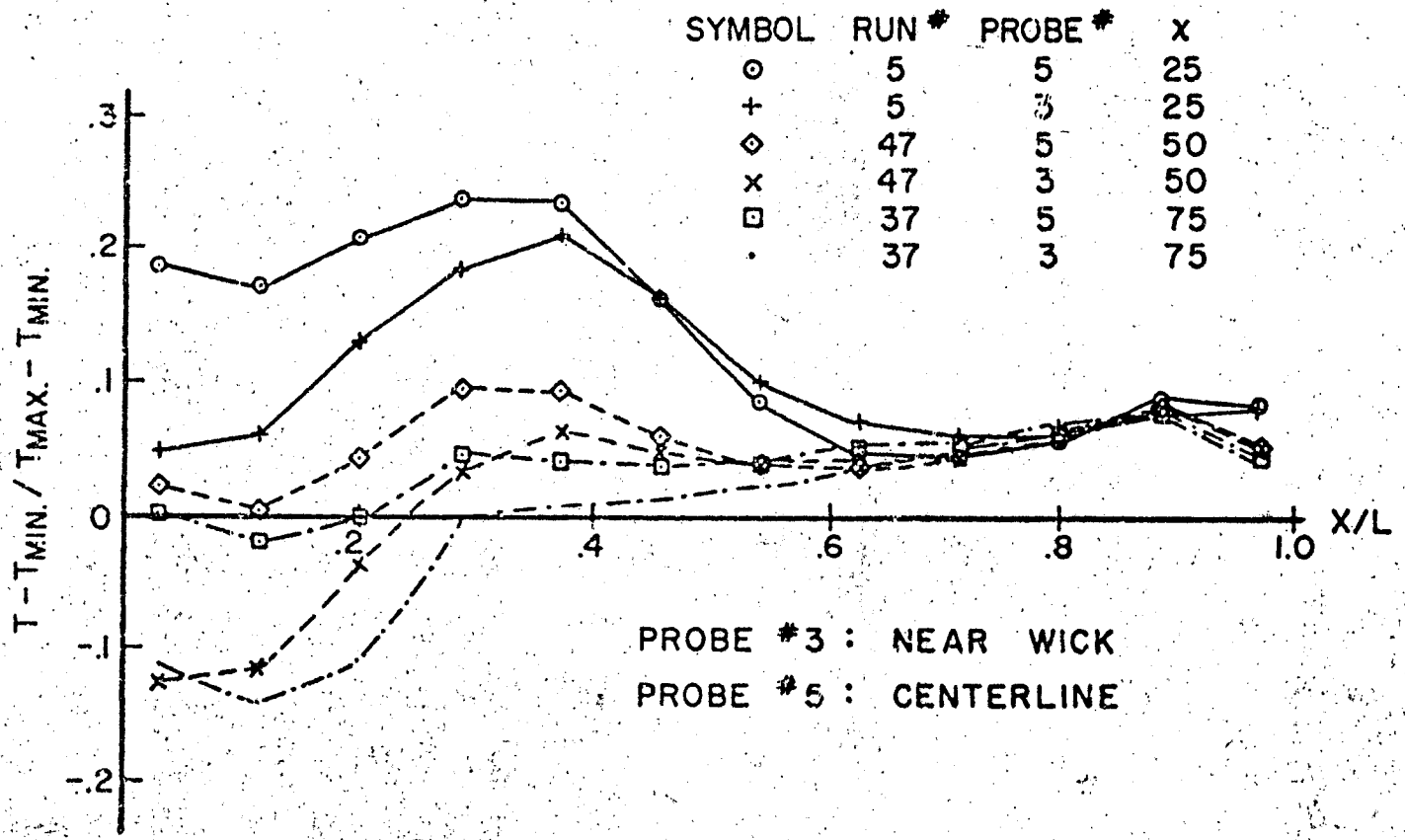

Figure 6.14 Comparison of Centerline and Nearwick Temperatures for Water-Methanol Mixtures, θ = 90°, P = 100w

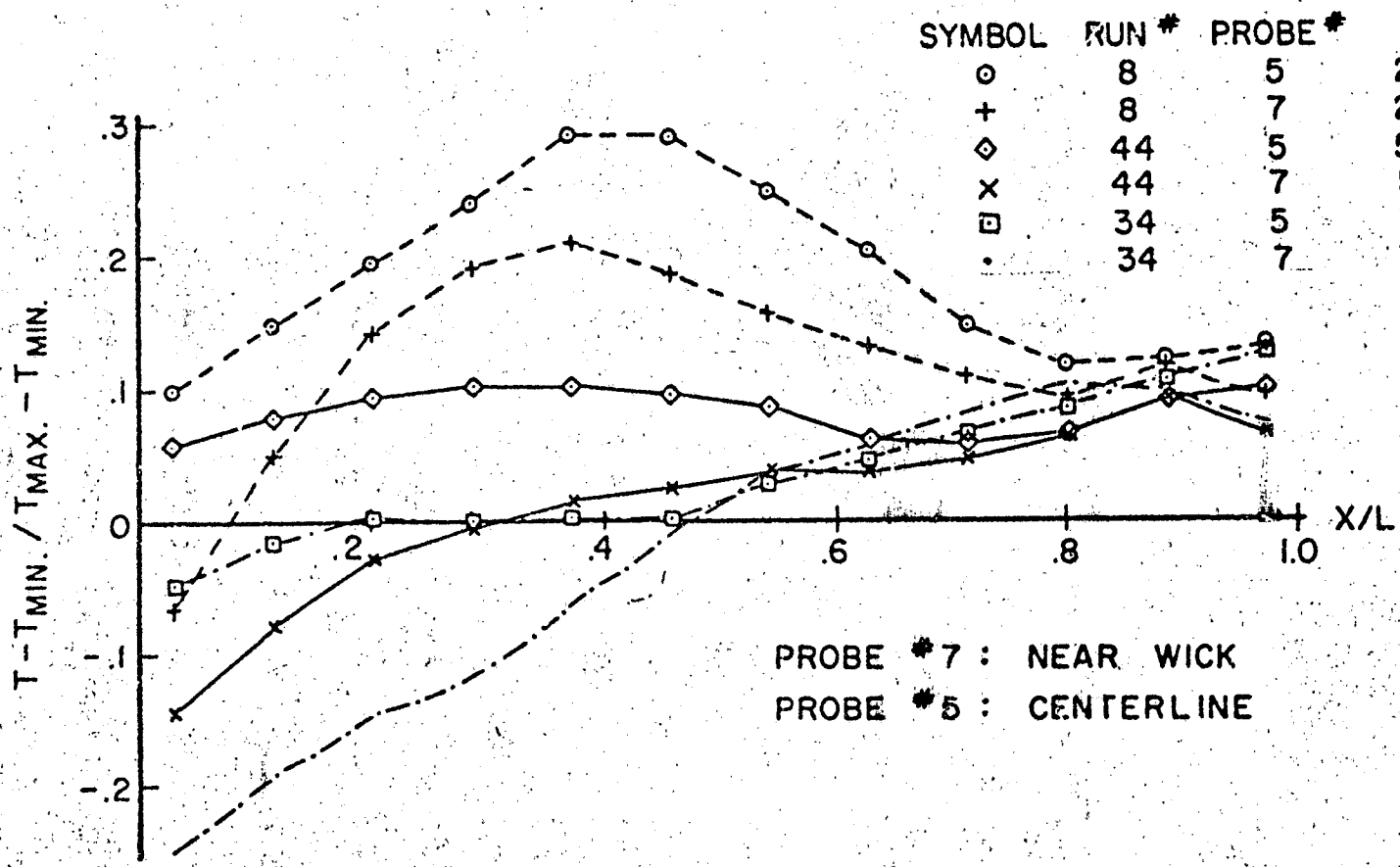

Figure 6.15 Comparison of Centerline and Nearwick Temperatures for Water-Methanol Mixtures, θ = 45°, P = 100w

CHAPTER VII: CONCLUSIONS AND RECOMMENDATIONS

A comprehensive literature collection composed of publications, papers presented at meetings and reports of varying nature, which appeared during the period from 1964 through midyear 1970 on heat pipe technology and on related topics, was classified and evaluated. Although it is to be expected that Russian heat pipe publications may well exist, none were found in the common literature indexing systems.

An experimental program was conducted which consisted of three parts. The first part involved the design, construction, and operation of a device to measure transient wicking heights in porous samples. The second part consisted of the design and operation of a conventional cylindrical heat pipe while the final phase of the investigation involved the design, construction, and experimentation with a two component coplanar heat pipe.

Conclusions

A critical evaluation of the literature leads to several conclusions regarding the state of the art of heat pipe technology. An abundance of data on heat pipe materials including working fluid properties, wick-fluid interactions, and material compatibility was generated in the course of a

sizeable number of research programs; but little effort was spent on a systematic classification and evaluation of materials in view of their potential for heat pipe application.

Generally the six interdependent processes which are assumed to effect the functioning of the heat pipe in the so-called heat pipe regime are in agreement with most qualitative observations. However, the evaporation mechanism, in particular, which is commonly regarded to take place at the liquid-wick vapor interface is the subject of some controversy.

Considerable effort has been spent on the prediction of the capillary limit, but only a marginal effort on the sonic and boiling limits. The entrainment limit requires even more attention because virtually no attempt has been made to formulate an analytical model.

Discrepancies between theoretical predictions and experimental observations of the four operating limits were found. The deviation was notably severe for the case of the boiling limit. Although the heat pipe promises potential solutions to problems of temperature control, passive heat transfer, heat flux conversion and variable thermal conductance, some of the heat pipe applications appear to have been suggested in view of eventual government funding of extensive research programs.

The techniques used and the data obtained during the course of this investigation lead to the following conclusions.

Construction details are given for a low cost apparatus for the measurement of wicking properties. It permits an accurate and continuous indication of the position of the advancing liquid front within a porous sample.

For the cylindrical heat pipe the axial temperature profiles as a function of power input behave as expected for a heat pipe employing a fixed temperature sink and a floating temperature source. The large temperature drop measured at the condenser end of the pipe is largely unaccounted for. Since the same behavior was observed by other investigators who used a fixed temperature sink, it appears that this phenomenon may be attributable to this particular mode of operation and not to the commonly accepted presence of a stagnant layer of noncondensable gas. The performance of the cylindrical heat pipe was significantly reduced (evidenced by the increase in evaporator wall temperature) as the inclination from horizontal was increased. The data showed that the maximum wicking height for the stainless steel screen, as it was installed in the pipe, was in the neighborhood of 12 cm. The number of screen layers used and the firmness with which they are pressed against the container wall certainly influences the wicking characteristics of the wick.

The data obtained with the coplanar heat pipe operated at a fixed sink temperature and with floating source temperatures lead to the following conclusions. The temperatures along the wick display considerable variation from the

evaporator to the condenser. This heat pipe worked more efficiently and transported more energy when operated in a horizontal position as compared to a situation with the evaporator above the condenser. In addition, the low vapor velocities permitted stratification to considerably influence the temperature distribution within the pipe (vapor chamber).

In regards to the behavior of two component heat pipes, the data indicated that under no conditions did complete separation of the components take place as deduced from a one dimensional argument. The two component heat pipe revealed the same temperature characteristics as a single component heat pipe when in a horizontal orientation. This behavior may be due to some mixing which took place in the liquid accumulated on the surface of the lower wick. Thus the entire vapor space, in effect, was in equilibrium with a constant composition fluid.

For the tests where the evaporator was located above the condenser, however, the excess liquid resided only at the condenser end of the pipe. For these cases, the axial temperature distributions obtained with a two component working fluid differed, to some extent, from those obtained with a single component working fluid. Such behavior indicates that a partial separation of the components did occur.

The effect which condensation on the windows had on the tendency toward component separation is unknown; however,

it can be argued that this effect was small for two reasons. First, once the condensation formed on the windows it appeared to remain relatively stable so that the condenser wick became the location of preferred condensation and thus played a dominant role in establishing the operating characteristics of the pipe. Second, the temperature distribution within the vapor core showed no changes in the cross axial direction (normal to the windows) while changes were evident normal to the wicks.

The merits of the heat pipe have been somewhat exaggerated. This is especially true for low temperature applications in a gravity field where the selection of the wick is of primary importance. Most of the wicks used are incompletely described in the literature. Often no cleaning procedure is reported even though this is as important as the wick selection itself. The use of the better "grooved" wicks requires special machining techniques which are not readily available to all investigators.

The isothermal nature of heat pipes which is so highly touted in the literature does not always occur. In fact, for fixed temperature condensers, it appears to be the exception rather than the rule.

While the heat pipe may be useful for high temperature and space applications, it should not be regarded as the ultimate solution to many ordinary heat transfer problems where greater economy, performance, and reliability are possible with more conventional heat transfer devices.

Recommendations

The study of the heat pipe literature leads to several recommendations. A coordinated materials research program is essential. In addition to assessing the desirability of potential wicking materials, this program should also provide for the investigation of the effect which various cleaning procedures and treatment techniques have on the wicking characteristics of potential heat pipe wick.

The influence which the external boundary conditions (i.e., either fixed or floating temperature) have on the operational characteristics of heat pipes is unclear. An experimental study in which a given heat pipe could sequentially be subjected to the various types of boundary conditions would be useful.

Additional work is needed on the theoretical predictions of the operating limits of heat pipes. In particular, the boiling and entrainment limits need more work.

Several recommendations are in order regarding an experimental extension of the work reported in this study. The behavior of the two component working fluid could be more easily detected by employing a heat pipe whose geometry dictated higher vapor velocities. If such a geometry was used, the consequence of stratification on the resulting temperature profiles could be neglected.

The use of the interferometer to measure the concentration distribution within the vapor space still appears feasible. However, major design changes in the test section are

necessary in order to avoid the condensation of the vapor on the inside of the windows. A design in which the windows are thermally insulated from both the ambient environment and the walls of the pipe should solve the condensation problem. Thermal insulation from the ambient conditions may be possible by using composite windows consisting of two pieces of glass with an evacuated space between them. Isolation of the windows from the test section walls, however, appears to be very involved.

The chemical analysis of the vapor with a gas chromatograph is desirable to ascertain the eventual separation into two components. Such a technique however, would virtually necessitate a direct connection of the chromatograph to the test section to insure that the vapor sample is not contaminated. An investigation of two component mixtures whose equilibrium curves exhibit an azeotropic point could be undertaken. In addition, the effect of the various types of boundary conditions on the characteristics of a two component heat pipe should be investigated.

LIST OF REFERENCES

LIST OF REFERENCES

1. Gaugler, R. S., "Heat Transfer Device," U. S. Patent 2,350,348, June 6, 1944.

2. Trefethen, L., "On the Surface-Tension Pumping of Liquids, or, a Possible Role of the Candlewick in Space Exploration," General Electric Technical Information Series, No. 61SD114, Feb. 1962.

3. Grover, G. M., Cotter, T. P., Erickson, G. F., "Structures of Very High Thermal Conductance," J. Applied Physics, Vol. 35, 1964, pp. 1990-1.

4. Cotter, T. P., "Theory of High Pipes," Los Alamos Scientific Lab., LA-3246-MS, Feb. 1965.

5. Katzoff, S., "Heat Pipes and Vapor Chambers for Thermal Control of Spacecraft," AIAA Thermophysics Specialist Conference, AIAA 67-310, April 1967.

6. Gray, V. H., "The Rotating Heat Pipe - A Wickless, Hollow Shaft for Transferring High Heat Fluxes," NASA TM X-52540.

7. Conway, E. C., and Kelley, M. J., "A Continuous Heat Pipe for Spacecraft Thermal Control," Aviation and Space: Progress and Prospects - Annual Aviation and Space Conference, June 1968, pp. 655-8.

8. Feldman, F. T., Jr., "Heat Pipe Design and Analysis," Northrop Corporate Laboratories - NCL 68-11R, February 29, 1968.

9. Feldman, F. T., Jr., and Whiting, G. H., "Applications of the Heat Pipe," J. Mechanical Engineering, Nov. 1968, pp. 48-53.

10. Harbaugh, W., "Heat Pipe Applications," Presented at Heat Pipe Technology and Manned Space Station Applications Technical Interchange, Huntsville, Alabama, May 27, 1969.

11. Basiulis, A. and Dixon, J. C., "Heat Pipe Design for Electron Tube Cooling," Paper No. 69-HT-25, Presented at the ASME-AIChE Heat Transfer Conference, Minneapolis, Minnesota, August 3-6, 1969.

12. Forrester, A. T., and Barcatta, F. A., "Surface Tension Storage and Feed Systems for Ion Engines," J. Spacecraft, Vol. 3, No. 7, July 1966, pp. 1080-85.

13. Langston, L., and Kunz, H. R., "Vapor Chamber Fin Studies," NASA CR-54882, first quarterly report, second quarterly report, third quarterly report, 1966.

14. Anand, D. K., Dybbs, A. Z., and Jenkins, R. E., "Effects of Condenser Parameters on Heat Pipe Optimization," J. Spacecrafts and Rockets, Vol. 4, No. 5, May 1967, pp. 695-6.

15. Cotter, T. P., Deverall, J., Erickson, G. F., and Grover, G. M., "Status Report on Theory and Experiments on Heat Pipes at Los Alamos," European Nuclear Energy Agency and Institution of Electrical Engineers, International Conference on Thermionic Electrical Power Generation, London, Sept. 20-25, 1965.

16. Andeen, G. B., Kern, E. R., Griffith, P., "The Heat Pipe," AEC Contract AT (30-1)-3496: Progress Report, June 30, 1965.

17. Kemme, J. E., "Ultimate Heat Pipe Performance," IEEE Conference Record of 1968 Thermionic Conversion Specialist Conference, Oct. 21-23, 1968, pp. 266-71.

18. Deverall, J. E., "Capability of Heat Pipes," Presented at Heat Pipe Technology and Manned Space Station Applications Technical Interchange, Huntsville, Alabama, May 27, 1969.

19. Cotter, T. P., "Heat Pipe Startup Dynamics," Thermionic Conversion Specialist Conference, Oct. 30 - Nov. 1, 1967, pp. 344-8.

20. Eastman, G. Y., "The Heat Pipe," Scientific American, Vol. 218, No. 5, May 1968, pp. 38-46.

21. Feldman, Jr., K. T., and Whiting, J. H., "The Heat Pipe," Mech. Eng., Feb. 1967, pp. 30-33.

22. Feldman, Jr., K. T., "The Heat Pipe, An Interesting Heat Transfer Device," Mech. Eng. News, Vol. 4, No. 2, 1968, pp. 24-27.

23. Deverall, J. E., and Kemme, J. E., "High Thermal Conductance Devices Utilizing the Boiling of Lithium or Silver," April 9, 1965, LA-3211, Los Alamos Scientific Laboratory.

24. Parker, G. H., and Hanson, J. P., "Heat Pipe Analysis," Advances in Energy Conversion Engineering, Aug. 1967, pp. 847-57.

25. Haskin, W. J., "Cryogenic Heat Pipe," Air Force Flight Dynamics Laboratory, Wright-Patterson Air Force Base, Ohio, AFFDL-TR-66-228, June 1967.

26. Frank, S., "Optimization of a Grooved Heat Pipe," Intersociety Energy Conversion Engineering Conference, Aug. 13-17, 1967, pp. 833-45.

27. Jeffries, N. P. and Zerkle, R. S., "Honeywell Heat Pipe Study," Report 1 and 2, Systems and Research Division, Honeywell, Inc., Minneapolis, Minnesota, 1968.

28. Neal, L. G., "Analytical and Experimental Study of Heat Pipes," TRW Report 99900-6114-R000, Jan. 1967, TRW Systems, One Space Park, Redondo Beach, California.

29. Phillips, E. C., "Low Temperature Heat Pipe Research Program," NASA Report No. CR-66792, 1966.

30. Frank, S., Smith, J. T., Taylor, K. M., "Heat Pipe Design Manual," Martin Nuclear Report MND-3288, Martin Marietta Corp., Baltimore, Maryland, Feb. 1967.

31. European Atomic Energy Community, Ispra, Italy, "Liquid Metals for Heat Pipes, Properties, Plots and Data Sheets," Report No. EUR-3655 E., No. N68-14750, Nov. 1967.

32. Hampel, V. E., and Koopman, R. P., "Reactivity Self-Control on Power and Temperature in Reactors Cooled by Heat Pipes," Lawrence Radiation Lab., Univ. of Calif., Livermore, UCRL-71198, Nov. 1, 1968.

33. Basiulis, A. and Dixon, J. C., "Heat Pipe Design for Electron Tube Cooling," Private Comm. from A. Basiulis, Hughes Electron Dynamics Division, 3100 W. Lomita Blvd., Torrance, Calif., 1969.

34. Scheidegger, A. E., The Physics of Flow Through Porous Media, New York, MacMillan, 1960.

35. McKinney, B. G., "An Experimental and Analytical Study of Water Heat Pipes for Moderate Temperature Ranges," Ph.D. Dissertation, University of Alabama, 1969.

36. Carnesale, A., Cosgrove, J. H., and Ferrell, J. K., "Operating Limits of the Heat Pipe," Proc. of Joint AEC/ Sandia Laboratories Heat Pipe Conference, Vol. 1, No. Sc-M-66-623, Oct. 1966, pp. 27-44.

37. Cosgrove, J. H., Ferrell, J. K., and Carnesale, A., "Operating Characteristics of Capillary Limited Heat Pipes," J. Nuclear Energy, Vol. 21, No. 7, July 1967, pp. 547-58.

38. Cosgrove, J. H., "Engineering Design of a Heat Pipe," Ph.D. Thesis, North Carolina State University, 1966.

39. Ferrell, J. K., and Carnesale, A., "A Study of the Operating Characteristics of the Heat Pipe," Oct. 1, 1966, ORO-3411-5, Fifth quarterly progress report.

40. Ferrell, J. K., and Carnesale, A., "A Study of the Operating Characteristics of the Heat Pipe," Quarterly Progress Reports #6 through #11, ORO-3411-6 through ORO-3411-11.

41. Ferrell, J. K. and Alleavitch, J., "Vaporization Heat Transfer in Capillary Wick Structures," AIChE Reprint 6, Presented at the ASME-AIChE Heat Transfer Conference, Minneapolis, Minnesota, August 3-6, 1969.

42. Shlosinger, A. P., "Heat Pipes for Space Suit Temperature Control," Aviation and Space: Progress and Prospects - Annual Aviation and Space Conference, June 1968, pp. 644-48.

43. Shlosinger, A. P., "Heat Pipe Devices for Space Suit Temperature Control," TRW Systems Report No. 06462-6005-RO-00, Nov. 1968, TRW Systems, One Space Park, Redondo Beach, California.

44. Shlosinger, A. P., Woo, W. Cafaro, C., and Bentilla, E. W., "Technology Study of Passive Control of Humidity in Space Suits," NASA Report No N66-14556, 1965.

45. Anon., "TRW Systems - Heat Pipe Experience and Technology," a promotional booklet available from TRW Systems, One Space Park, Redondo Beach, California.

46. Bohdansky, J., Buxbaum, C. A., and Grover, G. M., "The Use of a New Heat Removal System in Space Thermionic Power Supplies," European Atomic Energy Community, EUR 2229.3, 1965.

47. Busse, C. A., Caron, R., Geiger F., and Potzschke, M., "Performance Studies on Heat Pipes," European Nuclear Energy Agency and Institution of Electrical Engineers, International Conference on Thermionic Electrical Power Generation, London, Sept. 20-25, 1965.

48. Ranken, W. A., and Kemme, J. E., "Survey of Los Alamos and Euraton Heat Pipe Investigations," Thermionic Conversion Specialist Conference, IEEE, Oct. 1965, pp. 325-36.

49. Calimbas, A. T., Hulett, R. H., "An Avionic Heat Pipe," Paper No. 69-HT-16, Presented at the ASME-AIChE Heat Transfer Conference, Minneapolis, Minnesota, August 3-6, 1969.

50. McSweeney, T. I., "The Performance of a Sodium Heat Pipe," AIChE Preprint 7, Presented at the ASME-AIChE Heat Transfer Conference, Minneapolis, Minnesota, August 3-6, 1969.

51. Turner, R. C. and Harbaugh, W. E., "Design of a 50,000 watt Heat Pipe Space Radiator," Aviation and Space: Progress and Prospects - Annual Aviation and Space Conference, June 1968, pp. 639-43.

52. Turner, R. C., "The Configuration Pumped Heat Pipe - An Analysis and Evaluation," Private Comm. from R. C. Turner, RCA Electronic Components, Lancaster, Pa., 1969.

53. Phillips, E. C., and Hindermann, J. D., "Determination of Properties of Capillary Media Useful in Heat Pipe Design," Paper No. 69-HT-18, Presented at the ASME-AIChE Heat Transfer Conference, Minneapolis, Minnesota, August 3-6, 1969.

54. Ernst, D. M., "Evaluation of Theoretical Heat Pipe Performance," Thermionic Conversion Specialist Conference, Oct. 30 - Nov. 1, 1967, pp. 349-54.

55. Langsten, L. S. and Kunz, H. R., "Liquid Transport Properties of Some Heat Pipe Wicking Materials," Paper No. 69-HT-17, Presented at the ASME-AIChE Heat Transfer Conference, Minneapolis, Minnesota, August 3-6, 1969.

56. Ginwala, K., Blatt, T. A., and Bilger, R. W., "Engineering Study of Vapor Cycle Cooling Components for Space Vehicles," ASD-TDR-63-582, Sept. 1963, pp. 120-80.

57. Farran, R. A., and Starner, K. E., "Determining Wicking Properties of Compressible Materials for Heat Pipe Application," Aviation and Space: Progress and Prospects - Annual Aviation and Space Conference, June 1968, pp. 659-70.

58. Schwartz, J., "Performance Map of the Water Heat Pipe and the Phenomenon of Noncondensible Gas Generation," Paper No. 69-HT-15, Presented at the ASME-AIChE Heat Transfer Conference, Minneapolis, Minnesota, August 3-6, 1969.

59. Grover, G. M., "Theory and Recent Advances," Presented at Heat Pipe Technology and Manned Space Station Applications Technical Interchange, Huntsville, Alabama, May 27, 1969.

60. Deverall, J. E., and Kemme, J. E., "Satellite Heat Pipe," Los Alamos Scientific Laboratory Report No. LA-3278-MS, April 20, 1965.

61. Grover, G. M., "Heat Pipe Systems," Post Conference Report - International Conference on Thermionic Electrical Power Generation - 650908, London, pp. 12-16.

62. Busse, C. A., Caron, R., Cappelletti, C., "Prototypes of Heat Pipe Thermionic Converters for Space Reactors," European Nuclear Energy Agency and Institution of Electrical Engineers, International Conference on Thermionic Electrical Power Generation, London, Sept. 20-25, 1965.

63. Busse, C. A., Geiger, F., Potaschke, M., and Quataert, D., "Heat Pipe Life Tests at 1600°C and 1000°C," 1966 IEEE Conference Record of the Thermionic Conversion Specialist Conference, Nov. 1966, pp. 149-58.

64. Leefer, B. I., "Nuclear Thermionic Energy Converter," Proc. of the 20th Annual Power Sources Conference, May 1966, pp. 172-75.

65. Harbaugh, W. E., and Longsderff, R. W., "The Development of an Insulated Thermionic-Converter/Heat Pipe Assembly," Thermionic Conversion Specialist Conference, Nov. 1966, pp. 139-48.

66. RCA, "Heat Pipe Sweats to Harness Nuclear Reactor Heat," Electromechanical Design, Vol. 11, Oct. 1967, p. 20.

67. Shefsick, P. K., "Thermal Measurements of a Thermionic Converter/Heat Pipe System," Thermionic Conversion Specialist Conference, Nov. 1966, pp. 169-74.

68. Judge, J. F., "RCA Tests Thermal Energy Pipe," J. of Missiles and Rockets, Vol. 18, Feb. 14, 1966, pp.36-38.

69. Ernst, D. M., Levy, E. K., Shefsiek, P. K., "Heat Pipe Studies at Thermo Electron Corporation," IEEE Conference Record of 1968 Thermionic Conversion Specialist Conference, Oct. 21-23, 1968, pp. 254-57.

70. Ernst, D., "Heat Pipe Developments in Thermionics," Presented at Heat Pipe Technology and Manned Space Station Applications Technical Interchange, Huntsville, Alabama, May 27, 1969.

71. Ernst, D. M., and Eastman, G. Y., "Thermionic Two Piece Heat Pipe Converter," Proc. of the 21st Annual Power Sources Conference, 1967, pp. 132-8.

72. Johnson, G. D., "Compatibility of Various High-Temperature Heat Pipe Alloys with Working Fluids," IEEE Conference Record of 1968 Thermionic Conversion Specialist Conference, Oct. 21-23, 1968, pp. 258-65.

73. Bainton, K. F., "Experimental Heat Pipes," United Kingdom Atomic Energy Authority, AERE-M1610, 1965.

74. Hall, W. B., "Heat Pipe Experiments," Thermionic Conversion Specialist Conference, IEEE, Oct. 1965, pp. 337-40.

75. Bowman, B. R. and Crain, R. W., Jr., "An Ambient Temperature Water Heat Pipe," Private Comm. from R. Bowman, Mech. Engr. Dept., Washington State University, Pullman, Washington, 1969.

76. Bohdansky, J., Strub, H., and VanAndel, E. "Heat Transfer Measurements Using a Sodium Heat Pipe Working at Low Vapor Pressure," Thermionic Conversion Specialist Conference, Houston, Texas, Nov. 1966, pp. 144-8.

77. Allingham, W. D., and McEntire, J. A., "Determination of Boiling Film Coefficient for a Heated Horizontal Tube in Water-saturated Wick Material," J. of Heat Transfer, Paper No. 60-HT-11, 1960, pp. 1-5.

78. Anand, D. K., "On the Performance of a Heat Pipe," J. Spacecraft Rockets (Eng. Note), Vol. 3, No. 5, May 1966, pp. 763-65.

79. Anand, D. K., Dybbs, A. Z., and Jenkins, R., "Heat Pipe Application for Spacecraft Thermal Control," The Johns Hopkins University, Applied Physics Laboratory, AD 662241 - 100 pp., 1967.

80. Marto, P. J. and Mosteller, W. L., "The Effect of Nucleate Boiling on the Operation of Low Temperature Heat Pipes," Paper No. 69-HT-24, Presented at the ASME-AIChE Heat Transfer Conference, Minneapolis, Minnesota, August 3-6, 1969.

81. Moss, R. A., and Kelley, A. J., "Neutron Radiographic Study of Limiting Planar Heat Pipe Performance," Private Comm. from A. J. Kelley, Assistant Professor of Aerospace and Mechanical Sciences, Guggenheim Laboratories, Princeton University, Princeton, New Jersey, 1969.

82. Costello, C. P. and Redeker, E. R., "Boiling Heat Transfer and Maximum Heat Flux for a Surface with Coolant Supplied by Capillary Wicking," Chem. Eng. Prog. Symp. Series, Heat Transfer, Vol. 59, No. 41, 1963, pp. 104-13.

83. Dzakowic, G. S., Arcella, F. G., and Tang, Y. S., "Experimental Study of Vapor Velocity Limit in a Sodium Heat Pipe," Paper No. 69-HT-21, Presented at the ASME-AIChE Heat Transfer Conference, Minneapolis, Minnesota, August 3-6, 1969.

84. Deverall, J. E., Salmi, E. W., and Knapp, R. J., "Orbital Heat Pipe Experiment," NASA Report No. N67-37590, June 22, 1967.

85. Kemme, J. E., "Heat Pipe Capability Experiments," Proc. of Joint AEC/Sandia Laboratories Heat Pipe Conference, Vol. 1, Sc-M-66-623, Oct. 1966, pp. 11-26.

86. Kemme, J. E., "High Performance Heat Pipes," Thermionic Conversion Specialist Conference, Oct. 30 - Nov. 1, 1967, pp. 355-8.

87. Deverall, J. E., Salmi, E. W., and Knapp, R. J., "Heat Pipe Performance in a Zero - g Gravity Field," J. of Spacecrafts and Rockets, Vol. 4, No. 11, Nov. 1967, pp. 1556-7.

88. Deverall, J. E. and Salmi, E. W., "Heat Pipe Performance in a Space Environment," Thermionic Conversion Specialist Conference, Oct. 30 - Nov. 1, 1967, pp.359-62.

89. Deverall, J. E., "The Effect of Vibration on Heat Pipe Performance," Los Alamos Scientific Laboratory, Report LA-3798, Nov. 1967.

90. Bohdansky, J., Schins, H. E. J., "Heat Transfer of a Heat Pipe Operating at Emitter Temperature," European Nuclear Energy Agency and Institution of Electrical Engineers, International Conference on Thermionic Electrical Power Generation, London, Sept. 20-25, 1965.

91. McKinney, B. G., "An Experimental and Analytical Study of Water Heat Pipes for Moderate Temperature Ranges," NASA T. M., Report No. 53849, June 6, 1969.

92. Tien, C. L., "Two Component Heat Pipes," AIAA Paper No. 69-631, June 1969.

93. Dannenburg, K., "Space Station Program," Presented at Heat Pipe Technology and Manned Space Station Applications Technical Interchange, Huntsville, Alabama, May 27, 1969.

94. Madsen, J., "Spacecraft Thermal Modulation Using Heat Pipes," Presented at the Heat Pipe Technology and Manned Space Station Applications Technical Interchange, Huntsville, Alabama, May 27, 1969.

95. Bienert, W., "Heat Pipes for Electronic Equipment and Temperature Control," Presented at the Heat Pipe Technology and Manned Space Station Applications Technical Interchange, Huntsville, Alabama, May 27, 1969.

96. Anand, D. K., "Heat Pipe Application to a Gravity-Gradient Satellite," Aviation & Space: Progress and Prospects - Annual Aviation and Space Conference, June 1968, pp. 634-38.

97. The Johns Hopkins University, "The GEOS-2 Heat Pipe System and Its Performance in Test and in Orbit," Report No. S2P-3-25, NASA CR-94585, NASA N68-25540, April 29, 1968.

98. Deverall, J. E., "Total Hemispherical Emissivity Measurements by the Heat Pipe Method," Aviation and Space: Progress and Prospects - Annual Aviation and Space Conference, June 1968, pp. 649-54.

99. Schretzmann, K., "The Effect of Electromagnetic Fields on the Evaporation of Metals," Physics Letters, Vol. 24A, No. 9, April 24, 1967, pp. 478-79.

100. Bohdansky, J., and Schins, H. E. J., "New Method for Vapor-Pressure Measurements at High Temperatures and High Pressures," J. of Applied Physics, Vol. 36, No. 11, Nov. 1965, pp. 3685-4.

101. Heath, C. A. and Lantz, E., "Nuclear Thermionic Space Power System Concept Employing Heat Pipes," NASA TN D-4299, 1965.

102. Haller, H. C. and Lieblein, S., "Feasibility Studies of Space Radiators Using Vapor Chamber Fins," Proc. of Joint AEC/Sandia Laboratories Heat Pipe Conference, Vol. 1, No. Sc-M-66-623, Oct. 1966, pp. 47-68.

103. Haller, H. C., Lindow, B. G., and Aver, B. M., "Analysis of a Low Temperature Direct Condensing Vapor-Chamber Fin and Conducting Fin Radiators," NASA TND-3103, 1965.

104. Haller, H. C., "Analysis and Evaluation of a Vapor-Chamber Fin-Tube Radiator for High Power Rankine Cycles," NASA TND-2836, 1965.

105. Werner, R. W. and Carlson, G. A., "Heat Pipe Radiator for a 50-MWT Space Power Plant," Lawrence Radiation Laboratory, Report No. UCRL-50294, June 30, 1967.

106. Los Alamos Scientific Laboratory, Quarterly Status Report on Advanced Reactor Technology (ART) for period ending July 31, 1965, LA-3370-MS, 1965, pp. 58-62.

107. "Discussion of Heat Pipe Principles," Radio Corporation of America, Direct Energy Conversion Dept., Lancaster, Pennsylvania.

108. Roberts, J. J., Croke, E. J., Carter, R. P., Norco, J. E., "A Heat-Pipe-Cooled Fast-Reactor Space Power Supply," Argonne National Laboratory, Report No. ANL-7422, June 1968.

109. Ruhle, V. R., Steiner, D. Fritz, R., and Dagbjartsson, S., "Employment of Heat Pipes for Thermionic Reactors," Atomkern Energie, Vol. 10, Sept./Oct. 1965, pp. 399-404.

110. Brosens, P. J., "Thermionic Converter with Heat Pipe Radiator," Advances in Energy Conversion Engineering Conference, Aug. 13-7, 1967, pp. 181-9.

111. Busse, C. A., "Optimization of Heat Pipe Thermionic Converters for Space Power Supplies," European Atomic Energy Community, EUR 2534.e, 1965.

112. Bohdansky, J., "Thermionic Converter and Its Use in a Reactor," European Atomic Energy Community, Ispra, Italy, Report No. EUBU 5-4, 1965.

113. Frysinger, G. R. and Eastman, G. Y., "3 K.W. Flame Heated Thermionic Energy Converter," Proc. of the 20th Annual Power Sources Conference, May 1966, pp. 169-71.

114. Hall, W. B., and Kessler, S. W., "Advances in Heat Pipe Design," Proc. of the 20th Annual Power Sources Conference, May 1966, pp. 166-69.

115. Lazarids, L. J., and Pantazelos, P. G., "Tests on Flame Heated Thermionic Diode," Proc. of the 20th Annual Power Sources Conferences, May 1966, pp. 175-77.

116. Bohdansky, J., Salamon, K., VanAndel, E., "Integrate Cs-Graphite Reservoir System in a Heat Pipe Thermionic Converter," Thermionic Conversion Specialist Conference, Palo Alto, California, Oct. 30 - Nov. 1, 1967, pp.93-96.

117. Brosens, P., "Heat Pipe Thermionic Converter Development," NASA Report No. CR-93664, Dec. 1967.

118. Werner, K. W., "The Generation and Recovery of Tritium in Thermonuclear Reactor Blankets Using Heat Pipes," Lawrence Radiation Laboratory, Univ. of Calif., Livermore, UCID-15390, Oct. 3, 1968.

119. Wyatt, T., "Controllable Heat Pipe Experiment," Applied Physics Laboratory, SDO-1154, The Johns Hopkins University, March 1965.

120. Yuan, S. W. and Finkelstein, A. B., "Laminar Pipe Flow with Injection and Suction Through a Porous Wall," ASME Trans., Vol. 78, 1956, pp. 719-24.

121. Knight, B. K. and McInteer, B. B., "Laminar Incompressible Flow in Channels with Porous Walls," LA-DC-5309, Los Alamos, Sci. Lab., 1965.

122. Wageman, W. E. and Guevara, F. A., "Fluid Flow Through a Porous Channel," Physics of Fluids, Vol. 5, No. 6, Nov. - Dec. 1960, pp. 878-81.

123. Busse, C. A., "Pressure Drop in the Vapor Phase of Long Heat Pipes," Thermionic Conversion Specialist Conference, Palo Alto, Calif., Oct. 30 - Nov. 1, 1967, pp. 391-98.

124. Schindler, M., and Wassner, G., "Theoretical Considerations on Heat Transfer in Heat Pipes," Atomkern Energie, Vol. 10, Sept./Oct. 1965, pp. 395-98.

125. Streckert, J. H. and Chato, J. C., "Development of a Versatile System for Detailed Studies on the Performance of Heat Pipes," Tech. Report No. ME-TR-64, Dec. 1968, University of Illinois, Urbana, Illinois.

126. Chato, J. C. and Streckert, J. H., "Performance of a Wick-Limited Heat Pipe," Paper No. 69-HT-20, Presented at the ASME-AIChE Heat Transfer Conference, Minneapolis, Minnesota, August 3-6, 1969.

127. Levy, E. K., "Theoretical Investigation of Heat Pipes Operating at Low Vapor Pressures," Aviation and Space: Progress and Prospects Annual Aviation and Space Conference, June 1968, pp. 671-76.

128. Marcus, B. D., "On the Operation of Heat Pipes," TRW Space Technology Laboratory Report No. 99900-6114-R000, May 1965, TRW Systems, One Space Park, Redondo Beach, California.

129. Lyman, F. A. and Huang, Y. S., "Analysis of Temperature Distributions in Heat Pipe Wicks," Paper No. 69-HT-23, Presented at the ASME-AIChE Heat Transfer Conference, Minneapolis, Minnesota, August 3-6, 1969.

130. Gorring, R. L. and Churchill, S. W., "Thermal Conductivity of Heterogeneous Materials," Chamical Engineering Progress Symposium Series - Heat Transfer, Houston, Texas, Vol. 59, 1963.

131. Nissan, A. H., Hansen, D. and Walker, J. L., "Heat Transfer in Porous Media Containing a Volatile Liquid," Chemical Engineering Progress Symposium Series - Heat Transfer, Houston, Texas, Vol. 59, 1963.

132. Bressler, R. G. and Wyatt, P. W., "Surface Wetting Through Capillary Grooves," AIChE, Preprint 19, Presented at the ASME-AIChE Heat Transfer Conference, Minneapolis, Minnesota, August 3-6, 1969.

133. Galowin, L. S. and Barker, V., "Heat Pipe Channel Flow Distributions," Paper No. 69-HT-22, Presented at the ASME-AIChE Heat Transfer Conference, Minneapolis, Minnesota, August 3-6, 1969.

134. Miller, P. L. and Holm, F. W., "Investigation of Constraints in Thermal Similitude," Air Force Flight Dynamics Laboratory, Wright-Patterson Air Force Base, Ohio, Tech. Report AFFDL-TR-69-91, Vol. I, II.

135. Bosnjakovic, and Blackshear, Technical Thermodynamics, New York, Holt, Rinehart and Winston, Inc., 1965.

136. Landolt, and Bornstein, II Band, 2 Teil, Berlin, Springer Verlag, 1962.

137. "Alcohols," Union Carbide Chemicals Company, 270 Park Avenue, New York, New York, 1961.

138. Jacob, M., Heat Transfer, Vol. I, New York, John Wiley & Sons, Inc., 1949.

139. Holman, J. P., Heat Transfer, New York, McGraw-Hill Book Company, 1968.

140. Deverall, J. E., "Mercury as a Heat-Pipe Fluid," Paper No. 70-HT/SpT-8, Presented at the ASME Space Technology and Heat Transfer Conference, Los Angeles, California, June 21-24, 1970.

141. Schwartz, J., "Performance Map of an Ammonia (NH_3) Heat Pipe," Paper No. 70-HT/SpT-5, Presented at the ASME Space Technology and Heat Transfer Conference, Los Angeles, California, June 21-24, 1970.

142. Waters, E. D. and King, P. P., "Campatibility Evaluation of an Ammonia-Aluminum-Stainless Steel Heat Pipe," Paper No. 70-HT/SpT-15, Presented at the ASME Space Technology and Heat Transfer Conference, Los Angeles, California, June 21-24, 1970.

143. Joy, Patrick, "Optimum Cryogenic Heat-Pipe Design," Paper No. 70-HT/SpT-7, Presented at the ASME Space Technology and Heat Transfer Conference, Los Angeles, California, June 21-24, 1970.

144. Chi, S. W. and Cygnarowicz, Thomas A., "Theoretical Analyses of Cryogenic Heat Pipes," Paper No. 70-HT/SpT-6, Presented at the ASME Space Technology and Heat Transfer Conference, Los Angeles, California, June 21-24, 1970.

145. Ferrell, J. K. and Johnson, H. R., "The Mechanism of Heat Transfer in the Evaporator Zone of a Heat Pipe," Paper No. 70-HT/SpT-12, Presented at the ASME Space Technology and Heat Transfer Conference, Los Angeles, California, June 21-24, 1970.

146. Soliman, M. M., Graumann, D. W., and Berenson, P. J., "Effective Thermal Conductivity of Dry and Liquid-Saturated Sintered Fiber Metal Wicks," Paper No. 70-HT/SpT-40, Presented at the ASME Space Technology and Heat Transfer Conference, Los Angeles, California, June 21-24, 1970.

147. Marcus, B. D. and Fleischman, G. L., "Steady-State and Transient Performance of Hot Reservoir Gas-Controlled Heat Pipes," Paper No. 70-HT/SpT-11, Presented at the ASME Space Technology and Heat Transfer Conference, Los Angeles, California, June 21-24, 1970.

148. Bliss, Jr., F. E., Clark, E. G., and Stein, B., "Construction and Test of a Flexible Heat Pipe," Paper No. 70-HT/SpT-13, Presented at the ASME Space Technology and Heat Transfer Conference, Los Angeles, California, June 21-24, 1970.

149. Bilenas, Jonas A. and Harwell, William, "Orbiting Astronomical Observatory Heat Pipes - Design, Analysis, and Testing," Paper No. 70-HT/SpT-9, Presented at the ASME Space Technology and Heat Transfer Conference, Los Angeles, California, June 21-24, 1970.

150. Carlson, Gustav A. and Hoffman, Myron, A., "Effect of Magnetic Fields on Heat Pipes," Paper No. 70-HT/SpT-10, Presented at the ASME Space Technology and Heat Transfer Conference, Los Angeles, June 21-24, 1970

APPENDIX A: STRATIFICATION

Stratification had a significant influence on the steady state temperature field within the vapor space. It was especially important for the coplanar heat pipe because of the low vapor velocities which were prevalent in the vapor core.

Since the evaporator was located above the condenser for $\theta = 45°$ and $\theta = 90°$, stable operating conditions existed. That is, the lower density, higher temperature vapor tended to accumulate at the top of the vapor space in the evaporator while the higher density, lower temperature vapor resided in the condenser. Because heat addition took place at the top of the vaper space, no major convection currents occurred and the primary mode of energy transport (for pure stratification) was effected by conduction through the vapor space. Consequently, for a situation where no heat pipe action exists the temperature distribution within the vapor core must satisfy Laplace's equation under the assumption of consvant thermal conductivity of the vapor. In reality, however, it may vary with temperature up to approximately 15% from end to end.

The temperature distribution within the vapor space was determined by utilizing the analogy between thermal and

electrical systems. The vapor space was modeled on a sheet of Teledeltos paper. It was assumed that the vapor at the wick surface in the condenser was at some temperature T_c, and that the vapor at the wick surface in the evaporator was at another temperature, T_{II}. In the electrical analog, this implies that these surfaces were maintained at a constant voltage. All other boundaries of the vapor space were considered to be adiabatic and thus were open circuits in the electrical analog model. The resulting lines of constant voltage (and hence the analogous isotherms) were determined using a DC Null Detector and are illustrated in Figure A.1.

The dimensionless axial temperature distributions corresponding to each of the probe locations are presented in Figure A.2. These distributions are, of course, highly idealistic resulting from the assumed boundary conditions. In actuality, the temperatures at the wick surface in both the evaporator and condenser were not constant. Also the end walls undoubtedly were not adiabatic.

To verify whether conduction was indeed the dominant factor in establishing the stratified temperature distribution, ten tests were conducted. Each test employed a wick in only the evaporator end of the heat pipe. A sufficient amount of fluid was introduced into the coplanar pipe so that some excess liquid always remained in the condenser section. The pipe was evacuated until the liquid pool boiled, thus assuring that saturation conditions were

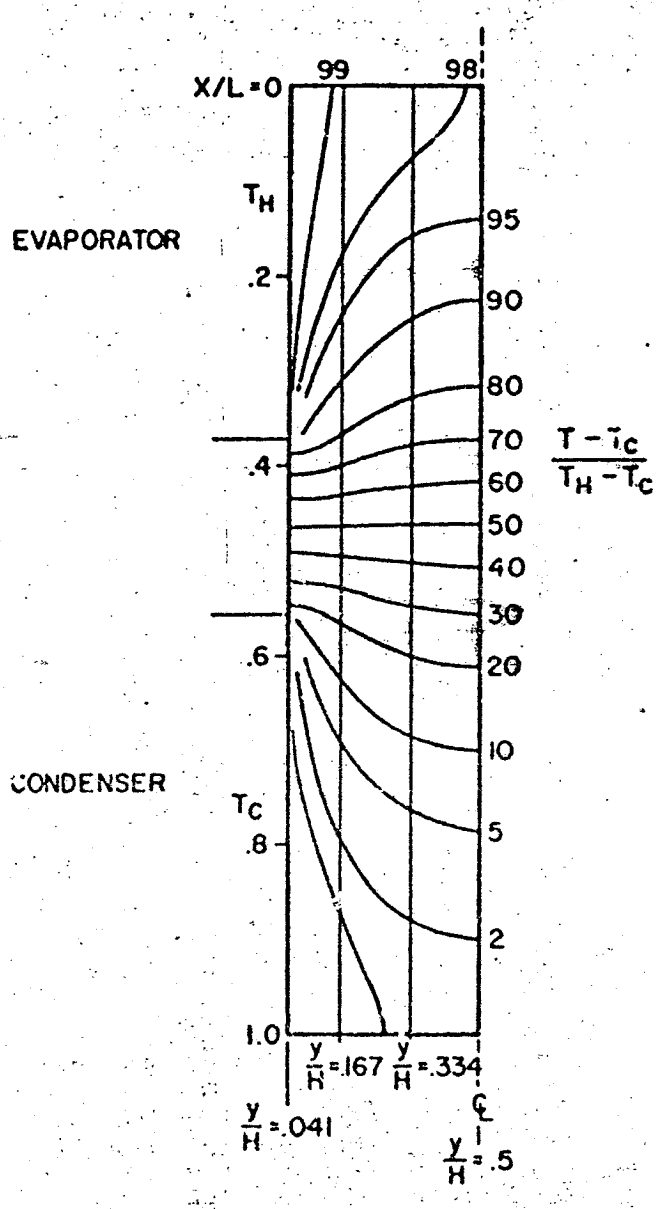

Figure A.1 Pure Conduction Isotherms in Vapor Space

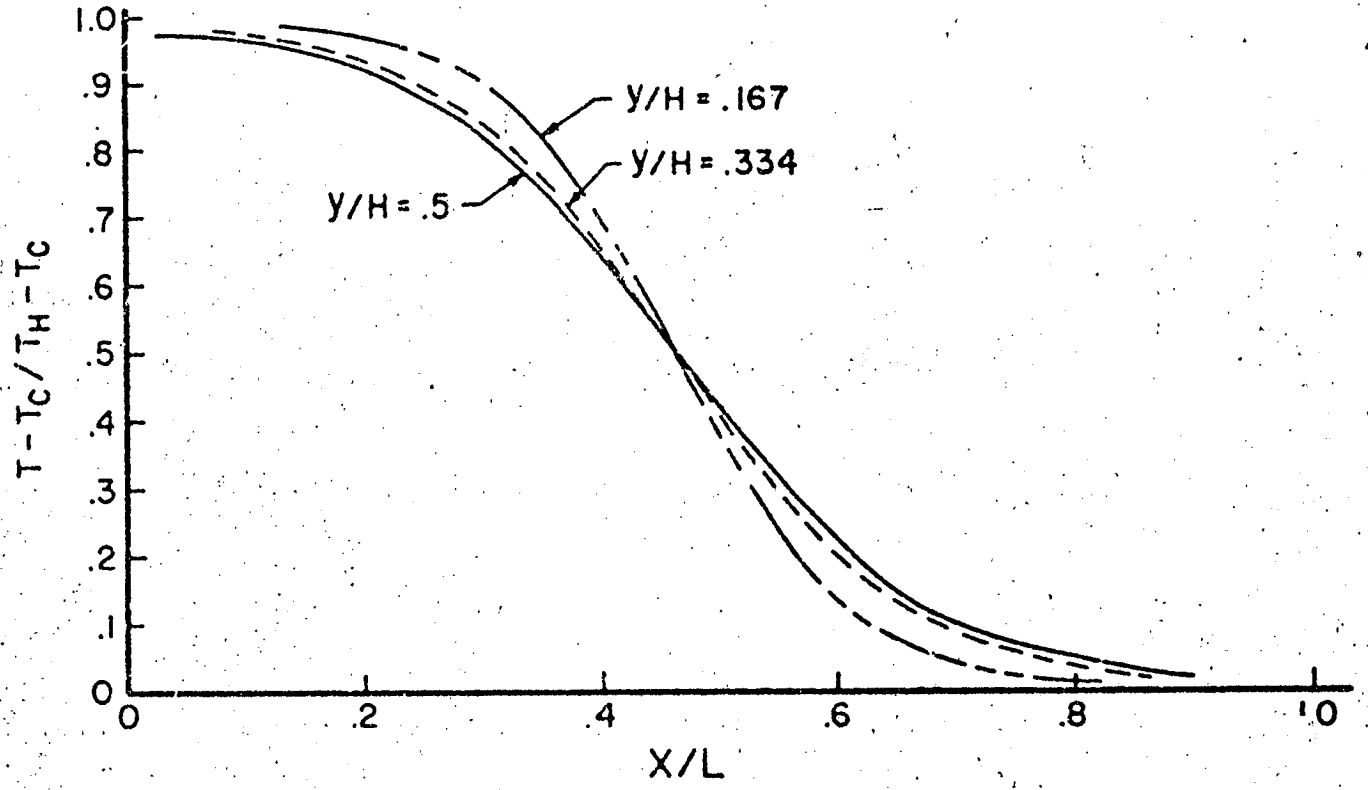

Figure A.2 - Pure Conduction Axial Temperature Distributions

initially present. The heaters were then energized and the resulting steady state temperature distributions in the vapor space were measured. Since the absence of a wick in the condenser section prevented liquid from reaching the evaporator, the wicks rapidly dried out and the resulting temperature distribution was determined solely by the occurrence of stratification. As expected, the dimensionless temperature distributions were essentially independent of composition, pressure, and temperature. Two such distributions are presented in Figures A.3 and A.4 for the centerline probe and for orientations of $\theta = 90°$ and $\theta = 45°$. Similar distributions were measured for the other probes.

The similarity between the measured distributions and those obtained with the electrical analog suggests that conduction does indeed establish the temperature field. The different values near the ends of the pipe are probably caused by the idealized boundary conditions which were employed in the electrical analog apparatus.

The experimentally determined stratification profiles for each probe were used for subsequent data comparisons with the stratification profile.

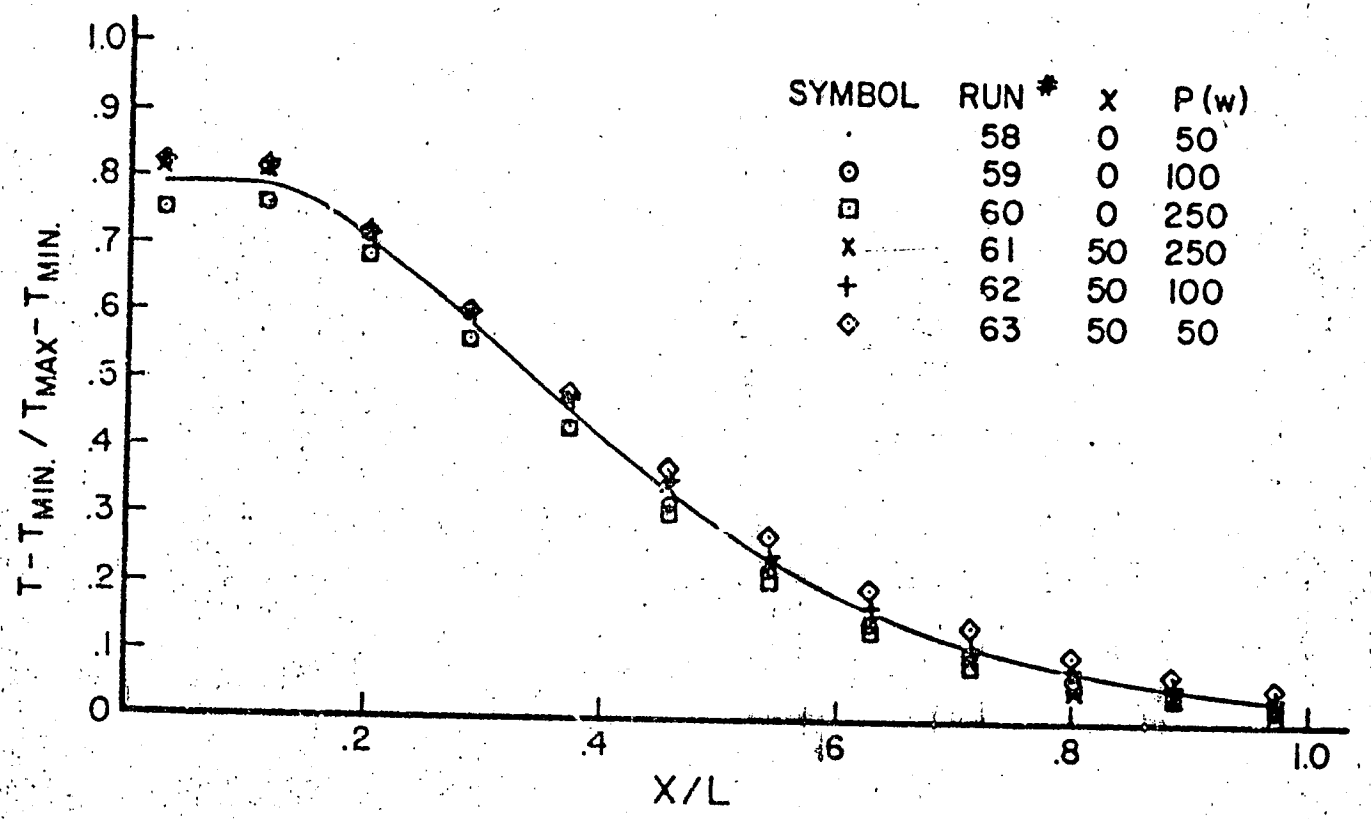

Figure A.3 Centerline Temperature Distribution for Pure Conduction, $\theta = 90°$

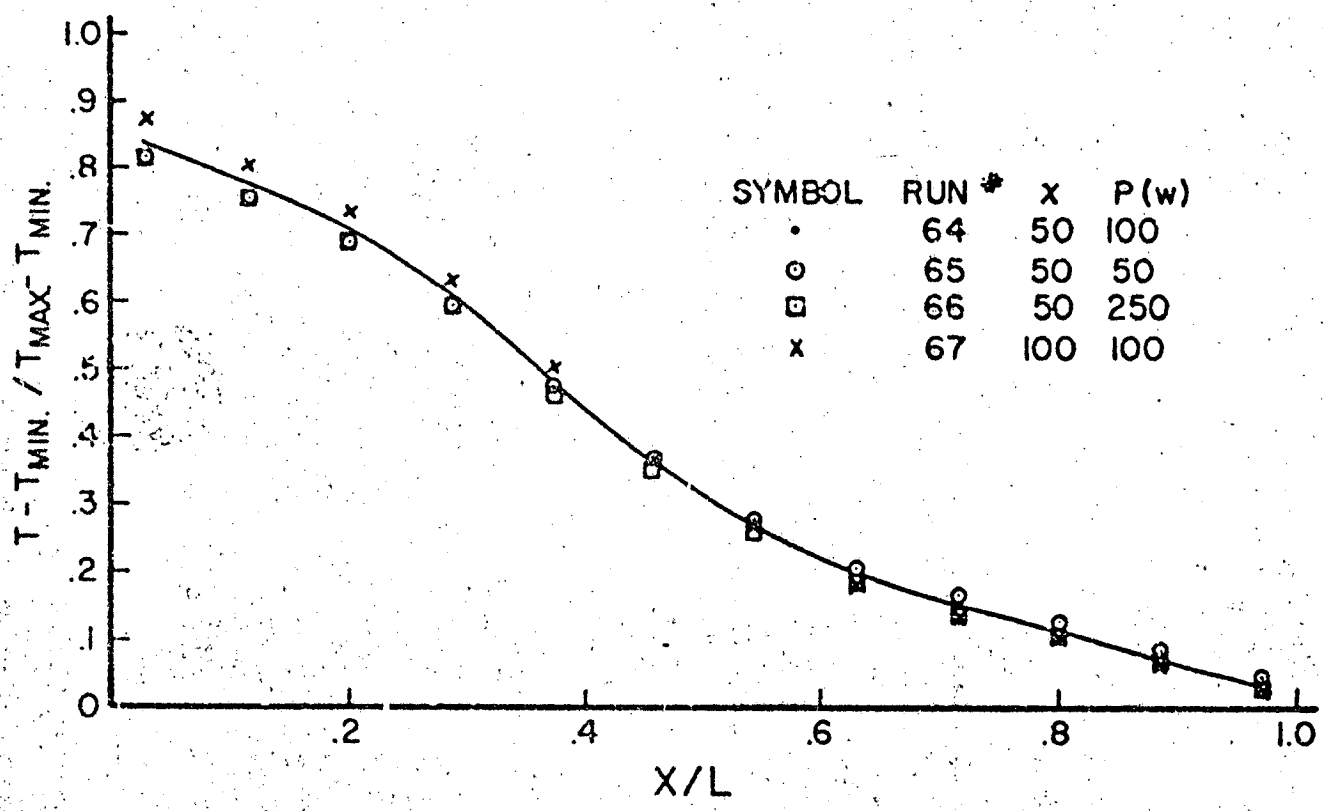

Figure A.4 Centerline Temperature Distribution for Pure Conduction, θ = 45°

APPENDIX B: PROBE CONDUCTION

The temperature measurement with a relatively high thermal conductivity probe in a medium of very low conductivity naturally leads to some errors. To assess the influence that the room temperature, T_o, imposes on the measurement of the vapor temperature, T_e, the following technique was used. The temperature actually measured at the probe tip, T, was related to T_o and T_e using the standard expression for the temperature distribution along a finite rod which protrudes from a heat source with heat losses to a constant temperature vapor environment as given by Jacob [138]. This expression is given as

$$\frac{\theta}{\theta_o} = \frac{(1 + P)e^{-mL}}{1 + Pe^{-2mL}} \qquad (B\text{-}1)$$

where

$$\theta = T - T_e \,, \quad \theta_o = T_o - T_e \qquad (B\text{-}2)$$

$$m = \left(\frac{hC}{kA}\right)^{\frac{1}{2}} \qquad (B\text{-}3)$$

and

$$P = \frac{km - h}{km + h} \qquad (B\text{-}4)$$

In the expressions, L is the length of the probe from the outside of the pipe, C is the probe circumference, A is the cross sectional area, h is the convective heat transfer coefficient, and K is the effective thermal conductivity of the probe. The dimensionless temperatures calculated with the above expressions are shown in Figure B.1 as a function of both the probe length and the convective heat transfer coefficient. It is readily apparent that large errors are encountered when h is small.

A conservative estimate of h was arrived at by assuming that the probes were orientated horizontally with free convection as the only mode of heat transfer to the surrounding vapor. Assuming a temperature difference of 5°F in the Grashof number and using an accepted correlation for the relationship of the Nusselt and Grashof numbers for free convection from a horizontal cylinder as given by Holman [139], the convective heat transfer coefficient was found to be approximately 2.5 Btu/hr ft^2°F. This value of h was used to calculate the actual vapor temperatures for all probe positions and all tests which were compared with the temperatures measured at the probe tip. It was found that the probe tip temperature was an accurate indication of the vapor temperature with the exception of the measurements taken at the last position in the condenser. With the exception of this last point the readings were in general accurate to within 1°F. The measurements taken at the

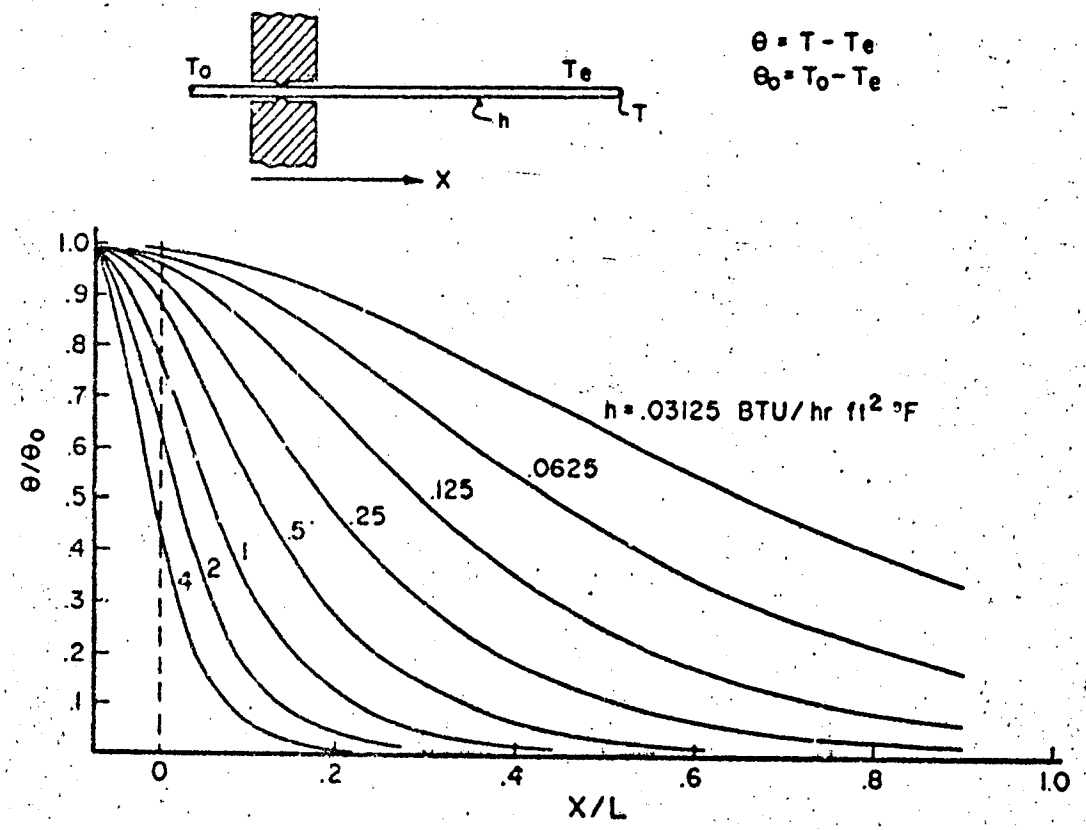

Figure B.1 Thermocouple Probe Temperature Distribution

extreme probe position were often in error by as much as 10°F. However, this occurred only for the high heat flux tests where the presence of forced convection certainly resulted in an increased value of h and thus smaller errors than are indicated by this approach.

APPENDIX C: RECENT LITERATURE

The articles discussed in this appendix were presented at the Space Technology and Heat Transfer Conference, Los Angeles, California, June 21-24, 1970. They are presented as a supplement to the previously discussed literature so that the present report is as up to date as possible.

Deverall [140] has found that the construction of mercury heat pipes for high heat transfer rates is feasible for operation between 200 and 360°C. Previously encountered wetting difficulties with mercury were virtually eliminated by the additions of magnesium and titanium.

Schwartz [141] tested an ammonia-stainless steel heat pipe. The operating characteristics were compared to the characteristics obtained with a geometrically identical heat pipe employing water as a working fluid [58]. It was found that the ammonia pipe was more efficient in transporting thermal loads than the water pipe up to an operating temperature of approximately 90°F. Above this temperature the ammonia pipes relative advantage declined rapidly until dry-out, at which point the water pipe was able to transport 30 percent more energy.

In a similar study, Waters and Kine [142] tested the ability of an ammonia heat pipe to operate for extended

periods without failure by fluid loss or by degradation of the energy transport mechanisms. The heat pipe used had an aluminum container and a stainless steel screen wicking structure. Accelerated time testing for both continuous heat pipe operation, and with alternating freeze-thaw cycles indicated no degradation in thermal performance. Subsequent metallurgical examination of the pipe revealed little material corrosion. The authors concluded that such a heat pipe should have a useful operating life in excess of 20 years when operated at about 80°F.

Heat pipes in the cryogenic temperature range have been theoretically considered by Joy [143]. Equations for the optimum pore size, optimum wick thickness ratio, and maximum heat transport were derived. The effect of gravity was found to play a major role and must be taken into consideration in cryogenic heat pipe design. The equations result in the selection of oxygen and a channel wick for an optimum cryogenic heat pipe design in the temperature range from 77 to 90°K.

Chi and Cygnarowicz [144] also presented a theoretical analysis of cryogenic heat pipes. The influence of liquid property variations was found to be significant. The theory compared favorably with the experimental results of Haskin [25].

Ferrell and Johnson [145] obtained experimental results for both the heat transfer coefficient and the critical heat

flux through saturated beds of monel and glass beads. The liquid in the neighborhood of the heater was supplied only by capillary action. Various wick inclinations were employed in the tests. The conduction mechanism through a thin liquid-bead layer in contact with the heating surface as proposed by Ferrell and Alleavitch [41] was found to be substantially correct.

Soliman, et al. [146] measured the effective thermal conductivity of both dry and water-saturated sintered fiber metal wicks. Correlations were found for the effective thermal conductivity in terms of the thermal conductivities of the solid and liquid phases and the wick porosity. Substantial differences in the effective conductivity were found when measured either along or across the fibers and this was attributed to the importance of the contact resistance between fibers.

The effect of the working fluid, in either the liquid or vapor phase, within the reservoir of hot reservoir gas-controlled heat pipes was investigated by Marcus and Fleischman [147]. It was found that the presence of liquid in the reservoir at startup results in temporary pressures and temperatures in excess of design conditions. A perforated non-wetting plug at the reservoir entrance was found to eliminate this problem.

Bliss, et al. [148] tested a flexible heat pipe subject to varying degrees of bend and various transverse and

longitudinal vibrations while in an unbent mode. It was discovered that flexible heat pipes are feasible and that the degree of bend had little effect on operation. The vibrational environment, in general, tended to increase the heat transfer capacity; however, critical longitudinal vibrational frequencies were found which caused cessation of heat pipe operation.

Bilenas and Harwell [149] describe the development and construction of a set of heat pipes designed to minimize structural temperature gradients for the Number 3 OAO Spacecraft to be launched in 1970.

Carlson and Hoffman [150] studied the influence of magnetic fields on heat pipes. Such effects were found to be important when electrically conducting working fluids (such as liquid metals) are used and the pipe axis is not aligned with the magnetic field. For such cases, the presence of a magnetic field always reduces the heat flux capability of the heat pipe. However, this outcome may be reduced by designing the pipe with a compound wick structure with a larger liquid flow passage and a proportionately smaller vapor flow passage than for the no-magnetic field design. The equations necessary for such a design are presented.